Research Center Borstel
Leibniz-Center for Medicine and Biosciences
Department of Molecular Infectiology
Director: Prof. Dr. U. Schaible

Division of Biophysics
Head: Prof. Dr. T. Gutsmann

‡

Characterization of

Reconstituted Bacterial Membranes

and Their

Interaction with Antimicrobial Peptides

‡

Dissertation

for Fulfillment of Requirements

for the Doctoral Degree

of the University of Lübeck

from the Department of Natural Sciences

Submitted by

Max Koistinen

from Frankfurt/M., Germany

Borstel, January 2012

_____

First referee: Prof. Dr. Thomas Gutsmann

Second referee: Prof. Dr. Christian Hübner

Date of oral examination: 4.6.2012

Approved for printing.
Lübeck, 7.6.2012

TABLE OF CONTENTS

LIST OF ABBREVIATIONS

A_0	surface area of the hydrophilic head group
AA	amino acid
AC	alternating current
AFM	atomic force microscopy
AMP	antimicrobial peptide
BCG	bacille Calmette-Guerin
BODIPY FL-PC	2-(4,4-difluoro-5,7-dimethyl-4-bora-3a,4a-diaza-s-indacene-3-pentanoyl)-1-hexadecanoyl-sn-glycero-3-phosphocholine
BODIPY	7-Nitro-2,1,3-benzoxadiazole-4-yl (NBD), 4,4-difluoro-5,7-dimethyl 4-bora-3a,4a-diaza-s-indacene-3-pentanoyl
bSM	sphingomyelin from porcine brain
C	carbon
c	speed of light in vacuum
CAD	computer-aided design
CD14	cluster of differentiation 14
CFU	colony forming units
chol	cholesterol
Cl	chloride
DOPC	dioleoyl-sn-glycero-3-phosphocholine
DPG	diphosphatidylglycerol
DSL	dynamic light scattering
E	transfer efficiency
E. coli	*Escherichia coli*
egg PC	phosphatidylcholine from chicken egg
FITC-PE	fluorescein-isothiocyanate-phosphadidylenthanolamine
FRET	Förster resonance energy transfer
FTIC	fluorescein-isothiocyanate
FTIR	Fourier transform infrared
G	glucosamine
GUV	giant unilamellar vesicle
H	hydrogen
hBD-3-l	linear derivative of human-β-defensin 3
hCAP18	human cationic antimicrobial peptide
Hep	heptose
Hepes	4-(2-hydroxyethyl)-1-piperazineethanesulfonic acid
HIV	human immunodeficiency virus
HPLC	high-performance liquid chromatography
I/O	input / output
I_D	donor fluorescence intensity in absence of an acceptor
I_{D+A}	donor fluorescence intensity in presence of an acceptor
IL-1, IL-6	interleukin -1, -6
IR	infrared
ITO	indium tin-oxide
K	potassium

kDa	kilo-dalton
Kdo	3-keto-3-deoxyoctonate
KI	potassium iodide
l	bond length
L	maximal length of an alkyl chain
l_{alkyl}	alkyl chain length in the fluid state
LBP	lipoprotein binding protein
l_c	liquid-crystalline
l_d	liquid-disordered
LL32	32 amino acid long fragment (AA: 104-135) of hCAP18
LL32-4A,	derivative of LL32; amino acids 15-18 have been replaced by alanine
l_o	liquid-ordered
LP	long pass
L-Pep 19-2.5	fragment of the limulus anti-LPS-factor protein
LPS	lipopolysaccharide
L_α	lamellar phase
M	monosaccharide
MALDI-TOF MS	matrix-assisted laser-desorption-time-of-flight mass spectrometer
MD2	myeloid differentiation factor 2
Mg	magnesium
MOM	mycobacterial outer membrane
n	number of carbons in an alkyl chain
Na	sodium
Na-Ph	sodium-phosphate
NBD- DHPE	N-(7-Nitro-2,1,3-benzoxadiazole-4-yl)- dihexadecanoyl-phosphatidylethanolamine
NBD	N-7-Nitro-2,1,3-benzoxadiazole-4-yl
NK-2,	active domain of the peptide NK-lysin from pig small intestine
P	phosphate
P_c	critical packing parameter
PC	phosphatidylcholine
PE	phosphatidylethanolamine
PG	phosphatidylglycerol
pH	*potentia hydrogenii*
PL	phospholipid mixture PE:PG:DPG 81:17:2 (w/w/w)
PMB	polymyxin B
PMBN	polymyxin B nonapeptide
PS	phosphatidylserine
r	distance
R	distance donor-acceptor
R_0	Förster-distance
Rh	rhodamin B
Rh-DHPE	N-(Rhodamin B sulfonyl)-dihexadecanoyl-phosphatidylethanolamine
s_0	ground state
s_1	first excited singlet state
SAXS	small-angle X-ray scattering
SM	sphingomyelin
s_o	solid-ordered

STM	scanning tunneling microscopy
SUV	small unilamellar vesicle
TDM	trehalose dimycolate
TFA	trifluoroacetic acid
TLR-4	toll-like receptor 4
TM	main phase transition temperature
TNF-α	tumor necrosis factor-alpha
V	volume
$\tilde{\nu}$	wavenumber
V_L	Lennard-Jones potential
ε	Lennard-Jones energy
Θ	bond angle
λ	wavelengths
ν	frequency
σ	Lennard-Jones radius

1 INTRODUCTION

1.1 CONTEXT AND AIMS

Humans, like all living organisms, are a subject to evolution and therefore permanently bound to compete with a hostile environment. While the hazard of ending up mauled by wildlife has vanished since the cultural and technological rise of mankind, the threat by infectious diseases remains. Despite vast advantages in medicine, certain bacterial infections are still hard or impossible to cure. Furthermore, bacteria are able to adapt to antimicrobial substances, rendering once reliable pharmaceuticals useless. To keep pace with evolving microorganisms, biomedical research requires an understanding of the underlying mechanisms and functional principles of infection and activity of antimicrobial substances. This thesis is settled between research on membrane associated mechanisms of medical relevant infections, their reduction to simpler biophysical membrane models and investigation of interactions between these models and antimicrobial peptides (AMPs) with activity against bacterial membranes (Fig. 1.1). Results obtained by use of membrane models allowed for both, predictions about the structural properties of natural membranes and predictions about the activity of the tested peptides *in vivo*. The diseases dealt with in this thesis are human tuberculosis caused by *Mycobacterium tuberculosis* and sepsis/septic shock, related to an infection with Gram negative bacteria and immunological reactions thereupon. Tuberculosis is rare in Germany but causes two million casualties per year worldwide. To investigate the properties of the mycobacterial cell envelope and possibly identify new substances with anti-mycobacterial activity, a simplified outer membrane of the tuberculosis pathogen was reconstituted. By this, the prepared membrane models contained the particular important mycobacterial glycolipid trehalose dimycolate (TDM). This molecule is linked to mycobacterial growth and virulence, but little is known about its conformation within membranes and its interactions with AMPs. These small cationic peptides are found in almost all classes of animal live, providing relative unspecific protection against invading pathogens. AMPs attained growing attention as new drugs against infectious diseases within the last decades, as the activity of generic antibiotics increasingly suffers from bacterial resistance. Because AMPs usually function by causing permeabilization of bacterial cell membranes, membrane models are well suited for investigation of their activity. The carried out experiments with mycobacteria mimicking membranes allowed for conclusions about the architecture of the cell envelope in real mycobacteria and revealed the antimicrobial potential of certain AMPs. Results from experiments using bacteria were compared with results from the reconstituted membranes to figure out, whether the model system can mimic the natural situation.
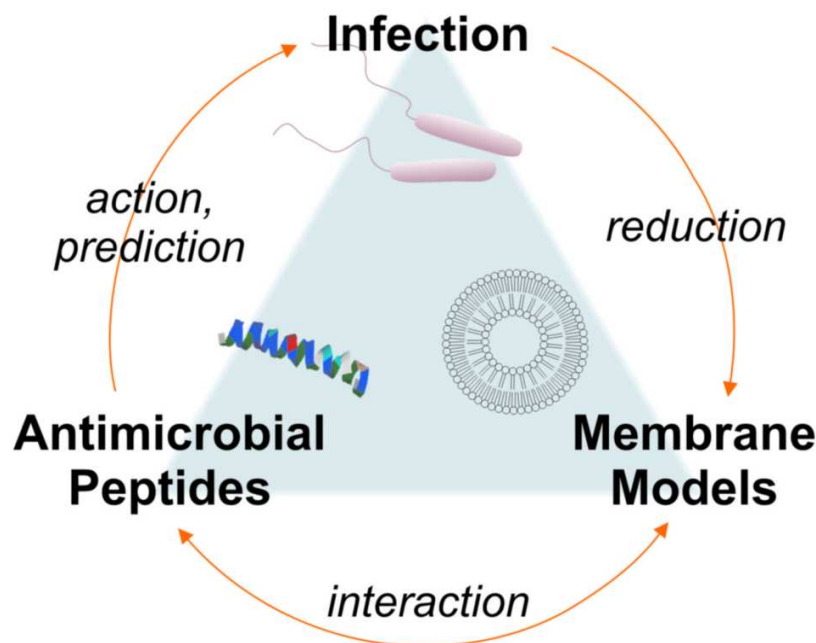
Fig. 1.1: **Schematic presentation of the general concept of this thesis.** To investigate aspects of infection, human and bacterial cell membranes are reduced to simplified membranes model. These better controllable mimics of nature are then used to study interactions with antimicrobial peptides. Obtained results allow for prediction of the peptides action on real cells.

The second medical relevant complex investigated in this thesis is Gram negative sepsis, a severe inflammatory condition of the whole body caused by a massive release of bacteria or bacterial fragments into the blood stream. As the immune system of the host reacts on the presence of bacteria with a widening of blood vessels, sepsis can be accompanied by a life threatening drop in blood pressure, known as septic shock. Sepsis, sometimes colloquially called blood poisoning, and septic shock cause about 150,000 infections in Germany per year (Engel et al., 2007). The ability of Gram negative bacteria to survive within a host is thereby connected to the asymmetric structure of their outer membrane, containing lipopolysaccharides (LPSs) in the outer leaflet and phospholipids in the inner leaflet. Besides their structural function within the bacterial cell, LPSs are also known to trigger strong immune reactions, when sensed by specific receptors on macrophages and other immune-cells. Both, the structural and the immunogenic function of LPSs can be impaired by AMPs, what makes these peptides valuable as pharmaceuticals. AMPs are suited to bind and permeabilize LPS membranes and in this way kill the bacteria, but also possess LPS-neutralizing activity. Here, a prevention of immune reactions can be archived by AMPs either by direct binding and inactivation of LPSs or by an AMP related inhibition of LPS-receptors on immune cells. Research on the prevention of sepsis dealt with eradication of

Gram negative infections by AMPs. Model membranes reflecting the natural asymmetry of the outer membrane of Gram negative bacteria were prepared and mixed with AMPs to test for permeabilization. Results contributed to a better understanding of interactions between lipids and LPSs and furthermore showed the activities of certain AMPs. For research on prevention of sepsis related septic shock, membrane models mimicking human macrophages were created. Macrophages carry LBP, CD14, TLR-4, and MD2 receptors on their surface, whose activation by LPS is the first step in an immunological cascade eventually causing septic shock. The functionality of these receptors has been reported to be connected to localization within special membrane areas, called lipid rafts. These lipid rafts were reconstituted in model membranes as domains rich in sphingomyelin and cholesterol. This setup allowed to investigate the ability of AMPs to alter the domain structure and eventually also prevent the emergence of lipid rafts and the function of CD14 receptors in real macrophages. The use of lipid raft mimicking structures provided information about the ability of the peptides to interact with eukaryotic membranes and contributed to a better understanding of the often stressed lipid raft concept.

1.2 BIOLOGICAL MEMBRANES

Biological membranes allow living cells to divide space into a defined inside and outside. The inner realm is usually filled with cytosol and can be further divided into compartments by other membranes. The outer realm is filled with interstitial fluid in tissues of multicellular organisms or consists of the media, which forms the outside environment for unicellular organisms. Cell or plasma membranes, which can be roughly described as a lipid bilayer with embedded proteins, surround all kinds of cells. According to the fluid mosaic model (Singer and Nicolson, 1972), which is further described in paragraph 1.2.3, membranes consist of a quasi two-dimensional layer, in which lipids and proteins diffuse laterally and are rather randomly distributed. Membranes do not only protect the interior from the outside but also regulate active and passive transport of vital substances into and out of the cell. Selective permeability of cell membranes allows certain molecules to pass, while transport of other molecules is hindered in one or both directions. In this way organisms are able to create and maintain cellular homeostasis, a state in which energy, charge, entropy and concentrations of certain substances differ from the surrounding. Cell membranes also contain embedded protein receptors, which are able to recognize specific molecules and transfer signals into the cell. This allows cells to react on signals from the outside and e.g. release signal molecules by themselves. Cellular signaling or communication is a cornerstone for the development of higher organisms, in which cells are not just accumulated but function as a hole. Cellular interactions also create a need to identify cells and discriminate between own and foreign cells in multicellular organisms. Therefore plasma

membranes host both, receptors to identify surrounding cells and markers to be recognized by others. Cell membranes also function as an anchor for other cellular structures like the cytoskeleton in eukaryotic cells, the extracellular matrix of animal cells or cell walls found around plant and bacterial cells. The diversity of cell membrane associated features is reflected in the variety of cell envelope compositions and membrane associated molecules (Darnell et al., 1986).

1.2.1 *PHOSPHOLIPIDS*

Different phospholipids constitute the essential part of cell membranes. Due to their amphiphilic structure, phospholipids spontaneously form lipid bilayers when embedded in water. In such a lipid bilayer the hydrophilic head groups of the phospholipids point outward towards the polar environment while the hydrophobic alkyl chains are orientated inward facing each other. With respect to their chemical structure, phospholipids can be divided into glycerol based glycerophospholipids (phosphoglycerides) (Fig. 1.2) and sphingosine based sphingolipids (Fig. 1.3). The term "phospholipids" in this thesis refers to glycerophospholipids. While eukaryotic membranes contain high rates of phosphatidylcholines (PC) (Boon and Smith, 2002) and the sphingolipid sphingomyelin (SM) (van Meer et al., 2008), phosphatidylethanolamines (PE) and phosphatidylglycerols (PG) are common lipids in membranes of Gram negative bacteria (Osborn et al., 1972). Especially bacterial cell membranes do also contain significant amounts of the diphosphatidylglycerol cardiolipin (DPG). This phospholipid with four alkyl chains is involved in regulation of the lamellar bilayer structure.
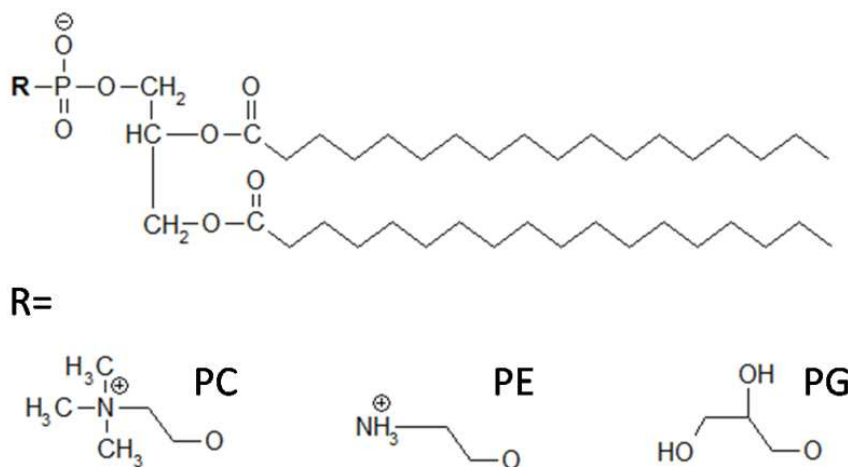
Fig. 1.2: **Structure of common glycerophospholipids.** Phospholipids consist of two hydrophobic alky chains of variable lengths and a polar head group. In all phospholipids the phosphate group carries a negative charge, while other residues can contain different charges. The structure of the head group residue determines the lipid type; phosphatidylcholine (PC), phosphatidylethanolamine (PE), phosphatidylglycerol (PG).
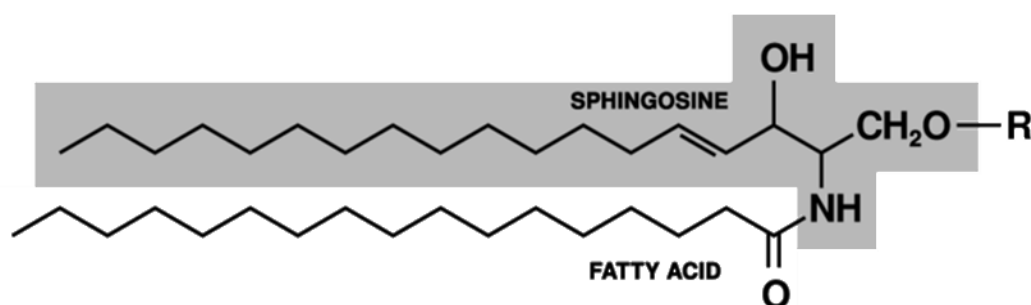
Fig. 1.3: **General structure of sphingolipids.** The lipid class is characterized by a sphingosine element, which contains a long, largely saturated alkyl chain. The second chain is of variable lengths and saturation. The polar head group residue (R) is equivalent to phospholipid head groups. For sphingomyelin (SM) R consists of the PC residue in Fig. 1.2.

1.2.2 PHASE BEHAVIOR

Lamellar phospholipid bilayers are able to exist in several phases, which are characterized by differential packing of the lipids within a lattice. Packing is mainly governed by the alkyl chains of the phospholipids, which can alternate between a linear extended conformation and a flexible kinked conformation. The chemical basis of these reorganization processes is the

shift between trans and gauche conformers within the alkyl chains of the lipids (Fig. 1.4). Changes arise from temperature dependent rotation around carbon single bonds (Marsh, 1991). At temperatures below their main phase transition temperature (T_M) lipid bilayers are in gel (solid-ordered (s_o)) phase. Here, the alkyl chains of the lipids exist in an all-trans (anti) conformation, which leads to a linear and rather inflexible orientation and allows for relative tight packing of the lipids. Lipids in gel phase membranes have therefore a low fluidity (lateral and rotational mobility) and a high degree of order (Stott et al., 2008). The term "order" in this context refers to the ordered conformation of the lipid´s alkyl chains. Above the T_M lipids are present in the liquid-crystalline phase (l_c), which is also referred to as lamellar phase (L_α) or liquid-disordered phase (l_d). In this phase also carbon chains with gauche conformation occur. These conformations produce kinks in the extended chains, whereby the tight packing of the lipids is disrupted. Spacing of the lipid head groups and lipid fluidity are increased, whereas the order of the fatty-acid chains is lowered (Sankaram and Thompson, 1990).
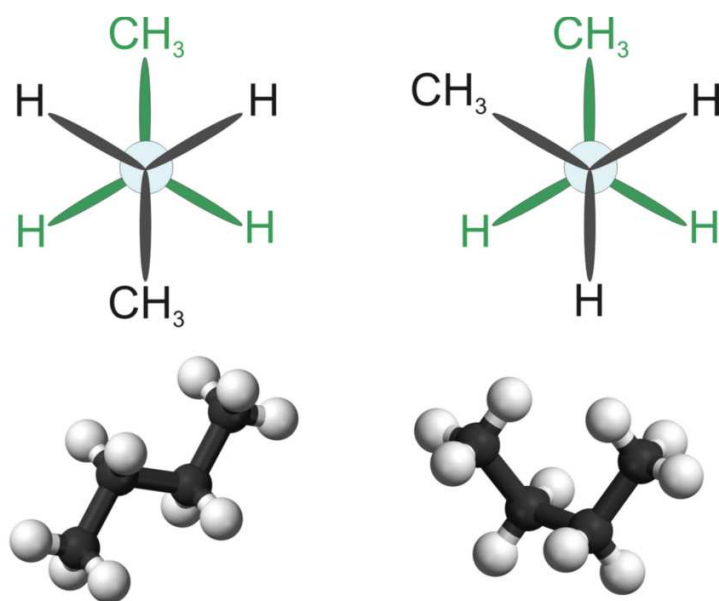
Fig. 1.4: **Trans conformation (left) and gauche conformation (right) by taking the example of butane.** The upper Newman projection shows the molecules viewed from the end of the chains. The lower ball-and-sticks models show the three-dimensional orientation. An energetically favored trans conformation leads to an extended chain with a staggered arrangement of the carbon atoms (left). At higher temperatures the formation of gauch isomers at particular C-C single bonds causes the chain to bend (right).

Besides phospholipids, human and animal cell membranes contain significant amounts of cholesterol, which contributes to the regulation of membrane permeability and fluidity (Bloch, 1991; Nielsen et al., 1999). On the one hand membrane fluidity is increased by

intercalation of cholesterol into the lipid lattice, inhibiting a tight packing of the lipids (Fig. 1.5). On the other hand the stiff cholesterol molecules limit the mobility of the alkyl chains of the lipids and promote the formation of trans isomers. By this, the degree of order is increased and the membrane is stabilized.

Fig. 1.5: **Effect of cholesterol on lipid bilayers.** Incorporation of cholesterol (red) between phospholipids (green) increases membrane fluidity by spacing of lipid head groups but also stabilizes membranes by limiting alkyl chain mobility.
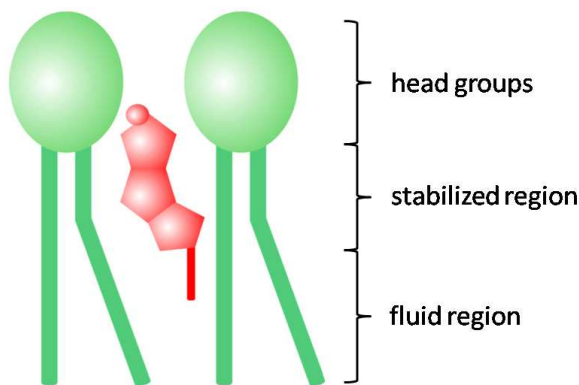
The effects of cholesterol lead to the formation of a new phase, called liquid-ordered (l_o) phase. This phase is characterized by fluidity similar to liquid-crystalline phases and enhanced order comparable to gel phases (Ipsen et al., 1987; McMullen et al., 2000). In membranes with high cholesterol content the phase transition of the lipids is broadened or abrogated. Stating from about 40 mol % cholesterol membranes are in the liquid-ordered phase irrespective of the temperature (Veatch et al., 2005). Interactions between SM and cholesterol are of special interest in cell biology and membrane biophysics, as they lead to the formation of SM-cholesterol rich domains in artificial model membranes and lipid rafts (cf. next paragraph) in natural cell membranes. Several models have been suggested to explain the clustering of cholesterol with SM: in the so called umbrella-model the head group of SM is suggested to be bent sideways by an intramolecular H-bond between the oxygen of its phosphate group and a hydroxyl group of the sphingosine element, which is missing in phospholipids. The lowered SM head group shields the cholesterol from unwanted contact with water molecules, while charged-pair coupling between the hydroxyl group of the cholesterol and the amino group of the SM head group stabilizes the system. By this, the cholesterol molecules obtain an orientation more perpendicular to the surface of the membrane and allow for tighter packing of SM and cholesterol (Aittoniemi et al., 2007). Other authors explain domain formation by H-bonds between cholesterol and the alky chains of the SM (Simons et al., 2004; Scherfeld et al., 2003; van Duyl, et al., 2003) or by hydrophobic interactions (Slotte, 1999; Holopainen et al., 2004). In all models the basis for domain formation is founded by

properties of the sphingosine element, which is present in sphingolipids but missing in other phospholipids.

1.2.3 THE FLUID MOSAIC MODEL AND MEMBRANE DOMAINS

In 1972 Singer and Nicolson developed the "fluid mosaic model" about the gross organization of lipids and proteins in biological membranes (Singer and Nicolson, 1972). This work condensed ideas and findings derived from earlier studies on the properties of erythrocyte membrane proteins (e.g. Fairbanks et. al. 1971) and proteins from various other membranes (e.g. Blasie et. al. 1969; Frye and Edidin, 1970; Cone, 1972). The "fluid mosaic model" describes membranes as structures, which are mainly governed by hydrophilic and hydrophobic interactions. Membrane lipids are grouped as a bilayer by interactions of the bulk water with the hydrophobic carbon chains and the hydrophilic head groups of the lipids. Peripheral membrane proteins are relatively soluble in aqueous buffers and are only weakly associated to the membrane, e.g. by electrostatic interactions. Integral membrane proteins are highly insoluble in aqueous buffers and are therefore partially embedded in the lipid bilayer. These proteins are thought to have an amphiphilic structure; nonpolar groups are buried in the hydrophobic middle of the lipid bilayer, while polar and ionic groups stick outward making contact with the polar solvent. While a small fraction of membrane lipids directly interacts with proteins, the main part of the phospholipids has an isotropic distribution within the fluid bilayer. Thus, membranes are thought as a virtually two dimensional solution of embedded proteins and lipids as a matrix. The randomly distributed mosaic of different lipids and proteins is in thermodynamic equilibrium and fluctuates over time, due to a relatively high lateral mobility of the molecules. The "fluid mosaic model" has remained the standard conceptualization for membrane architecture for decades, but the emergence of new findings points out some of the overgeneralizations it contains. One of the most debated topics, I would like to elaborate on, is the suggested patchiness of membranes. For reviews see *Engelman, 2005* and *Almeida et al., 2005*. Since the 1970s theoretical and experimental studies showed phase separations and formation of domains in model membranes. Separation of lipids was either into gel and liquid-crystalline phases (Shimshick and McConnell, 1973(I); Freire and Snyder, 1978) or into liquid-ordered and liquid-crystalline phases, when cholesterol was present (Shimshick and McConnell, 1973(II)). With gel phases considered to be unphysiological in cholesterol rich human and animal cell membranes, mainly the domain coexistence of liquid-ordered and liquid-crystalline domains was thought to be of particular biological interest (Ahmed et al., 1997). Evidence for phase separations in liquid membranes led to the formation of the lipid raft concept (Simons and Ikonen, 1997). Ordered domains or "rafts" rich in sphingolipids, glycolipids, cholesterol and certain proteins are thought to exist in cell membranes in the liquid-ordered phase, while the

surrounding fluid matrix is in the less ordered liquid-crystalline phase (Rietveld and Simons, 1998; Brown and London, 2000). The emergence of rafts is connected to the ability of sphingolipids to interact and cluster with cholesterol (Ramstedt and Slotte, 2002) also causing a characteristic insolubility of rafts in detergents such as Triton X-100 (Hanadaet al., 1995; Brown and London, 2000). Rafts are thought to be involved in many important biological processes in cell plasma membranes (Rajendran and Simons, 2005) and membranes of the Golgi apparatus (Gkantiragas et al., 2001) including (immune receptor) signal transduction (Field et al., 1997; Brown and London, 1998; Solomon et al., 1998; Baird et al., 1999; Kawabuchi et al., 2000; Moffett et al., 2000; Rajendran and Simons, 2005), cell shaping and development (Huwiler et al., 2000, Huttner and Zimmerberg, 2001), membrane fusion (Chamberlain et al., 2001; Lang et al., 2001), protein trafficking (Simons and Ikonen, 1997; Lafont et al., 1999; Ikonen, 2001), sorting of membrane lipids (Simons and van Meer, 1988), sorting of membrane proteins (Rodgers et al., 1994; Arreaza and Brown, 1995; Field et al., 1997; Brown and London, 1998; Moffett et al., 2000; Galbiati et al., 2001) and provision of docking sites for certain pathogens and toxins (Valeva et al., 2006).

The lipid raft concept appeared to be helpful to better explain many observations in cells but remained controversial. The identification of raft associated proteins by detergent based assays is often criticized for giving false-positive results (Lichtenberg et al., 2005), while disagreement about the existence or morphology of rafts is often due to the inability to directly observe this kind of domains *in vivo* connected to the use of possibly improper methods for indirect verification (Shaw, 2006). In addition, the cholesterol content of the outer leaflet of natural cell membranes is so high that according to biophysical models the biggest part, if not all, of the membrane surface would be in the liquid-ordered phase (Munro, 2003). By this, lipid rafts were no special compartment of the plasma membrane and would be unable to fulfill most of their suggested functions, e.g. the local increase of protein concentration by recruitment of proteins into lipid rafts. Furthermore, different experiments (e.g. Jacobson et al., 2007; Hancock, 2006) indicate a small and transient character of rafts, which contradicts with observations of stable micrometer-sized SM-cholesterol rich domains in model membranes and the idea of enduring domains necessary for the proposed biological functions. After considerable debate a consensus definition of lipid rafts (here called membrane rafts) was drawn up at the interdisciplinary Keystone Symposium on Lipid Rafts and Cell Function in 2006: *"Membrane rafts are small (10-200 nm), heterogeneous, highly dynamic, sterol- and sphingolipid-enriched domains that compartmentalize cellular processes. Small rafts can sometimes be stabilized to form larger platforms through protein-protein and protein-lipid interactions."*(Pike, 2006). This definition accounts for the transient nature of small rafts below the resolution of optical microscopy and allows also for long-lived structures, which are necessary for biological function. Model membranes exhibiting a liquid-ordered / liquid-crystalline phase separations have been reconstituted in this thesis for a general investigation of lipid phase behavior and to be able to test the effects of different antimicrobial substances on liquid-ordered domains.

1.3 GRAM NEGATIVE BACTERIA

Gram negative bacteria constitute a category of bacteria with common cell envelope architecture. The name Gram negative refers to the impossibility to stain these bacteria with crystal violet by the Gram staining protocol (Salton and Kim, 1996). The majority of Gram negative bacteria is pathogenic, including medical relevant human pathogenic species like *Legionella pneumophila*, *Pseudomonas aeruginosa*, *Proteus mirabilis*, *Salmonella typhi* and some *Escherichia coli* serotypes. Gram negative bacteria display a cell envelope characterized by an inner phospholipid membrane and an outer asymmetric membrane, with phospholipids in the inner and lipopolysaccharide (LPS) in the outer leaflet (Fig. 1.6) (Nikaido and Vaara, 1985). The properties of LPS are further explained in the following paragraph. The inner lipid membrane of Gram negative bacteria is negatively charged, due to the occurrence of anionic lipids like PG. For example the inner membrane of *Salmonella typhimurium* contains PE:PG:DPG in a ratio of 81:17:2 (w/w/w) (Osborn et al., 1972). This lipid mixture was also used for the preparation of artificial membranes in this thesis. The periplasmatic space between the inner and outer membrane contains a peptidoglycan layer and the periplasm, a gel-like fluid rich in proteins. Compared to Gram positive bacteria the peptidoglycan layer is only weakly extended. Lipoproteins connect peptidoglycan and outer membrane and stabilize the structure. Channel-like membrane proteins (porins) pervade the relative impermeable outer membrane and allow for transport of substances into the cell. The upper molecule size for transportation is 600 Da (Benz and Bauer, 1988). Reconstitution of membrane models mimicking the outer membrane of Gram negative bacteria has been carried out during this thesis. Experiments with these membrane models were intended to investigate interactions between lipids and LPSs as well as permeabilization effects of possibly antimicrobial substances.
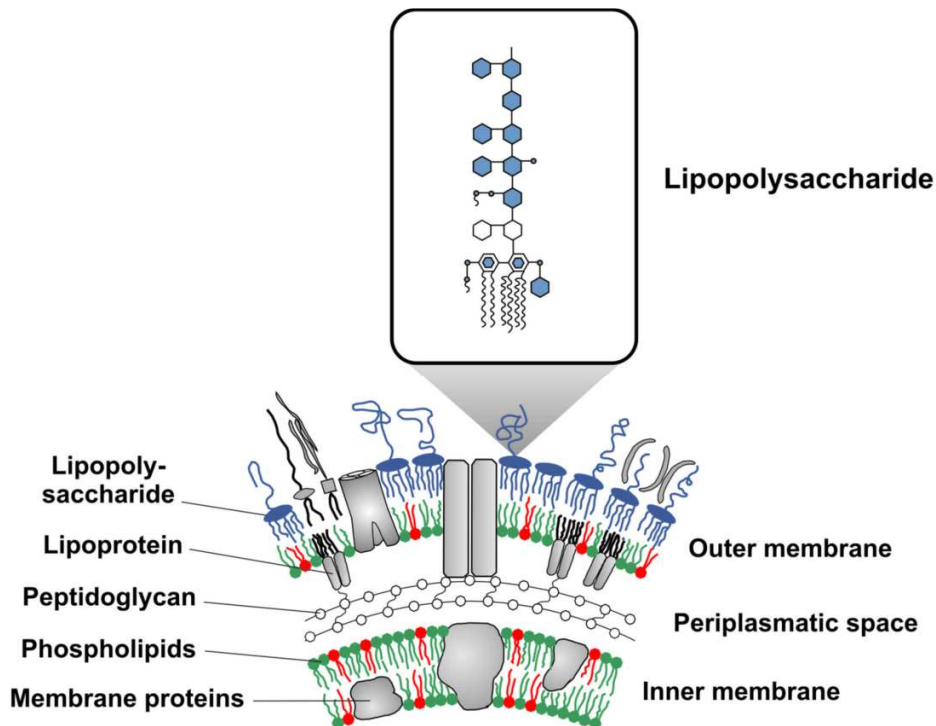
Fig. 1.6: **Structure of the Gram negative cell envelope.** An inner lipid membrane contains high rates of zwitterionic PE (green) and anionic PG (red). The outer membrane is composed of an inner lipid leaflet and an outer LPS leaflet (blue). LPSs are anchored by their lipid part in the membrane, while the sugar groups reach outward. The cell envelope is held together by a thin peptidoglycan layer between inner and outer membrane.

1.3.1 LIPOPOLYSACCHARIDES AND SEPSIS

LPSs from the outer membrane of Gram negative bacteria consist of a lipid part and a glyco (polysaccharide) part (Fig. 1.7). The lipid part, which is known as lipid A, anchors the LPS in the bacterial membrane. It consists of a glucosamine disaccharide with four attached alkyl chains. These groups usually possess 12 to 14 carbon atoms and partly carry further alkyl chains, leading to a total of 4 to 7 chains connected to the sugars (Zähringer et al., 1994). Lipid A possesses a negative charge due to its phosphate groups. In some species lipid A carries a further monosaccharide, e.g. aminorabinose, connected to one of the phosphate groups. The glyco part of LPS undergoes strong variation among different bacteria species. It consists of a variable number of diverse monosaccharides. Directly associated with lipid A are two or three units of 2-keto-3-deoxyoctonate, followed by three partly phosphorylated heptoses of variable kind and a small number of different other monosaccharides. These elements combined constitute the inner and outer core region of the LPS. The outer core is

connected to the O-specific chain, consisting of a number of repetitive elements, usually different di-, tri-, or polysaccharides (Rietschel et al., 1987; Kleinig, 1999). Branching of the chain and chemical modifications of the sugars are possible. The O-specific chain is usually present in wild type bacteria, causing a high heterogeneity in bacterial outer membranes. As an example over 160 individual structures from different *E. coli* strains are known (Raetz and Whitfield, 2002). LPSs with O-specific chains cause a smooth bacteria morphology and are therefore also named S- or smooth-form LPSs. LPSs lacking the O-specific chain cause a rather rough morphology and are termed R- or rough-form LPSs (Rittig et al., 2003). The shortest naturally occurring LPSs, named deep rough LPSs, consist only of the lipid A part with attached 2-keto-3-deoxyoctonate (Raetz, 1993) and were also used for experiments in this thesis.

P: Phosphate group; G: Glucosamine; M: Monosaccharide; Kdo: 2-Keto-3-Deoxyoctonate; Hep: Heptose
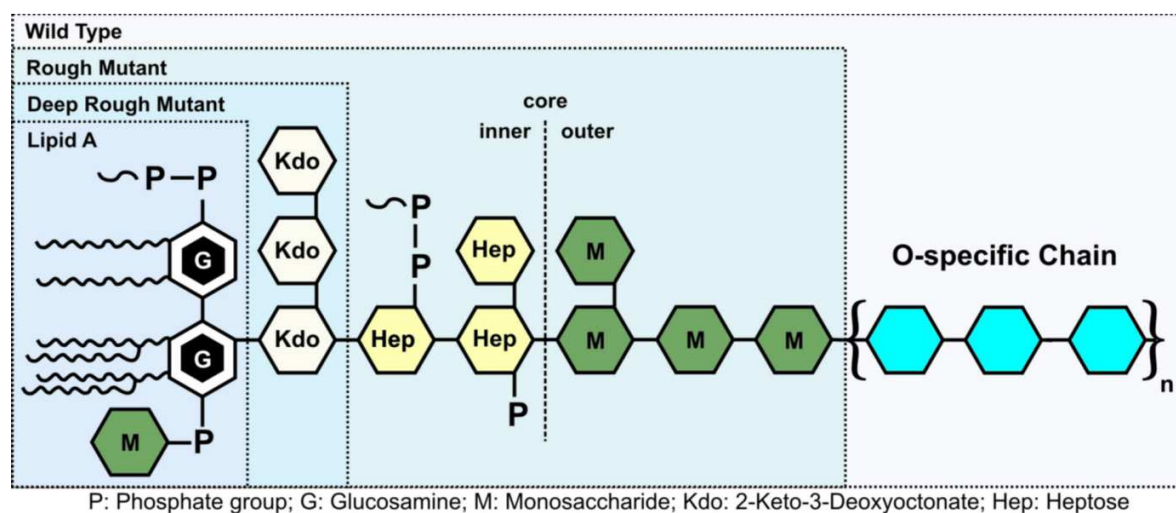
Fig. 1.7: **Generalized structure of an LPS.** The lipid part of the molecule (lipid A) is connected to a variable number of monosaccharides.

LPSs are of particular medical interest, because they contribute to the bacteria´s pathogenity by protecting them from certain antibiotics and chemicals (Salton and Kim, 1996) and also trigger strong immunologic reactions within the host. The lipid A part of LPSs, which functions as endotoxin, binds to the CD14/TLR4/MD2 receptor complex on monocytes, macrophages, dendritic cells and B-cells. Binding to these immune-cells promotes the secretion of cytokines (TNF-α, IL-1, IL-6) and nitric oxide, which trigger further cellular responses and finally cause an inflammation of the affected tissue (Rivest et al., 2000). Inflammation as a response to invading bacteria is intended to remove these bacteria from the host. To promote the access of immune-cells to infected tissues, blood flow and permeability in neighboring blood vessels are increased. In addition, a chemotactic gradient towards the infection site is established by collateral cells to attract neutrophil granulocytes (Cotran et al., 1998). To kill or damage bacteria and promote host defense mechanisms

(Hasday, 2000) the body temperature is also increased locally or system wide, eventually leading to the symptom of fever (Thompson, 2005). The downside of these mechanisms is the possible evocation of a septic shock as an overreaction to a local or generalized infection. Especially if bacteria of bacterial components like LPSs are massively released to the blood streams, an overreaction of the immune system is likely and leading to sepsis, an inflammatory state of the whole body. This process is often associated with fewer, a high respiratory rate and a widening of all blood vessels, causing a life threatening drop in blood pressure, known as septic shock (Karima et al., 1999). With respect to the described medical relevance, parts of this thesis deal with the use of LPS in model membranes. Research is intended to create a deeper insight into the role of LPS in Gram negative bacteria and to test different AMPs for their potential to permeabilize LPS containing membranes. The model derived data allow for identification of AMPs also able to kill real bacteria and possibly function as new pharmaceuticals. Besides a killing of Gram negative bacteria by AMPs, also the neutralization of LPS by AMPs was investigated. Neutralization is crucial, as LPSs are still immunologically active even after killing of the bacteria and are often released from damaged bacterial membranes. An ideal AMP would therefore be able to kill Gram negative bacteria and additionally neutralize LPSs. While a neutralization is generally also possible by direct interactions between AMPs and LPSs, this thesis focuses on an indirect mechanism based on the CD14 receptor complex. This LPS recognition receptor is probably only functional, when incorporated into lipid rafts (Schmitz and Orsó, 2002), allowing to speculate about a silencing of the receptor and a possible prevention of septic shock by acting on the lipid raft structure. To investigate this possibility, lipid raft mimics in model membranes were created and mixed with AMPs.

1.4 MYCOBACTERIA AND TUBERCULOSIS

Mycobacteria are a bacterial genus sharing a unique cell envelope architecture. The taxon includes pathogens like *Mycobacterium leprae* or *Mycobacterium tuberculosis (M. tuberculosis)*, from which the latter causes tuberculosis in humans, killing about 2 million people per year worldwide (Glickman and Jacobs, 2001). *M. tuberculosis* is present in humans at least since antiquity and was identified and described in 1882 by Robert Koch. Despite the development of effective antibiotics in the 1950s and 1960s, in 2007 there were an estimated 13.7 million active tuberculosis cases, 9.3 million new cases, and 1.8 million deaths (World Health Organization, 2009). Tuberculosis in humans usually attacks the lungs, leading to symptoms like chronic cough, coughing up blood, fever, weight loss, night sweats and overall exhaustion. The active disease is easily communicable by droplet infection, leading initially to an asymptomatic latent infection, which is present in about one third of

the world´s population (World Health Organization, 2010). In about 10% of the latent cases the disease develops into the active form, causing about 50% mortality in untreated patients. Reasons for the ongoing threat by tuberculosis are manifold. The complex, costly and long-winded antibiotic therapy of patients overextends the possibilities of public health in poor countries, while the rise of HIV-associated and multi drug-resistant strains impairs the situation. Extinction of the disease or at least a profound protection by vaccination is currently impossible, due to the limitations of the available Bacille Calmette-Guerin (BCG) vaccination. Furthermore, the lack of a quick and reliable diagnosis for tuberculosis promotes its spread. For a review on the topic see *Hanekom et al., 2010. M. tuberculosis* shows like other mycobacteria resistance to antimicrobial agents, active against other Gram negative or positive bacteria (Johnson et al., 2006). The difficulties in removing pathogenic mycobacteria from the host organism by the immune system or by antibiotics are partially linked to the unusual structure of the mycobacterial cell envelope. Although the exact setup is unknown, the suggested models for the envelope agree in the existence of an inner phospholipid membrane rich in PE and PG connected to an outer cell wall (Fig. 1.8) (Tonge, 2000). The mycobacterial cell wall can be subdivided into an inner peptidoglycan layer and an outer membrane. This characteristic mycobacterial outer membrane (MOM) is especially hydrophobic, waxy, rich in mycolic acids and trehalose dimycolate (TDM) and does also contain phospholipids (Brennan and Nikaido, 1995). The inner peptidoglycan layer and the MOM are held together by a network of the polysaccharide arabinogalactan, which is covalently bound to the peptidoglycan on one end and to mycolic acids of the MOM on the other (Brennan and Nikaido, 1995). The set up of the cell wall provides a high degree of impermeability to antibiotic agents (Brennan and Nikaido, 1995; Jarlier and Nikaido, 1994; Nikaido, 1994), protection against oxidative radicals (Yuan et al., 1995) and desiccation resistance (Harland et al., 2008) as well as biochemical possibilities to manipulate the host immune system. Remarkably *M. tuberculosis* infects primarily macrophages, a cell type which usually kills pathogenic microorganisms. The mode of entry and persistence within macrophages is still under debate, but some of the suggested mechanisms are also based on properties of components of the mycobacterial cell wall (Meena and Rajni, 2010). The given examples demonstrate the importance of research on tuberculosis and especially the role of the MOM for mycobacterial pathogenity. Investigations in this thesis were especially focused on the role of one important component of the MOM, namely the glycolipid trehalose dimycolate (TDM). The molecule is described in detail in the next paragraph.
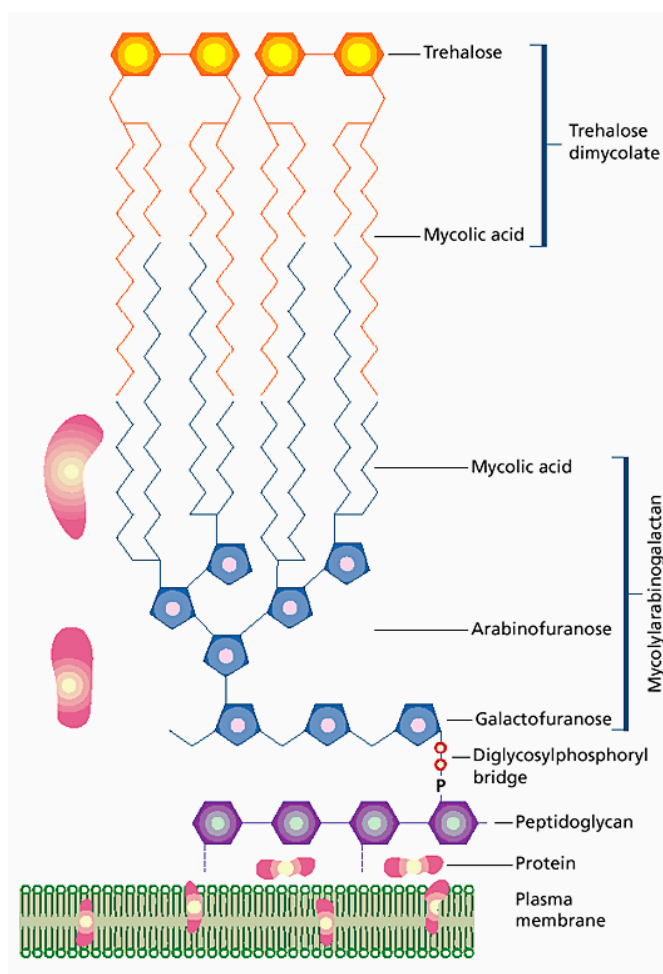
Fig. 1.8: **Simplified structure of the mycobacterial cell envelope** (image after Tonge, 2000). On top of a lipid plasma membrane the envelope consists of an inner peptidoglycan layer and an outer hydrophobic mycolate layer. These two layers are held together by the polysaccharide arabinogalactan and by lipoarabinomannans. Trehalose dimycolate is mostly located in the outer leaflet of the outer layer, where it contributes to hydrophobicity and mechanical stability (n.b.: the structure shown above is not universally accepted and further debated on in the Discussion section.).

1.4.1 TREHALOSE DIMYCOLATE

Trehalose dimycolate (TDM), which is also known as cord factor, consists of a trehalose sugar connected to four alky chains via two mycolic acid groups (Fig. 1.9) (Noll et al., 1956). The molecule is found in the outer layer of the MOM. There is a multitude of evidence for the connection between mycobacterial virulence and TDM (Hunter et al., 2006(I)), including but not limited to the findings that TDM is abundant in virulent *M. tuberculosis* (Bloch, 1950; Hunter et al., 2006(II)), large amounts of TDM exist on the

surface of virulent but not on avirulent mycobacteria (Bloch, 1955), TDM is the most toxic lipid of *M. tuberculosis* and causes the induction of granulomas (a special type of inflammation) (Syed and Hunter, 1997; Behling et al., 1993), TDM enhances acute and chronic tuberculosis in mice (Bloch and Noll, 1955), TDM causes virulent mycobacteria to grow in serpentine cords (Bloch,1955; Hunter et al., 2006(II)), TDM removal from the *M. tuberculosis* surface promotes killing of the pathogen in macrophages and mice (Indrigo et al., 2003; Silva et al., 1985; Lima et al., 2001), reduced ability for TDM production correlates with reduced *M. tuberculosis* virulence (Armitige et al., 2000) and alterations in TDM mycolic acids influence *M. tuberculosis* virulence (Rao et al., 2005).
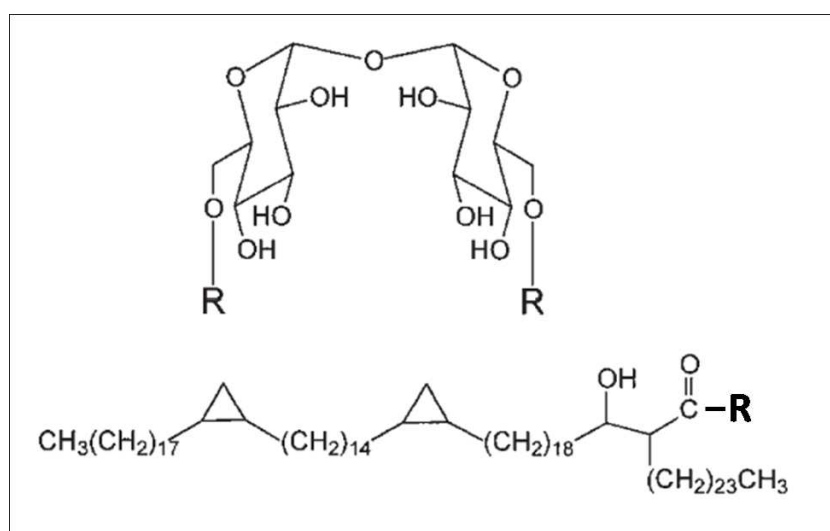

Fig. 1.9: **Chemical structure of TDM.** The upper structure shows a trehalose sugar, which forms the head group of TDM. Connected to it are two mycolic acids with two alkyl chains each. The two longer of these alkyl chains are known as meromycolic chains, while the other are termed short chains. TDM alkyl chains sometimes contain one of more cyclopropane rings (image after Tonge, 2000; altered).

In contrast to the extensively investigated immunological effects of TDM, the underlying conformation and physical state of the molecule in the MOM are not completely known. This might be due to the lack of a widely accepted model of the mycobacterial cell wall as well as to the inconstancy of biological TDM conformations, of which at least three types are suggested; the immunological properties of TDM are believed to be based partly on excess TDM on the surface of the mycobacterial cell wall (Hunter et al., 2006(I)), which is suggested to exists primarily as TDM micelles or small aggregates (Retzinger et al., 1981; Retzinger et al., 1982; Youmans, 1979(I)), whereas the TDM toxicity is linked to a second conformation of free monolayers (Retzinger et al., 1982; Youmans 1979(II); Goren and Brennan, 1979). The third conformation of TDM is found in the outer leaflet of the MOM, where membrane bound TDM is associated with other elements of the outer membrane, e.g.

phospholipids, glycolipids, mycolic acids and membrane proteins (cf. previous paragraph). In this thesis artificial membrane models of the MOM were created to investigate the biophysical features of membrane-bound TDM. Besides its structural properties, also interactions with antimicrobial substances were of particular interest to illuminate the role of TDM in drug resistance and possibly glean out new anti-mycobacterial drugs.

1.5 MEMBRANE MODELS

Research in the field of natural sciences and also this work are often connected with a reductionist view on things. Reductionism is the idea, that systems are completely determined by their parts and interactions of them. It states that complex phenomena can be understood by reduction to underlying simpler or more fundamental aspects (Nagel, 1961). Reductionism can be thought as a general philosophical framework or can be applied to certain scopes only. The generalized view of reductionism is often criticized for its rejection of emergent phenomena, which are impossible to be explained by description of the involved parts. However, if carefully applied to isolated aspects of science, reductionism can contribute to gain a deeper insight into complex phenomena. In an attempt to understand the complexity of biological membranes our biophysical approach reduces them to the fundamental lipid bilayer and eventually a few different species of biological molecules. This resulting model membrane, yet simple enough to be controlled and described, is meant to reflect the properties of naturally occurring membranes. Results obtained using the membrane model should be transferable to certain extends to the *in vivo* situation. Therefore, the use of models is to walk a fine line between too simple models with low biological relevance and to complex models hard to understand and handle. A holistic alternative to reductionism is claimed by the newly emerging field of systems biology, trying to describe biological organisms as a whole (Noble, 2006; Kitano, 2002) but not having caused a paradigm shift in biosciences up to now. In this thesis membrane models were not only set up as simple lipid bilayers made of one lipid species but were further adapted to their biological origins. Models of eukaryotic membranes contained characteristic lipids like PC and SM as well as cholesterol, allowing formation of SM-cholesterol rich domains. Models for the MOM contained the bacterial lipids PE and PG as well as the mycobacterial glycolipid TDM. Models for the outer membrane of Gram negative bacteria contained PE, PG, DPG and characteristic LPSs. These models also resembled the natural asymmetry of Gram negative outer membranes with LPS exclusively in the outer membrane leaflet and phospholipids in the inner. Besides mimicking natural membrane architecture, also environmental parameters like temperature, pH value and concentrations of salt ions were intended to approximate *in vivo* conditions whenever possible. In this thesis, different membrane models were set up as solid supported bilayers and multilayers for atomic force

microscopy (AFM) measurements, as free standing mono- or bilayers for conductivity measurements and as vesicles of different sizes for fluorescence spectroscopy and microscopy (Fig. 1.10). These membrane systems are explicitly described in the Materials and Methods section and further debated on in the Discussion section. The individual properties and limitations of the different membrane systems vary and combinations are necessary to obtain a maximal amount of information. For a review on membrane systems and their applications see *Chan and Boxer, 2007*.
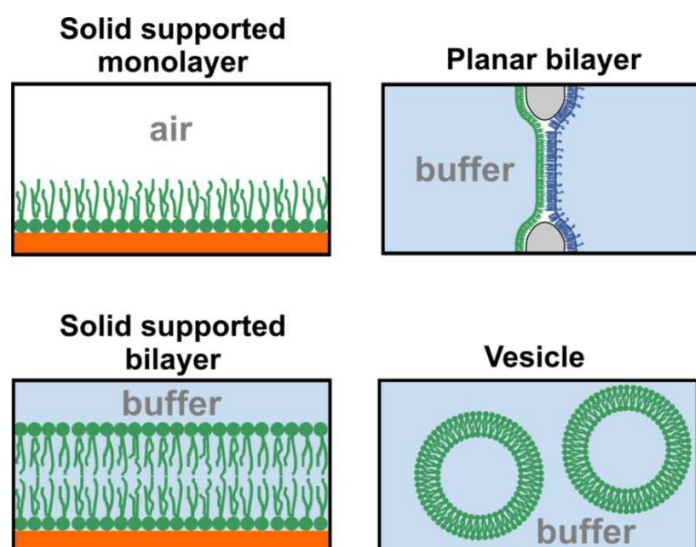

Fig. 1.10: **Different membrane systems used in biophysical research.** Planar mono- or bilayers on a solid support are suited for topography scans and force spectroscopic measurement by AFM. Unsupported planar bilayers allow for measurement of membrane conductivity and can be observed by fluorescence microscopy. Vesicles of different sizes feature a spherical bilayer with a more natural membrane curvature. While small vesicles are suited for fluorescence and IR spectroscopic experiments, larger vesicles allow for direct observation by optical microscopy.

1.6 ANTIMICROBIAL PEPTIDES AND THE INNATE IMMUNE SYSTEM

Antimicrobial peptides (AMPs) are components of the innate immune system, acting directly on invading pathogenic microorganisms. Unlike the highly specific adaptive immune system, the innate immune system does not create long-lasting immunity (Alberts et al., 2002). Cells and mechanisms of this nonadaptive system provide immediate and unspecific protection for the host. Innate immunity is the dominant defense strategy in evolutionary older organisms like protozoa, plants, fungi and insects (Janeway et al., 2001). In vertebrates, including humans, the innate immune system functions as a first line of defense,

bridging the time span till the slower adaptive immune system is able to react. More recent studies also indicate that the innate immune system activates the dominant adaptive immunity (Gudmundsson and Agerberth, 1999; Hancock and Scott, 2000; Yang et al., 2001). Unlike the highly specific antibodies of the adaptive immune system AMPs show a broad range of activity against bacteria, fungi, viruses and protozoa (Boman, 1995). The first AMP was isolated from the pupae of the *Cecropia* moth in the early 1980s (Steiner et al., 1981). Since then several hundred different AMPs have been identified in all classes of plant and animal life. Medical use of these simple to synthesize peptides in natural or artificially modified forms gained growing attention as alternatives to classic antibiotics. In humans several histatins, lactoferricin, six α-defensins, four β-defensins, and the human cationic antimicrobial peptide hCAP18 have been identified (Cederlund, 2011). Although these peptides are structurally diverse, they share common properties like a positive net charge and a size of 12-50 amino acid (AA) residues. Many AMPs possess an amphiphilic character, which means that hydrophobic and charged residues form spatially separated regions within the molecule (Zasloff, 2002). The chemical structure of the antimicrobial peptide LL32, which was also used for experiments in this study, was modeled to demonstrate this amphiphilic character (Fig. 1.11). For further information on LL32 see Materials and Methods section.
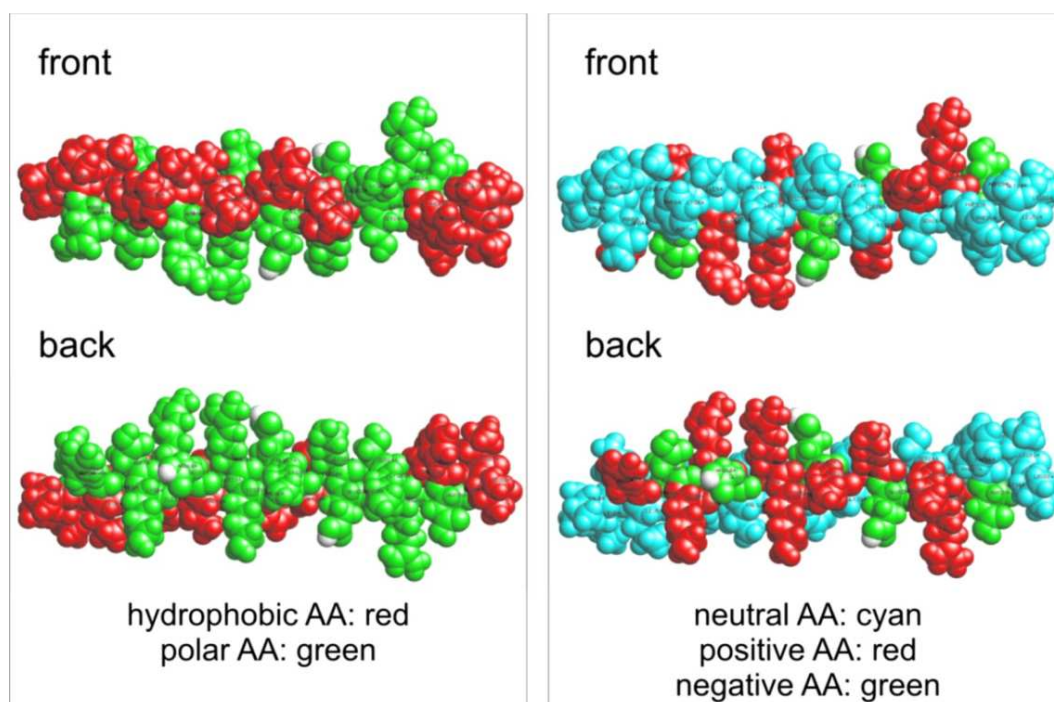
Fig. 1.11: **Amphiphilic structure of AMPs by the example of LL32.** The structure of the α-helical peptide was modeled using the molecule editors/visualizers Avogadro 1.0.1 (http://avogadro.openmolecules.net) and RasMol 2.7.5 (www.rasmol.org). Left panel: hydrophobic amino acids (red) are located on one side along the helix and polar amino acids (green) along the other. Right panel: Neutral amino acids (cyan) constitute a region mostly congruent with the hydrophobic amino acids while charged (polar) amino acids (red, green) are located at the opposite side of the molecule. The N-terminal end of the LL32 helix is pointed to the left.

In contrast to the classic opinion, AMPs do not only kill bacteria by disruption of bacterial membranes, but are also able to act inside the bacterial cell, e.g. by blocking of nucleic acid, cell wall or peptide synthesis. For a review on AMPs and possible modes of action against microorganism, see *Zasloff, 2002*; *Brogden, 2005*. Investigations in this thesis are focused on AMPs, which act on bacterial membranes. For most, if not all, AMPs the initial contact with microorganisms is electrostatic, based on interactions of the cationic peptides with negatively charged bacterial membranes. For interactions with outer membranes of Gram negative bacteria, a self promoted uptake of certain AMPs into the membrane has been suggested (Hancock, 1997). Here, AMPs initially break the electrostatic cross linking of neighboring LPSs by divalent cations (Ca^{2+} or Mg^{2+}), subsequently triggering a destabilization of the membrane and a promoted uptake of further AMP molecules. For the binding and subsequent disruption of the membrane several models exist. These can be basically divided in two groups;

- The **carpet-like model** and similar models, in which AMP molecules bind more parallel to the surface of the target membrane forming a layer or carpet. AMPs are scattered across the membrane causing mechanical stress and at higher concentrations finally subvert the bilayer by formation of micelles or rather unordered pores (Brogden, 2005).

- The **barrel-stave** and **toroidal-pore model**, in which the peptides are incorporated perpendicular to the membrane surface (trans-membrane) already at low concentrations and cause the formation of defined trans-membrane pores (Neville et al., 2006).

Besides the induction of defined or unordered lesions in membranes, also the fusion or aggregation of bacterial membranes has been suggested as a mode of action for certain AMPs (Daugelavicius et al., 2000; Cajal et al., 1996). In this thesis the activities of several AMPs and the antibiotic polymyxin B (PMB) were investigated by means of membrane models mimicking the cell membrane of macrophages, bacterial lipid membranes, the outer membrane of Gram negative bacteria and the outer membrane of mycobacteria.

2 MATERIALS AND METHODS

2.1 LIPIDS AND STEROLS

For the preparation of vesicles, planar bilayers and monolayers the following lipids and sterols were used: L-α-phosphatidylcholine from chicken egg (**egg PC**); 1, 2-dioleoyl-sn-glycero-3-phosphocholine (**DOPC**); *E. coli* L-α-phosphatidylethanolamine (**PE**); *E. coli* L-α-phosphatidylglycerol (**PG**); *E. coli* cardiolipin (diphosphatidylglycerol, **DPG**); Octadecanoyl sphingomyelin from porcine brain (**bSM**) and cholesterol from ovine wool (**chol**) (all purchased from Avanti Polar Lipids, Alabaster, AL, USA)

The fatty acid distributions of the used natural lipid mixtures can be found on the homepage of the manufacturer: http://avantilipids.com.

The following fluorescent lipid conjugates were used: N-(Rhodamine B sulfonyl)-dihexadecanoyl-phosphatidylethanolamine (**Rh-DHPE**); N-(7-Nitro-2,1,3-benzoxadiazole-4-yl)-dihexadecanoyl-phosphatidylethanolamine (**NBD-DHPE**); 2-(4,4-difluoro-5,7-dimethyl-4-bora-3a,4a-diaza-s-indacene-3-pentanoyl)-1-hexadecanoyl-sn-glycero-3-phosphocholine (**BODIPY FL-PC**) and Fluoresceinisothiocyanate-phosphadidyl-enthanolamine (**FITC-PE**) (all obtained from Molecular Probes, Eugene, OR, USA). In the used samples the fluorophors rhodamine B (**Rh**), 7-Nitro-2,1,3-benzoxadiazole-4-yl (**NBD**), 4,4-difluoro-5,7-dimethyl-4-bora-3a,4a-diaza-s-indacene-3-pentanoyl (**BODIPY**) and fluorescein-isothiocyanate (**FTIC**) were attached to the lipid head groups.

Lyophilized lipids, sterols and fluorescent lipids were solved in chloroform (Merck KGAA, Darmstadt, Germany) prior to use. Samples solved in chloroform were stored at about -20 °C.

2.2 LIPOPOLYSACCHARIDES

To reconstitute bacteria mimicking membranes, natural salt forms of two types of deep rough mutant LPSs (cf. Introduction) were used;

- LPS R45 from *Proteus mirabilis* strain R45

- LPS WBB01 from *Escherichia coli* strain WBB01

Fig. 2.1 shows the chemical structures of the two LPSs. Molecules were extracted from bacteria cultures by the phenol/chloroform/petroleum ether method (Galanos et al., 1969), purified, and lyophilized afterwards. Furthermore, LPS R45 was also used in a fluorescent form, labeled with the fluorophor FITC. Labeling was done in our lab by amide coupling of the fluorophor to one of the LPS arabinoses. LPSs were solved in chloroform:methanol 9:1 (v/v) prior to use. To fully solve the LPS R45, extensive shaking and heating of the sample up to 80 °C were necessary. Samples solved in chloroform or methanol were stored at about -20 °C.
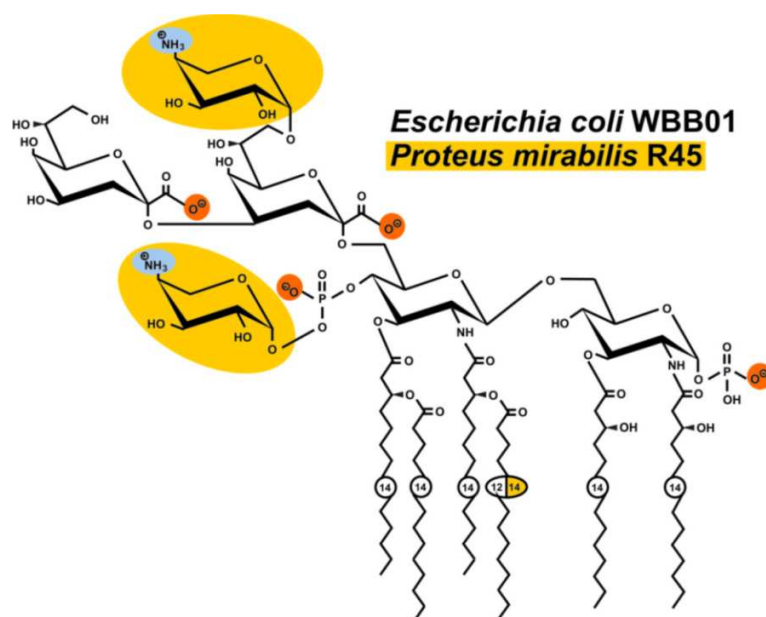
Fig. 2.1 **Structure of the LPSs used in this thesis.** The yellow shaded elements are only present in LPS R45. Positively charged groups are shaded blue, negatively charged groups red.

2.3 TREHALOSE DIMYCOLATE

To investigate the properties of mycobacterial membranes, reconstituted membrane mimics with incorporated TDM (cf. Introduction) were used. The mycobacterial glycolipid TDM descended from *M. tuberculosis*. TDM was extracted from bacterial cultures by Ulrich Schaible at the London School of Hygiene and Tropical Medicine. For details on the extraction and purification protocol see *Fischer et al., 2001*. TDM samples were stored as lyophilized powder at 4 °C and solved in chloroform prior to use. Mass spectrometric

analysis of the provided TDM was done by Buko Lindner at the Research Center Borstel using a matrix-assisted laser-desorption-time-of-flight mass spectrometer (MALDI-TOF MS, Bruker GmbH, Bremen, Germany). Results showed that TDM molecules in the sample differed in their molecular mass due to different alkyl chain length. An average molecular mass of 2749 g/mol was calculated from the TDM mass spectra (data not shown). For practical reasons TDM concentrations were, however, mostly given in mg per ml and TDM rates in weight percent. For the chemical structure of TDM see Fig. 1.9 in the Introduction section.

2.4 PEPTIDES

Peptides with potential activity against microorganisms were investigated in this work. These peptides were abbreviated "AMPs" for antimicrobial peptides, although not all peptides belonged to the group of naturally occurring antimicrobial peptides as an element of the innate immune system (cf. Introduction). The peptides are further described below:

- **LL32**, a 32 amino acid long fragment (AA: 104-135) of the 18 kDa human cationic antimicrobial peptide (hCAP18,); member of the α-helical cathelicidin peptide family. Sequence: LLGDFFRKSKEKIGKEFKRIVQRIKDFLRNLV

- **LL32-4A**, a synthetic derivative of LL32; amino acids 15-18 have been replaced by alanine, which is known to stabilize α-helices (Rohl et al., 1999). Sequence: LLGDFFRKSKEKIGAA AARIVQRIKDFLRNLV

- **hBD-3-l**, a synthetic derivative of human-β-defensin 3; while the natural folded form possesses 3 disulfide bonds, this molecule is linear due to elimination of the bonds by amino acid replacement (exchange of cysteins by serins); member of the defensin peptide family. Sequence: GIINTLQKYYSRVRGGRSAVLSSLPKEEQIGKSSTRGR KSSRRKK

- **L-Pep 19-2.5**, fragment of the limulus anti-LPS-factor protein; further modified by amino acid replacements. Sequence: GCKKYRRFRWKFKGKFWFWG (patent pending by Klaus Brandenburg, Research Center Borstel)

- **NK-2**, active domain of the peptide NK-lysin from pig small intestine. Sequence: KILRGVCKKIMRTFL RRISKDILTGKK

- **Polymyxin B (PMB)** and **Polymyxin B nonapeptide (PMBN)**, cyclic peptide-antibiotics produced by *Bacillus polymyxa*. Structure and further information are given by *Vaara, 1992*.

The peptides LL32, LL32-4A, hBD-3-l, L-Pep and NK-2 were obtained as lyophilized powder from Rainer Bartels (Research Center Borstel). Fluorescent derivatives of these substances were also created by Rainer Bartels by N-terminal addition of the fluorophors NBD or Rh. Peptides were synthesized by the solid-phase peptide synthesis technique (Coin et al., 2007) on an automatic peptide synthesizer (model 433 A, Applied Biosystems, Carlsbad, CA, USA). Reversed-phase HPLC was used to purify the peptides. 95 % purity was confirmed by mass spectrometry (Buko Lindner, Research Center Borstel using a MALDI-TOF MS, Bruker GmbH, Bremen, Germany). PMB and its nonapeptide (PMBN) were commercially available from Sigma Aldrich (Deisenhofen, Germany). Stock solutions of all substances were prepared in aqueous 0.01 % trifluoroacetic acid (TFA) (Riedel-de Haën, Seelze, Germany) solutions, which had a stabilizing effect on the peptides.

2.5 BUFFERS AND SOLUTIONS

When possible, experiments were carried out in buffer solutions to obtain *in vivo* like conditions. All buffers were prepared with purified water (0.055 µS/cm at 25 °C; Milli-Q Advantage A10, Millipore, Billerica, MA, USA). The standard buffer, which was used for most experiments, was 100 mM KCl (Sigma Aldrich, Deisenhofen, Germany), 5 mM Hepes (4-(2-hydroxyethyl)-1-piperazineethanesulfonic acid) (Merck, Darmstadt, Germany) buffer. A pH of 7 was adjusted with KOH (Merck, Darmstadt, Germany). For some experiments (e.g. with free standing bilayers) 100 mM KCl, 5 mM Hepes, 5 mM $MgCl_2$ (Merck, Darmstadt, Germany) (pH 7) was used, because preparations in $MgCl_2$ containing buffer provided more stable bilayers. GUVs could not be prepared in buffers with high salt concentrations and were therefore prepared either in purified water or in 10 mM sodium-phosphate (Na-Ph)-buffer at pH 7.4. Na-Ph-buffer was prepared from Na_2HPO_4 and NaH_2PO_4 (both Merck, Darmstadt, Germany). Buffer capacity was between pH 5 und 8. Figure legends in the Results section indicate which buffer was used for the respective experiments.

2.6 ELECTROFORMATION OF GUVs

Giant unilamellar vesicles (GUVs) were used as cell-sized membrane mimics, to investigate peptide membrane interactions and phase separation in membranes. Due to their size observation with an optical microscope was possible. Because the preparation of GUVs is

less straight-forward than the preparation of small unilamellar vesicles (SUVs), the metrology is described in detail. GUVs were prepared by a method called electroformation (Angelova and Dimitrov, 1986). Since this method was introduced over 20 years ago, it has become one of the most sophisticated tools for the preparation of GUVs. Although many different electroformation protocols have been suggested within the last decades, they were mostly based on a common principle: dried lipid multilayers are rehydrated in purified water or buffer, while an alternating current (AC) field is applied. The AC field induces a weak periodic motion of the medium facilitating the detachment of the lamellar lipid bilayers. Hydrated bilayers form mushroom-like structures and finally GUVs come into being (Fig. 2.2). Electrostatic interactions between the electric field and charged groups within the lipids as well as redistribution of counter-ions contribute to the process of electroformation (Dimitrov and Angelova, 1988).
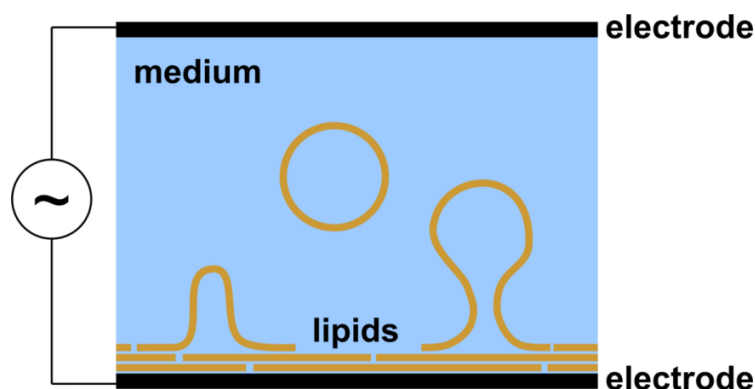

Fig. 2.2: **GUVs pinch off from stratified bilayers on top of an electrode during electroformation.** Lipids are dried onto one or both electrodes and rehydrated with water or buffer. An alternating (sinus) electrical field promotes the formation of mushroom-like structures and finally GUVs.

Own preparations using electroformation followed two different protocols, which are referred to as protocol (i) and (ii) in this work. Both protocols (i) and (ii) provided GUVs with diameters between 1-80 µm. While protocol (i) was well suited for the preparation of high GUV concentrations in purified water, preparations of GUVs in buffer followed protocol (ii). The advantages and disadvantages of the two protocols are further described in the Results section. Figure legends in the Results section also indicate, which of the protocols was used for the respective experiments.

Protocol (i) was derived from *Veatch, 2007* and slightly modified: phospholipids and fluorophors dissolved in chloroform were adjusted in the desired mixture and a concentration of 1 mg/ml was set. Fluorescently-labeled lipids were usually used in a molar ratio between 1:100 and 1:500 (labeled lipid / total lipid) [n.b. in this thesis ratios without any further descriptions refer to molar ratios]. The figure legends in the Results section

indicate the respective fluorophors and ratios used in the experiments. 100 µl of the 1 mg/ml lipid solution were placed on indium tin oxide (ITO) coated glass slides (PGO, Iserlohn, Germany) with a sheet resistance of <20 Ohm (sometimes also referred to as Ohm/sq). The ITO coating functioned as an electrical conductor, by which the slides were able to work as electrodes in the later electroformation process. The organic solvent was evaporated by heating up the sample, while the lipids were spread out to form thin films on the slides. Due to hydrophobic interactions the lipids formed piles of stratified bilayers on the surface of the slide. Last traces of solvent were removed by placing the sample in a vacuum chamber for about one hour. To setup an incubation chamber (Fig. 2.3), a rectangular silicone frame was created by hardening of liquid silicone (Sylgard 184 Silicone, Dow Corning, Midland, MI, USA) and used as a 5 mm spacer between the ITO slides. The so assembled chamber was filled with about 500 µl of purified water using a syringe and penetrating the silicone frame with a drain tube. Care was taken to remove all air bubbles from the chamber. Immediately after the chamber was filled with liquid, a 10 Hz, 1.5 V AC-field (sinus) was applied to the ITO electrodes using a function generator (Voltcraft 7202, Conrad Electronic SE, Hirschau, Germany). The chamber was incubated for 5 hours at about 55 °C and was allowed to cool down to room temperature slowly.
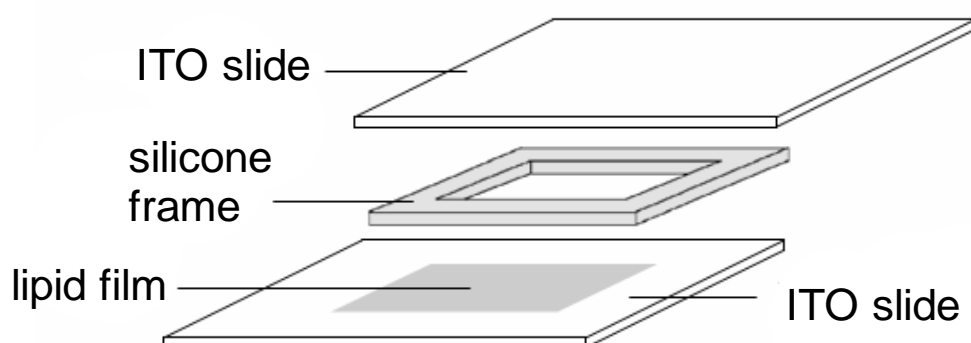
Fig. 2.3: Setup of the incubation chamber used for electroformation of GUVs in protocol (i).
Two ITO coated glass slides and a silicone frame formed a fluid filled cavity, in which the electroformation of GUVs from planar lipid films occurred.

The second protocol (ii) was derived from *Pott et al., 2008* and was further modified. Desired mixtures of chloroform-solved lipids and fluorophors were adjusted to a concentration of 1 mg/ml. 30 µl of this solution were dried onto two pieces of platinum wire (lengths 10 cm, diameter 0.75 mm) (Advent Research Materials, Oxford, GB) by putting small droplets on the wire and drying them under a nitrogen stream. When GUVs with incorporated TDM or LPS needed to be prepared, these molecules were mixed with the lipids in chloroform prior to application to the platinum wire. The wires were used as

electrodes instead of ITO coated slides and were placed in a 1 ml disposable syringe, by which a spacing of 2 mm was adjusted between each other using a plastic spacer. The syringe was filled up with about 800 µl of purified water or 10 mM Na-Ph-buffer and was sealed. Now, a 500 Hz AC-field (sinus) was applied by a function generator (Voltcraft 7202, Conrad Electronic SE, Hirschau, Germany). During electroformation the electrical tension was increased in three steps; 70 mV for 5 minutes followed by 626 mV for 20 minutes and 1.74 V for 90 minutes. The sample was tempered at about 55 °C during electroformation and was allowed to cool down slowly.

GUVs prepared by both protocols were best used directly after the sample had cooled down, but could also be stored over night at room temperature.

2.7   PREPARATION OF SMALL UNILAMELLAR VESICLES

Small unilamellar vesicles (SUVs) with a diameter less than 1 µm were used as a membrane system in fluorescence spectroscopic experiments. SUVs were also needed for the preparation of solid supported bilayers by spreading of vesicles. SUVs were prepared as follows: lipids, LPSs or TDM and eventually fluorophors were solved in chloroform or chloroform:methanol 9:1 (v/v) and adjusted to the desired ratios. A certain volume (often 100 µl) of this solution with a total lipid concentration of 1 mg/ml was placed in a 1.5 ml glass vial and dried at about 50 °C under a nitrogen stream until no more solvent was visible. The sample was then dried for a few more minutes to remove further traces of the solvent. Afterwards the dried lipids were rehydrated in 1000 µl buffer and sonicated (Sonifier Cell Disruptor B15, Branson Ultrasonics Corporation, Danbury, CT, USA) for two minutes. To promote the adjustment of phase equilibrium within the vesicles, the solution was cooled down to about 5 °C and heated up to 50 °C twice. Usually SUVs were prepared in a nominal concentration of 0.1 or 1 mg of total substance per ml. The exact compositions and concentrations used for the respective experiments are given in the Results section.

2.8   PREPARATION OF ASYMMETRIC VESICLES

Asymmetric vesicles provided a membrane mimic, which was able to model the asymmetry of certain natural membranes, e.g. outer membranes of Gram negative bacteria. Asymmetry

in this context refers to an uneven distribution of molecule species between the inner and outer leaflet of the membrane. Preparation of asymmetric vesicles was done according to a modified protocol first described by *Pautot et al., 2003*. While the original protocol was only used to prepare asymmetric phospholipid/phospholipid vesicles, our modified protocol was also used for the preparation of asymmetric LPS/phospholipid vesicles (n.b.: syntax for the description of asymmetric vesicles in this thesis is "outer leaflet / inner leaflet". An e.g. LPS R45/DOPC asymmetric vesicle would consist of LPS R45 in the outer leaflet and DOPC in the inner leaflet.). My coworker Annemarie Brauser adopted the protocol cited above for the use of LPS and made initial preparations. During my thesis I contributed to the establishment of this preparation method and implemented minor changes in the protocol. The final protocol, after which asymmetric vesicles have been prepared, is described in the following (cf. Fig. 2.4). To prepare the inner leaflet, 0.1 mg of the desired lipids and eventually fluorescent labels were placed in a 20 ml glass vial and solved in 2 ml dodecane (ReagentPlus, Sigma Aldrich, Deisenhofen, Germany) to gain a final concentration of 0.05 mg/ml. The vial was sonicated (Sonifier Cell Disruptor B15, Branson Ultrasonics Corporation, Danbury, CT, USA) for 30 minutes to make sure all lipids were completely solved. Afterwards 1 ml 100 mM KCl, 5 mM $MgCl_2$, 5 mM Hepes (pH 7) buffer was added and the solution was stirred by a magnet stirrer at 500 rpm for three hours at room temperature. By this, an emulsion of µm-sized buffer droplets within the dodecane came into being. The polar lipid head groups gathered in the buffer droplets, while their hydrophobic alkyl chains loomed into the surrounding dodecane. To prepare the outer leaflet 0.1 mg of the desired lipids or LPSs and eventually fluorescent labels were placed in a 20 ml centrifugation tube and solved in dodecane:silicone oil (AR200, Sigma Aldrich, Deisenhofen, Germany) 99:1 (v/v). The centrifugation tube was sonicated for 30 minutes to solve the molecules completely. The silicone oil in the solution was used to slightly increase the overall density, by which a mixing with the dodecane solution of the inner leaflet was prevented later. 1 ml of 100 mM KCl, 5 mM $MgCl_2$, 5 mM Hepes (pH 7) buffer was pipetted to the bottom of the centrifugation tube to form a sub layer below the dodecane. The solution was allowed to rest for 3 hours at room temperature. During this time the lipid or LPSs solved in the dodecane gathered at the phase boundary, by which their polar head groups were orientated downwards into the aqueous phase, while the hydrophobic alkyl chains pointed upward into the dodecane. Afterwards 300 µl of the previously prepared buffer-dodecane emulsion were carefully pipetted to the centrifugation tube. The solution was added as small droplets to the surface of the upper dodecane phase. Afterwards the centrifugation tube was centrifuged for 10 min at 120 g to force the buffer droplets into the lower buffer phase. By this, the droplets, which already carried the inner leaflet, ran through the lipid or LPS layer at the phase boundary and collected molecules as an outer vesicle leaflet. After centrifugation the final vesicle solution was slowly removed with a pipette. Vesicles were directly observed by microscopy or stored overnight at room temperature for observation on the next day.
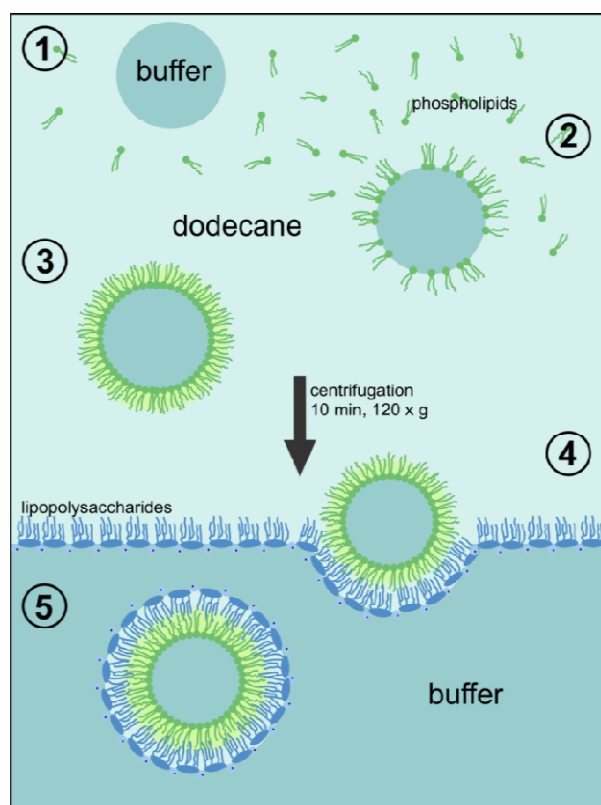
Fig. 2.4**: Principle of the preparation of asymmetric vesicles.** (1): Buffer droplets are created in a dodecane solution by stirring; (2): Solved phospholipids gather with their polar head groups in the buffer; (3) Lipids form the inner leaflet of the later asymmetric vesicles; (4) Lipid loaded droplets are centrifugated through an LPS monolayer at a dodecane-buffer phase boundary; (5) While passing through the monolayer, the droplets collect the LPSs as an outer leaflet of the asymmetric vesicles. Picture by courtesy of Annemarie Brauser.

2.9 PREPARATION OF LANGMUIR-BLODGETT FILMS

To prepare solid supported monolayers the Langmuir-Blodgett technique (Blodgett and Langmuir, 1937; Langmuir and Schaefer, 1938) was used in combination with a Langmuir film balance (Munitech, Munich, Germany) (Fig. 2.5). The basic setup of such a film balance is described explicitly by *Albrecht et al., 1978*. For the preparation of lipid monolayers a 1 cm times 2 cm wide piece of mica was submerged into the film balance basin in 100 mM KCl, 5 mM Hepes buffer at pH 7. On the surface of the buffer a DOPC, DOPC:TDM 10:1 (w/w), or DOPC:TDM 1:1 (w/w) monolayer was spread out by addition of chloroform-solved molecules. After evaporation of the chloroform the polar lipid head groups submerged into the buffer, while the polar alkyl chains pointed towards the air. A moveable barrier was used to adjust a lateral pressure of 20 mN/m. Now, the submerged

mica was pulled out of the liquid, passing the surface in a 90° angle. Pulling velocity was 1 µm/s. While the hydrophilic mica passed the monolayer of spread out lipids or TDM molecules, the head groups of the molecules bound to the mica surface and formed a monolayer on it.
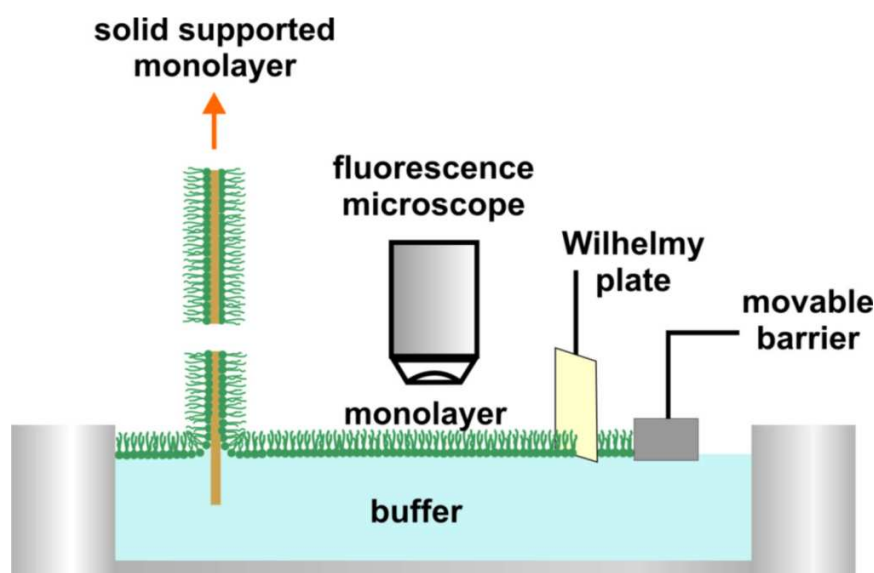

Fig. 2.5**: Schematic setup of a Langmuir film balance with an attached fluorescence microscope.** Lipids are spread to form a monolayer on the buffer surface. A movable barrier adjusts the lateral pressure of the lipids, which is measured by the Wilhelmy plate. Solid supported monolayers can be obtained from the spread out lipids by pulling a piece of mica through the layer (see also Roes et al, 2005).

2.10 PREPARATION OF SOLID SUPPORTED BILAYERS

Solid supported bilayers for AFM measurements were prepared by spreading of vesicles (Jass et al., 2000) (Fig. 2.6). An about 1 cm times 2 cm wide piece of mica (cf. paragraph 2.14.1) was glued to the bottom of a small petri-dish and cleaned by removing the uppermost layer of the sheet silicate with a piece of sticky tape. Afterwards 100 µl of a 0.1 mg/ml SUV solution were placed on the mica and incubated for 15 minutes at about 20 °C. Free floating vesicles came into contact with mica and spread to form a planar bilayer. Now, the petri-dish was filled with 2 ml of buffer to flush away free vesicles above the mica and prevent the sample from dehydration. The planar bilayer on the mica was then ready to be investigated by AFM.
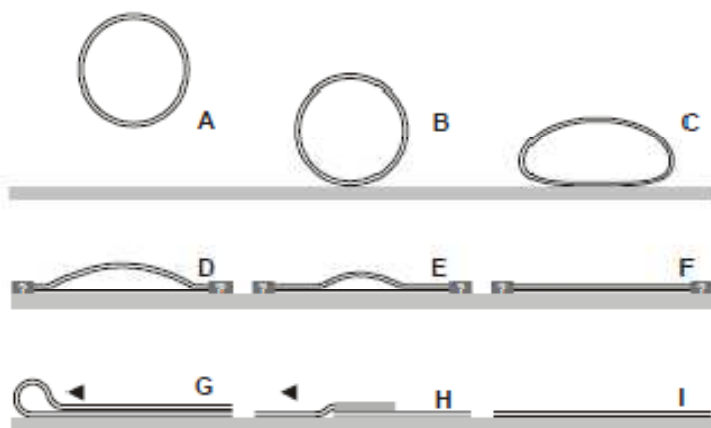
Fig. 2.6: **Illustration of the formation of solid supported bilayers by spreading of vesicles** (image from Jass et al., 2000). (A-C): A buffer solved vesicle comes into contact with the solid support and starts to flatten. (D-F): Starting from the vesicle rim two planar bilayers on top of each other come into being. (G-I): The loose upper bilayer is flushed away or moves to unoccupied parts of the solid support, uncovering the basic solid supported bilayer.

2.11 PREPARATION OF SOLID SUPPORTED MULTILAYERS

Besides bilayers with incorporated TDM, also TDM multilayers were investigated by AFM. Solid supported TDM multilayers were prepared by air drying of TDM solved in chloroform. 20 µl of a 0.5 mg/ml TDM solution were distributed over an about 1 cm times 2 cm wide piece of clean mica, which was glued to the bottom of a small petri-dish. 400 µl of purified water were placed at the rim of the petri-dish to keep the sample slightly hydrated. Care was taken not to touch the sample with water droplets directly. Petri-dish and sample were allowed to rest for about 15 minutes at 20 °C, by which the chloroform evaporated. Afterwards the water was removed and the sample was ready to be investigated by AFM.

2.12 FLUORESCENCE MICROSCOPY

Fluorescence microscopy (cf. Lichtman and Conchello, 2005) in this work was performed with two different devices; a Leica TCS SP1 spectral confocal microscope (Leica Microsystems Heidelberg GmbH, Heidelberg, Germany) using a HCX Plan Apo 63x (oil) lens and a Olympus IX 70 fluorescence microscope (Olympus America Inc., Center Valley,

PA, USA) with an LP Plan Fl 40x lens (Olympus America Inc., Center Valley, PA, USA). Both used fluorescence microscopes were of the inverse type, i.e. the lens was located below the sample. For the observation of GUVs usually the Olympus IX 70 microscope was used because of its easy handling and straight-forward data procession. Excitation of the sample occurred from 460 to 490 nm while the fluorescence emission was observed at wavelengths over 510 nm (510 nm long pass, LP). These values were suited to use NBD, Bodipy FL, FITC or Rh as fluorophors. As light source a 100 W mercury-vapor lamp (U-LH100HG, Olympus America Inc., Center Valley, PA, USA) was used. Fluorescence was recorded with a black and white CCD camera (C8484-05G, Hamamatsu Photonics Deutschland GmbH, Herschingen, Germany). In the resulting grey-scale images, dark areas represented low fluorescence intensity, while bright areas represented high intensity. Other experiments, however, required particularly small structures or the use of more than one type of fluorophor in the sample. In these cases the Leica TCS SP1 microscope was preferred because of its higher magnification and better variety of excitation end emission wavelength. This microscope had lasers at 458, 476, 488, 514, 543 und 633 nm for excitation and spectral fluorescence detection available. Excitation and emission wavelength were chosen in a way that the fluorophors NBD and Rh could be discriminated from each other, when used together in one sample. NBD was in all experiments excited at 488 nm and its fluorescence was recorded from 500 to 550 nm. Because Rh labels did not emit any significant amounts of light at wavelength of 550 nm or below, the recorded signal could be assigned to NBD. Rh was excited at 543 nm and its fluorescence was measured from 580 to 650 nm. Because NBD labels could not be excited at a wavelength of 543 nm, the recorded signal can only have originated from Rh. When the fluorophor FITC was used, the same wavelengths as applied for NBD were chosen. FITC was used for fluorescence quenching experiments with $CaCl_2$ (Merck, Darmstadt, Germany) as a quencher. In the shown images NBD and FITC fluorescence were assigned to green color, while Rh fluorescence was assigned to red. These colors resembled approximately the natural color impressions of the fluorophors. The Leica TCS SP1 microscope allowed for high sample-to-background intensity ratios, when the confocal effect was used. By this, a circular aperture within the beam path eliminated light, which was not derived from the focal plane. The downside of this effect was a relative low depth of field, especially at high magnifications. Therefore imaging of spherical μm-sized GUVs did not provide an image of the whole vesicle, but led to the depiction of a cross-section, in which the membrane appeared as a circle. A z-stack of many cross-sections could later be combined, showing the whole vesicle (used only in Fig. 3.16). Unfortunately, the recording of a z-stack took several seconds and could therefore only be applied to resting vesicles. Free floating vesicles, however, allowed but for the recording of single pictures.

For fluorescence microscopy 20-30 μl of the desired sample were simply placed on a glass slide prior to observation and covered with a cover glass at room temperature. AMPs or other substances were applied to the sample by mixing small amounts of the substances directly on the glass slide before the cover glass was attached. The Olympus IX 70 microscope was also used in combination with a homemade temperature cell (Fig. 3.5). This

device was developed in cooperation with Sebastian Stengl, an electrical engineering student from the University of Applied Sciences Lübeck, who absolved an internship in our lab. The design and functionality of the build temperature cell are described in detail in the Results section. When the cell was used, about 500 to 800 µl of a GUV suspension were applied to the body of the cell. Afterward the cell was sealed and placed on the sample table of the Olympus IX 70 microscope. The sample table of the Leica TCS SP1 contained microelectronics and was not suited to carry more than 100 g weight, preventing the use of the temperature cell. Figure captions in the Results section indicate the respective sample temperatures and which microscope was used for the experiments. Post processing of recorded images included adjustment of brightness and contrast as well as merging several pictures of a z-stack into a single image. These steps were carried out using the free software graphics editor GIMP2 (by The GIMP Development Team, www.gimp.org).

2.13 FLUORESCENCE SPECTROSCOPY

Fluorescence spectroscopy was used to investigate interactions of fluorescent labeled AMPs with lipid vesicles and TDM aggregates. In contrast to fluorescence microscopy, the spatial origin of the fluorescence signals is not resolved in this method but all signals at the same wavelength are summed up. In fluorescence spectroscopy samples are usually located in a glass cuvette containing a multitude of solved molecules or supramolecular structures, from which a small portion is labeled by a fluorophore. Light of a light source (often xenon arc or mercury-vapor lamps) passes through a filter or monochromator and excites the fluorophors in the sample. Fluorescence is emitted in all directions and the fluorescence intensity is recorded by a detector perpendicular to the axis of the incident light. This setup allows avoiding direct illumination of the detector by light from the spectrometer light source. However, inelastic (Raman) scattering of light from the incident beam can be recorded and erroneously considered as fluorescence. A second filter or monochromator in front of the detector allows picking a range of wavelengths, at which the fluorescence is observed. The fluorescence of a label can be altered by a number of different molecular processes including changes in hydrophobicity and polarity of the microenvironment, dipole-dipole-coupling with other molecules, impact of solvent molecules, changes in micro viscosity and movement or chemical modification of the label itself. By selection of adequate fluorophors, fluorescence spectroscopy can reveal information about molecular processes within the sample. For a broad discourse on fluorescence and fluorescence spectroscopy the textbook *Lakowicz, 1999* is highly recommended.

Measurements in this thesis were done using a Fluorolog 3 fluorescence spectrometer (HORIBA Jobin Yvon GmbH, Unterhaching, Germany) with diffraction grating

monochromators to isolate the incident and fluorescent light. Light source was a 450 W xenon short arc lamb (UXL-450S-O, Ushio Deutschland, Steinhöring, Germany). Fluorescence was amplified by photomultipliers prior to recording. The used spectrometer was built in so called T-shape configuration (Fig. 2.7) with two identical detection systems.
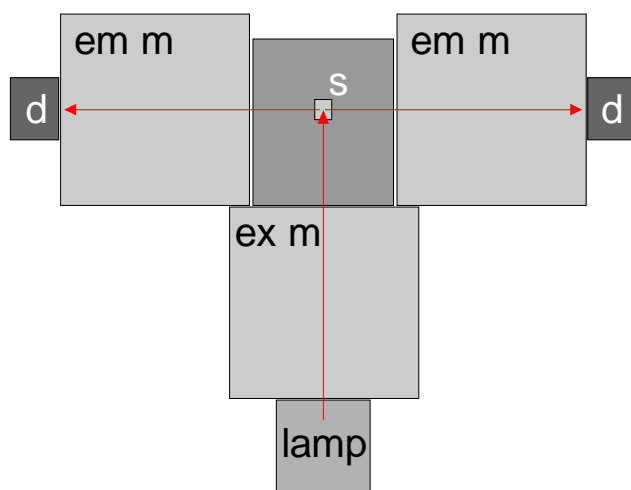

Fig. 2.7**: Schematic setup of the used fluorescence spectrometer in t-configuration.** Incident light is produced by a xenon arc lamp and passes the excitation monochromator (ex m) before it hits the sample (s). Two identical arms with an emission monochromator (em m) and a photomultiplier/detector (d) allow for simultaneous recording of fluorescence at two different wavelengths.

The actual fluorescence spectroscopic measurements shown in this work were based on the phenomenon of Förster resonance energy transfer (FRET) as described in detail in the next paragraph.

2.13.1 FÖRSTER RESONANCE ENERGY TRANSFER BASED EXPERIMENTS

One implementation of fluorescent spectroscopy is the measurement of Förster resonance energy transfer (FRET) (Förster, 1948), named after its discoverer Theodor Förster. For a review on the topic see *Miyawaki, 2011*. FRET is based on radiationless energy transfer from one molecule to another by long range electrostatic interactions (dipole coupling). To allow energy transfer, the fluorophors need to possess an overlap of donor emission and acceptor excitation spectra. This prerequisite was given for the used fluorophors NBD (donor) and Rh (acceptor), which are therefore called a FRET pair. Furthermore, the

efficiency for energy transfer in a sample depends on the orientation of donor and acceptor dipoles. Efficiency is highest for parallel oriented dipoles and zero for perpendicular dipoles. In a multitude of solved and relatively mobile fluorophors, as used in the experiments, a certain rate of donor and acceptor labels is always appropriately oriented (Lakowicz, 1999). Furthermore, the efficiency of FRET is highly dependent on the distance (R) between the involved molecules (equation 1).

$$E = \frac{1}{1+\left(\frac{R}{R_0}\right)^6}$$
(Equation 1)

E: transfer efficiency; R: distance donor-acceptor, mean distance when a multitude of molecules is observed; R_0: Förster-distance, R at which E= maximal/2.

The transfer efficiency can be experimentally determined by observation of donor fluorescence quenching. To do so, the donor intensity is measured first in absence and afterwards in presence of an acceptor. From these intensities the transfer efficiency is given by:

$$E = 1 - \frac{I_{D+A}}{I_D}$$
(Equation 2)

E: transfer efficiency; I_{D+A}: donor fluorescence intensity in presence of an acceptor; I_D: donor fluorescence intensity in absence of an acceptor.

For the actual experiments in this thesis SUVs made of PE:PG 1:1 (w/w) labeled 1:500 with NBD-DHPE were prepared in 100 mM KCl, 5 mM Hepes buffer (pH 7) as described previously. TDM aggregates labeled 1:500 with NBD-DHPE were prepared in the same way. A solution of each sample was diluted with 100 mM KCl, 5 mM Hepes buffer (pH 7) to a final concentration of nominal 5 µg/ml total substance and a volume of 2 ml. The solution was filled in a 3.5 ml glass cuvette (model 101-QS, Hellma GmbH & Co. KG, Müllheim, Germany) and placed in the fluorescence spectrometer. Afterwards the Rh labeled AMPs LL32-Rh, LL32-4A-Rh or hBD-3-l-Rh were titrated to the samples. Every 100 seconds 10 µl of a 0.01 mg/ml peptide solution were added. Sample temperature was kept constant at 37 °C. A small magnet stirrer in the sample cuvette provided an even distribution of peptides and vesicles/aggregates. Between the peptide additions the NBD fluorescence was continuously excited at 470 nm and recorded at 531 nm. A binding of the AMPs to the vesicles/aggregates brought donor and acceptor labels into close contact, which increased the transfer efficiency and led to a quenching of the donor fluorescence (Fig. 2.8). The mean NBD fluorescence intensity was later plotted against the respective peptide concentration to show the different binding capabilities of the used AMPs.
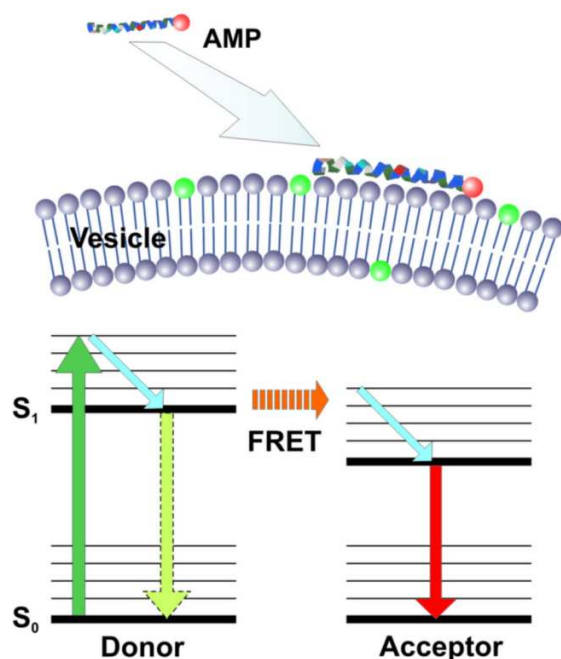
Fig. 2.8**: Principle of the used FRET based binding assay.** Upper image: schematic illustration of AMP binding to a vesicle membrane; lower panel: simplified Jablonski diagram for the unbound (left) and bound (right) condition. NBD (green) labeled vesicles are excited (green arrow). In absence of an Rh (red) labeled AMP NBD fluorescence can be recorded (dotted green arrow). If AMPs bind to the vesicle membrane, Rh labels approach the NBD and FRET conducts the energy to the Rh by dipole-dipole interactions. Rh fluorescence can be measured (red arrow), while the NBD fluorescence is quenched. Due to vibrational energy losses (cyan arrows) NDB and Rh fluorescence are increasingly redshifted.

2.14 ATOMIC FORCE MICROSCOPY

Atomic force microscopy (AFM) allowed for the investigation of planar lipid bilayers with a resolution in the nanometer range. The method was used to obtain information on the TDM organization in lipid bilayers and the effect of AMPs thereupon. AFM was first introduced by Binnig and Quate (Binnig and Quate, 1986) and has developed to a widely used method for the investigation of nanoscopic structures. Unlike to electron microscopy or scanning tunneling microscopy (STM), on which first AFM devices were based, AFM samples do not need to be electrically conductive and measurements must not be performed in vacuum. This made the method also attractive for research in biosciences, where experiments under physiological conditions are desired. AFM measurements are based on interactions between the sample and a small tip (<25 nm in diameter) connected to a transition bar known as cantilever (Fig. 2.9). For AFM scans sample and cantilever tip are moved relative to each other in x- and y-direction, which describe the plain of the sample. A laser beam is reflected

from the upper side of the cantilever, sensed by a four-segment photo detector and the deflection is calculated. If the cantilever tip experiences differences in sample height, it will cause the cantilever to bend, by which the laser beam is deflected. The now altered deflection is evaluated by a feedback loop controlling the z-position of the cantilever. The z-position of the cantilever holder is regulated by tension dependent stretching of a piezo crystal. A position sensor measures the piezo`s extension and provides the absolute position of the cantilever holder. This signal, called LVDTz, is used to reconstitute the height profile (topography) of the sample.
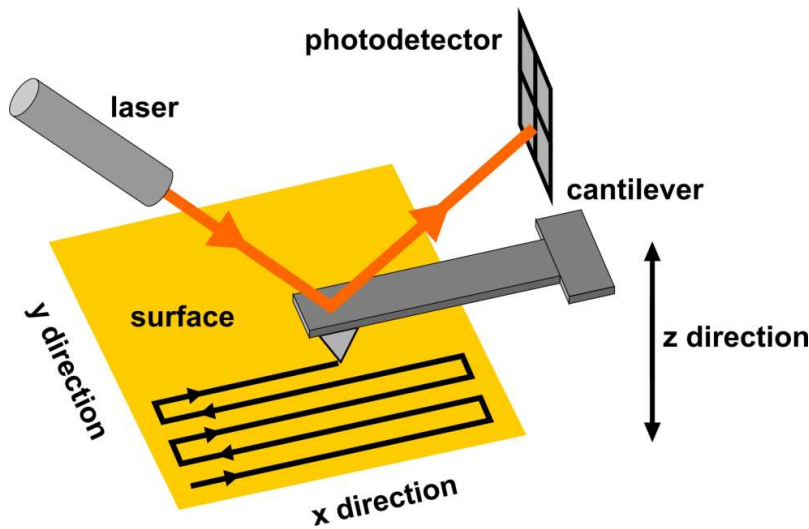

Fig. 2.9**: Schematic illustration of an AFM scan.** The tip of a cantilever scans the sample surface in x and y direction. Height differences cause the cantilever to bend and alter the illumination of a photo detector by a reflected laser beam. If the illumination exceeds a certain set-point, a feedback circuit adjusts the cantilever in z direction obtaining initial illumination. The z positions of the cantilever are used to reconstitute the sample topography.

AFM measurements can either be done in AC (alternating current) or in contact mode. In contact mode the tip slides over the sample surface. It thereby touches the sample and experiences a repulsive force. This force is a result of the Pauli exclusion principle, which states that identical fermions, like electrons, protons and neutrons, may not occupy the same quantum state simultaneously. A consequence of this principle is that matter cannot be condensed to any extend, but causes a repulsion. In AC mode, also known as tapping mode, the cantilever is triggered to perform a periodic motion in z-direction above the sample (Martin et al., 1987). The freely oscillating cantilever possesses a certain amplitude, phase and frequency, which are measured by the periodic changes in the deflection signal. In amplitude-modulated scans, as performed in this work, recording of the sample topography is derived from interactions between sample and cantilever amplitude. During scanning the cantilever tip periodically approaches the sample but does not necessarily touch the sample

38

surface. While the tip approaches, it first senses an attractive force, caused by relatively long ranged van-der-Waals interactions between induced dipoles in tip and sample (Fig. 2.10). Starting from distances of about 0.6 nm also a repulsive force emerges as a result of the Pauli exclusion principle. Superposition of attractive and repulsive forces gives the Lennard-Jones potential (V_L), describing approximately the interactions between two unbound uncharged atoms (*equation 3*).

$$V_L = 4\,\varepsilon\left[\left(\frac{\sigma}{r}\right)^{12} - \left(\frac{\sigma}{r}\right)^6\right]$$

(Equation 3)

V_L: Lennard-Jones potential; ε: Lennard-Jones energy describing the depth of the potential well.; σ: Lennard-Jones radius, r at which $V_L=0$; ε and σ are material constants; r: distance between the particles.

Repulsive forces prevail at distances below about 0.45 nm, while attractive forces predominate between about 0.45 and 0.7 nm. Attractive and repulsive forces interact with the tip during an AFM scan and change the amplitude of the cantilever oscillation. A feedback loop senses these alterations via changes in deflection and adjusts the cantilever z-position until the amplitude matches the set-point amplitude again. As in contact mode scans, the sample topography is reconstituted from the cantilever z-positions.
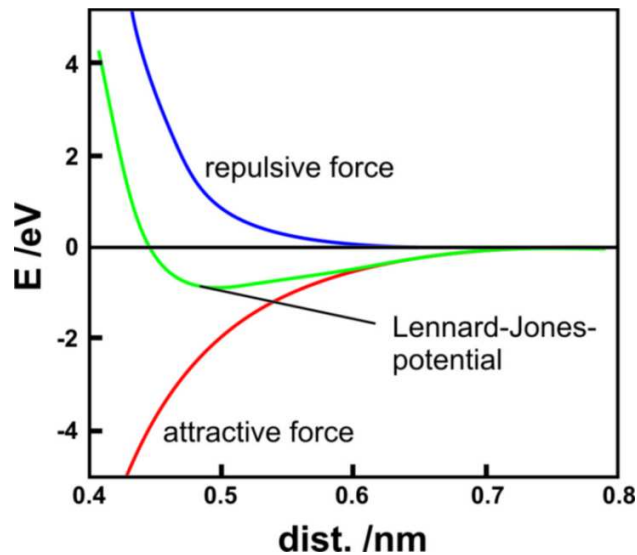

Fig. 2.10: **Lennard-Jones potential as a result of attractive and repulsive forces between approaching molecules.** Van-der-Waals interactions attract the cantilever tip to the sample, while forces based on the Pauli exclusion principle cause repulsion. Superposition of attractive and repulsive forces gives the Lennard-Jones potential.

2.14.1 MICA

AFM measurements work best with relative even samples, which are typically fixed to a solid support to prevent a dislocation during the measurement. Muskovit Mica (standard quality #54, Plano, Wetzlar, Germany) was used as substrate for solid supported monolayers, bilayers and multilayers. The sheet silicate is widely used for AFM measurements. It consists of many plan parallel crystalline layers with a thickness in the nanometer range. The uppermost layers can be separated from a bulk of mica with a strip of sticky tape. This brings up a very even and clean surface, suited to carry lipid membranes. Furthermore, clean mica possesses a hydrophilic surface with a negative charge and therefore promotes the attachment of phospholipid head groups. A disadvantage of mica is its light brown color and therefore limited translucency, narrowing its use in some combined AFM/fluorescence microscopy experiments.

2.14.2 TOPOGRAPHY SCANS

A MFP-3D atomic force microscope (Asylum Research, Santa Barbara, CA, USA) was used in this thesis, providing a resolution of up to 2 nm in horizontal (x and y) and 0.3 nm in vertical (z) direction. The actual horizontal resolution in the recorded images was lower, as 10 µm times 10 µm sized images were sampled in 256 lines with 256 pixels each. By this, no structures smaller than the pixel-size (about 39 nm) could be resolved, but scanning could be done much faster. Lipid bilayers were measured in 100 mM KCl, 5 mM Hepes buffer (pH 7) to gain more physiological conditions. OMCL-RC800 PSA2 (WS lever) cantilevers (Olympus OPTICAL CO., Tokyo, Japan) with pyramidal tips were used for all experiments with lipid bilayers. These cantilevers had a nominal spring constant of 0.76 N/m and a resonance frequency of 71 kHz in air. As most AFM measurements in this thesis were carried out in buffer on relatively soft samples, cantilevers with this rather low spring constant were favorable to minimize the amount of damage of the sample. Multilayers were measured in contact mode in air using the same cantilevers as for bilayers. Samples were prepared as described in the paragraphs above. Scan speed for AFM scans was usually 25 µm/s or as indicated in the figure legends in the Results section. Samples were mostly investigated at about 20 °C. When heating of samples was necessary, it was accomplished using a Bio Heater Stage Kit (Asylum Research, Santa Barbara, CA, USA). If AMPs were added to solid supported bilayers in buffer, 50 µl of the respective AMP solved in TFA were given as droplets to the surface of the buffer, in which the sample rested. By this, the AFM head was temporarily removed to gain a better access to the petri-dish. Final AMP concentrations are indicated in the figure legends in the Results section. Further image

processing (flattening, plane fitting and careful removal of single artifacts) was done using MFP-3D software under IGOR Pro (Lake Oswego, OR, USA).

2.14.3 FORCE SPECTROSCOPIC MEASUREMENTS

While AFM scans provided information about the topography of the sample surface, AFM based force spectroscopic measurements were suited to investigate sample thickness and stiffness (Franz et al., 2002; Vinckier and Semenza, 1998). In this kind of experiments the x- and y-position of the cantilever tip is kept constant, while the tip is moved in z-direction towards the sample. At a certain position the tip hits the sample surface and eventually penetrates to the solid support on which the sample rests. The pathway of these so called force graphs gives information about the force needed to penetrate the sample and the distance covered thereby (Fig. 2.11).
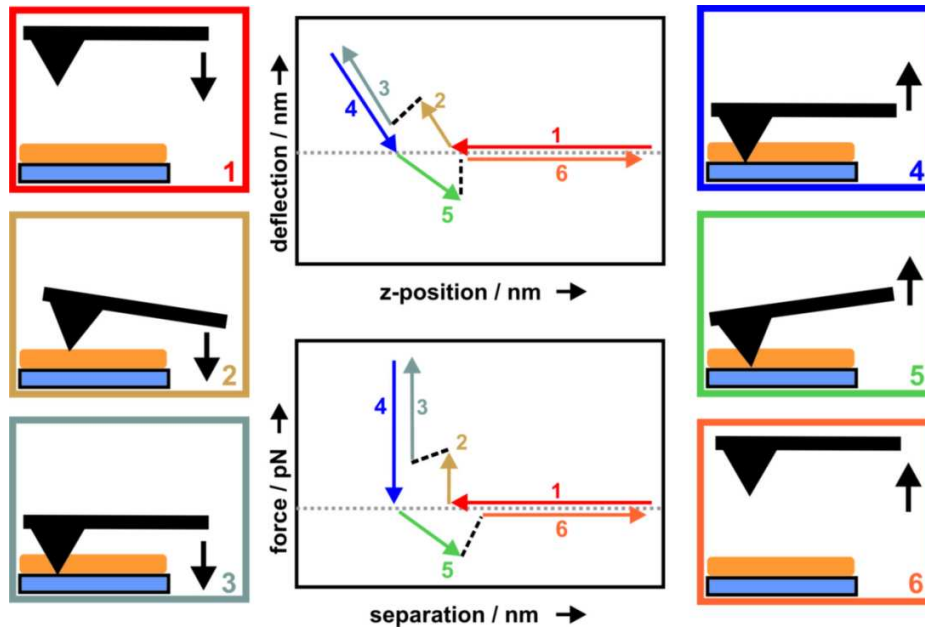
Fig. 2.11**: Principle of a force-spectroscopic measurement.** A deflection vs. z-position graph (mid, upper panel) describes the position of the laser beam on the detector as a function of the position of the cantilever holder. From these values a force vs. separation graph (mid, lower panel) can be calculated. Here, the force, which is applied to the sample, is plotted against the distance between cantilever tip and sample. (1): The cantilever tip approaches the sample; (2): Tip presses on the sample, bends and breaks through the sample; (3): Tip presses on the solid support; (4): Tip is pulled back; (5): Tip is pulled back further, bends and detaches from the sample; (6): The tip is released and removed from the sample. In own measurements only steps 1 to 3 were evaluated to investigate sample stiffness and thickness.

Deflection of the laser beam and absolute z-position of the cantilever are recorded during a force spectroscopic experiment. They can be plotted as a deflection vs. z-position graph. To gain information about sample thickness and stiffness from these values, some calculations need to be done. First the deflection values measured in volt need to be translated into deflection values in nanometers. This means that the measured changes at the photo detector need to be connected with the underlying displacement (bending) of the cantilever. It applies:

$$\mathrm{Defl\,[nm] = Defl\,[V] * InvOLS\,(nm/V)} \qquad \textit{(Equation 4)}$$

InvOLS: inverse optical lever sensitivity; the value describes the bending (in nm) necessary to cause a certain change in deflection. It is given by the first derivative of a deflection vs. z-position plot, in which the cantilever bends on a solid substrate.

Finally the force (F) applied to the cantilever during a force spectroscopic measurement is given by:

$$\mathrm{F\,[pN] = Defl\,[nm] * k\,(pn/nm)} \qquad \textit{(Equation 5)}$$

k: spring constant of the cantilever; values provided by the manufacturer were not accurate enough, so the spring constant needed to be determined for every cantilever in a separated experiment. The thermal noise method was used (Hutter and Bechhoefer, 1993). Here, the integral over the resonance peak of a free oscillating cantilever is used to determine the spring constant. The necessary fitting of the thermal graph and all calculations were implemented into the MFP-3D measurement software under IGOR Pro (Lake Oswego, OR, USA).

To adjust the units of the x-axis, the recorded absolute positions of the cantilever holder in z-direction (LVDTz) need to be translated into distances between sample and cantilever tip. These distance values, called separation (Sep), can be obtained as follows:

$$\mathrm{Sep\,[nm] = LVDTz\,[nm] - Defl\,(nm)} \qquad \textit{(Equation 6)}$$

The separation between tip and sample equals the z-position of the cantilever reduced by the distance caused by bending of the cantilever. Now, it is possible to plot force vs. separation curves, as shown in the Results section. Own force spectroscopic measurements were implemented using a MFP-3D atomic force microscope (Asylum Research, Santa Barbara, CA, USA) and OMCL-RC800 PSA2 (WS lever) cantilevers (Olympus OPTICAL CO., Tokyo, Japan) with pyramidal tips. The AFM was set into contact mode. Experiments on solid supported bilayers took place in 100 mM KCl, 5 mM Hepes buffer (pH 7) at about 20 °C. Cantilever descent velocity was 100 nm/s, sample rate 10 kHz. The respective spring constants of the used cantilevers and final concentrations of eventually added AMPs are given in the figure descriptions in the Results section.

2.15 FOURIER TRANSFORM INFRARED SPECTROSCOPY

Infrared (IR) spectroscopy was used to determine phase transition temperatures of different phospholipids, LPSs, TDM and mixtures of the aforementioned. Information about the existing phases in the samples helped to explain effects observed using other methods.

In IR spectroscopy a sample is illuminated with radiation in the IR spectrum. Most of the radiation passes through the sample and is recorded by a detector, while radiation of certain wavelengths is absorbed. Electromagnetic waves in the IR spectrum possess relatively low energies and are therefore unable to cause electronic transitions. Molecules absorb specific IR frequencies, which match the energy difference between two energy levels of molecular vibration. Only molecules with a dipole moment (spatial separation of charge due to differences in electronegativity) are able to absorb in the IR spectrum, because it is the molecule´s dipole moment which interacts with the electric field vector of the wave. Many chemical groups like CH_3, C-C-H, C=O, O-H, S-H, N-H, etc. possess a dipole moment and are therefore IR active. Because of this, IR spectroscopy is suited to generate a "fingerprint" of complex molecules (Jackson and Mantsch, 1996). Fourier transform infrared (FTIR) spectroscopy (Griffiths and de Haseth, 1986) is the most abundant method for IR spectroscopy today and was also used in this thesis. Old IR spectrometers of the dispersive type use a prism or dispersive grating to separate the radiation of an infrared source into individual frequencies. By this, transmitted intensities of individual frequencies are measured one after another and the overall time to measure the IR spectrum of a sample is relatively high. FTIR spectrometers are, however, able to record all frequencies of an IR source simultaneously, which is accomplished much faster. To do so the radiation passes an interferometer before it hits the sample. Interferometers consist of a beam splitter, which divides the incoming IR radiation and reflects half of it to a moving mirror, while the other half is transmitted to a static mirror. The radiation is reflected off from both mirrors and concurs at the beam splitter. While the pathway of one beam is constant, the pathway of the other beam is constantly changing due to the movement of the mirror. By this, the beam, which leaves the interferometer, is a result of two interfering beams, called an interferogram. The signal intensity of the interferogram can be considered as a function of the position of the moving mirror and every data point in the signal has information about all frequencies emitted from the IR source. After the measurement individual frequencies need to be calculated from the interferogram by a Fourier transformation.

For historical reasons positions of IR absorption peaks are often not given as frequencies but as wavenumbers ($\tilde{v}$) with the unit cm^{-1}. It applies:

$$\tilde{v} = \frac{v}{c} = \frac{1}{\lambda} \qquad\qquad (Equation\ 7)$$

$\tilde{v}$: wavenumber; v: frequency; c: speed of light in vacuum; λ: wavelengths

An IFS 55 FTIR spectrometer (Bruker GmbH, Bremen, Germany) was used. Lipid, LPS or TDM vesicles/aggregates were prepared in 100 mM KCl, 5 mM Hepes buffer (pH 7) or 100 mM KCl, 5 mM $MgCl_2$, 5 mM Hepes buffer (pH 7) at concentrations of 20 mM. Figure legends in the Results section indicate, which buffer was used for the respective experiments. About 10 µl of each sample were sealed between to IR transparent CaF_2 crystals and placed into the beam path. The sample was heated from about 5 to 65 °C with a rate of 1 °C per minute. An IR interferogram was recorded from 4000 to 700 wavenumbers at every degree Celsius. Fourier transformation of the data was done by Opus 6.5 (Bruker Optik GmbH, Ettlingen, Germany). Only the absorption of CH_2 symmetric stretching vibrations at around 2852 cm^{-1} was used to determine the phase transition. The position of the absorption maximum moved slightly towards higher wavenumbers, when the alkyl chains of the sample became more flexible. To determine the phase transition, the position of the absorption maximum was plotted as a function of temperature. The steepest increase, i.e. highest point in the first derivative, of the graph indicated the phase transition temperature.

2.16 Conductivity Experiments

Conductivity experiments were carried out to measure the membrane conductivity of untreated and AMP treated planar lipid membranes. Changes in conductivity are able to reveal the membrane permeabilization properties of AMPs (Wiese and Seydel, 1999). Planar lipid bilayers were prepared according to the Montal-Mueller technique (Montal and Mueller, 1972). About 5 µl of chloroform-solved lipids or LPSs with a concentration of 1 mg/ml were spread onto the surface of 100 mM KCl, 5 mM $MgCl_2$, 5 mM Hepes buffer (pH 7) on two opposing compartments connected by a small hole (about 150 µm in diameter) in a Teflon foil (Kastilo GmbH, Ulm, Germany) (Fig. 2.12). Afterwards the buffer level was increased on one and on the other side, which led first to the formation of a lipid monolayer and then to a bilayer across the hole. Bilayers could be symmetric or asymmetric depending on the used lipids or LPSs. For conductivity measurements electrodes were placed in the buffer in both compartments and a voltage of -20 mV was applied. The negative voltage refers to the polarity of the bilayer, which had a defined inner and outer side. Like in natural cells the inner side had a negative membrane potential compared to the outside. With respect to the *in vivo* situation, AMPs were always added to the buffer on the outside leaflet. Asymmetric LPS / phospholipid membranes had the LPS leaflet on the outside and the lipid leaflet on the inside. The membrane between the compartments functioned as an electrical resistance. This allowed measuring the membrane conductivity as a parameter for the permeabilization of bilayers by AMPs. After a bilayer was prepared, its conductivity was measured for a few minutes to make sure the membrane was stable. Afterwards AMPs were added to a final concentration of 1.7 µg/ml. Measurement signals were amplified with a

patch-clamp amplifier (L/M-PCA, List-Medical, Darmstadt, Germany) and transferred to a PC using an input/output (I/O) card (PCI-6036E, National Instruments Germany GmbH, Munich, Germany). Control of the measurement and data procession were performed by homemade software running in a LabVIEW 7.1 (National Instruments Germany GmbH, Munich, Germany) environment.
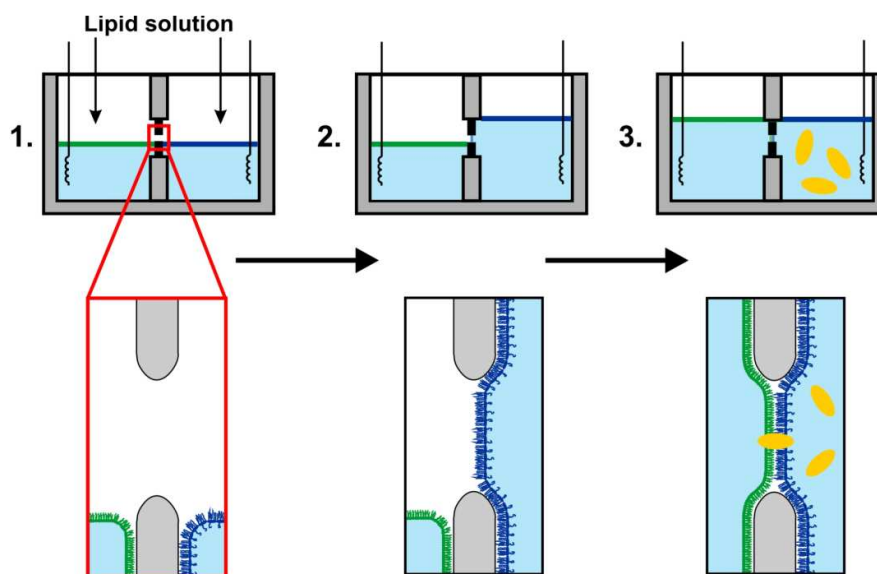

Fig. 2.12: **Schematic illustration of the preparation of planar lipid bilayers.** (1): Chloroform-solved lipids or LPSs (green and blue) of identical or different composition are spread to form monolayers on the surface of buffer. Buffer and samples are located in two identical compartments, connected by a small hole in a Teflon foil. (2-3): When the buffer level is increased on one and finally both sides, first a lipid monolayer and afterwards a bilayer is formed. (3): The final bilayer can be exposed to membrane active substances (yellow), which eventually permeabilize the membrane. Electrodes on both sides of the bilayer measure the conductivity as a parameter of membrane permeabilization.

The described setup was also combined with a fluorescence microscope. This allowed for visualization of fluorescently-labeled symmetric and asymmetric planar lipid bilayers. Observations were made with respect to phase separation and occurrence of domains in the bilayers. The partly homemade microscope was realized in our lab by a former PhD student named Sven Hagge. Case and mechanical parts of the device were manufactured by Eastern Scientific (Rockville, MD, USA). The microscope used a mercury short arc lamb (HBO 103W/2, Osram, München) for illumination, while a fluorescence filter (455DF70, Omega Optics, Brattleboro, VT, USA) and a dichroic filter (515DRLP, Omega Optics, Brattleboro, VT, USA) selected the wavelength for excitation (455 nm) and emission (515 LP). An M Plan APO 50x lens (Mitutoyo America Corporation, Aurora, IL, USA) was used. Fluorescence was recorded with a CCD camera (C 8484-02, Hamamatsu Photonics

Deutschland GmbH, Herschingen, Germany). For visual observation leaflets were labeled 1:100 with NBD-DHPE. Experiments with symmetric and asymmetric bilayers were carried out at 37 °C.

2.17 BIOLOGICAL EXPERIMENTS WITH MYCOBACTERIA

To get the complete picture, besides biophysical research on the activity of different AMPs on mycobacteria mimicking membrane models, also experiments with real mycobacteria were implemented. Experiments were carried out by our collaborators Ulrich Schaible from the Research Center Borstel and Sam Willcocks from the London School of Hygiene and Tropical Medicine in London. *M. tuberculosis* (wild type H37Rv) pre-cultures were grown in 7H9 broth (BD Biosciences, Oxford, UK) with 10 % Middlebrook ADC enrichment (BD Biosciences, Oxford, UK) and 1 % Tween 80 (BD Biosciences, Oxford, UK). For AMP testing 10^6 bacilli were incubated at 37 °C in a 96 well plate in 100 µl purified water: RPMI 1640 (Gibco, Invitrogen, Paisley, UK) 4:1 (v/v). Plates contained 30 µg/ml of either hBD-3-l, LL32 or LL20 or no AMP as a control. When two different peptides were combined, the concentration of each was reduced by half. After 24 hours of incubation serial dilution was performed by repeatedly transferring 10 µl of the lysate to 90 µl of an aqueous solution of 1 % BSA (w/v) (Invitrogen, Paisley, UK), 1 % Tween 80 (v/v). 50 µl of these mixtures were then plated onto Difco Mycobacteria 7H11 agar (BD Biosciences, Oxford, UK) supplemented with Middlebrook OADC enrichment (BD Biosciences, Oxford, UK). Counts of colony numbers were implemented 5 to 7 weeks after plating. Results of these experiments are shown in the Discussion section (Fig. 4.7).

3 RESULTS

3.1 ESTABLISHMENT OF GUVS AS A MEMBRANE MODEL

The implementation of GUVs as a membrane system was a central task of this thesis. GUVs were established as model membranes for various investigations of lipid-lipid and lipid-peptide interactions. The preparation of GUVs from certain lipids (e.g. egg PC) in purified water (Fig. 3.1) was rather straight forward. However, to extend the possibilities of the GUV membrane model, several challenges arose:

- For a model mimicking biological processes GUVs should be suspended in buffer containing salt ions instead of purified water (see paragraph 3.2: GUVs in Buffer).

- Temperature control during the fluorescence microscopic observation of GUVs was necessary to adjust more physiological conditions or trigger certain temperature dependent effects like phase transition of lipids (see paragraph 3.3: Set up of a Temperature Cell).

- GUVs made of lipid compositions similar to those in bacterial membranes needed to be prepared for certain experiments (see paragraph 3.4: PMB-induced Fusion of Vesicles).

- For the investigation of lipid-raft mimicking structures and their interaction with antimicrobial peptides, GUVs with observable SM-cholesterol rich domains needed to be prepared (see paragraph 3.5: Investigation of SM-cholesterol rich Domains in GUVs).

- For an approximation of the membrane model towards mycobacteria or Gram negative bacteria, GUVs with incorporated TDM (see paragraph 3.8.1: Structural Properties of TDM) or LPS (see paragraph 3.6: LPS Containing GUVs and Asymmetric Vesicles) needed to be prepared.

Alterations in preparation techniques and parameters finally led to two different protocols;

- Protocol (i) using ITO covered glass slides as electrodes, applying a constant potential of 1.5 V and a relatively low frequency of 10 Hz during electroformation. This protocol provided good results for uncharged and sufficient results for charged lipids in purified water and was superior, when high concentrations of GUVs were needed.

- Protocol (ii) using platinum wire as electrodes. Here, a 500 Hz field was combined with a stepwise increase in potential. This setup allowed for the preparation of GUVs in purified water as well as in buffer and also succeeded to produce GUVs with incorporated charged lipids and LPS in sufficient quality. TDM containing GUVs could also be prepared, but preparations were often of poor quality. Generally concentrations of GUVs prepared by this protocol were about tenfold lower than with protocol (i).

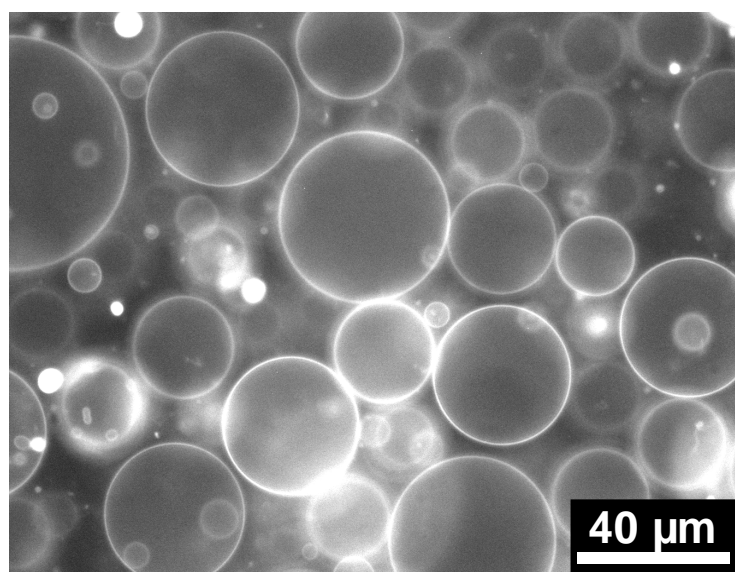For a detailed description of the protocols see Materials and Methods section.

Fig. 3.1**: GUVs made of egg PC were formed in purified water by electroformation using protocol (i).** GUVs were labeled with BODIPY FL-PC in a molar ratio of 1:500 for fluorescence microscopy with an Olympus IX 70 fluorescence microscope. Sample temperature was 21 °C.

3.2 GUVs in Buffer

GUVs are best prepared in purified water, which, however, limits the biological relevance of the model system. Attempts to prepare GUVs in sugar solutions and exchange the outer medium by buffer of same osmotic strength after the preparation have been suggested by *Estes and Mayer, 2005*. This procedure appeared to be time consuming and tricky, because GUVs were easily destroyed due to mechanic and osmotic stress during medium exchange. Furthermore, sugar molecules trapped inside the GUVs could influence the results of later experiments. To avoid these adversities, GUVs were directly prepared in buffer using

protocol (ii). Due to the involvement of electricity during the GUV preparation, the process was dependent on the conductivity of the medium. Solved salt ions increased the conductivity and hindered GUV formation. However, alterations in current and frequency allowed adjusting the protocol for the preparation of GUVs in 10 mM Na-Ph-buffer. GUVs made from natural lipids mixtures like egg PC (Fig. 3.2) as well as mixtures of lipids and cholesterol like DOPC:bSM:cholesterol 2:2:1 (Fig. 3.9) were prepared in 10 mM Na-Ph-buffer at pH 7.4. Preparations using 100 mM KCl, 5 mM Hepes buffer also provided some GUVs, but included many lipid fragments (data not shown). In preparations using protocol (i) with a 10 Hz field very few GUVs were formed in 10 mM Na-Ph-buffer and no GUVs at all developed in 100 mM KCl, 5 mM Hepes buffer (data not shown). The possibility to prepare GUVs in 10 mM Na-Ph-buffer is an improvement of the method, but a systematic tryout of different preparation conditions might lead to further improvement at even higher salt concentrations.
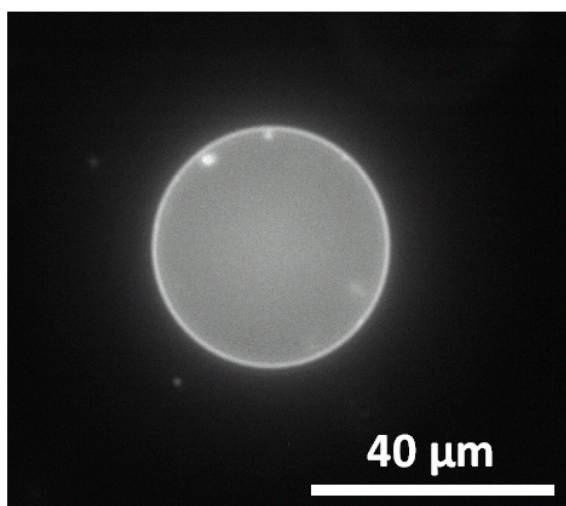
Fig. 3.2**: GUVs made of egg PC formed in 10 mM Na-Ph-buffer prepared by electroformation using protocol (ii).** GUVs were labeled 1:500 with NBD-DHPE for fluorescence microscopy with an Olympus IX 70 fluorescence microscope. Sample temperature was 21 °C.

3.3   SET UP OF A TEMPERATURE CELL

Although most experiments in this work were carried out at room temperature, temperature control was crucial for certain experiments. To be able to adjust the temperature of a GUV solution during fluorescence microscopy, two different homemade temperature cells were constructed. The design of a rather simple temperature cell is shown in Fig. 3.3. A glass slide

carrying the sample was attached to the lower part of the chamber. A hole in the chamber fitted the lens of the inverse fluorescence microscopes. A heating foil attached to the lid of the chamber heated the sample during observation. The foil was regulated by a commercial temperature controller (LCD-Temperatur-Schaltstufe, assembly kit obtained from Conrad Electronic SE, Hirschau, Germany). The temperature cell was only able to heat up the sample, while cooling proceeded passively by heat dissipation. Therefore no temperatures below room temperature could be adjusted. Furthermore, the sample, which was covered by a cover glass, had contact to the air inside the chamber. This led to evaporation of the medium and limited observation times at elevated temperatures to a few minutes. Due to these limitations this temperature cell was only used in the beginning of my thesis as a first prototype, but not for experiments shown in this work.
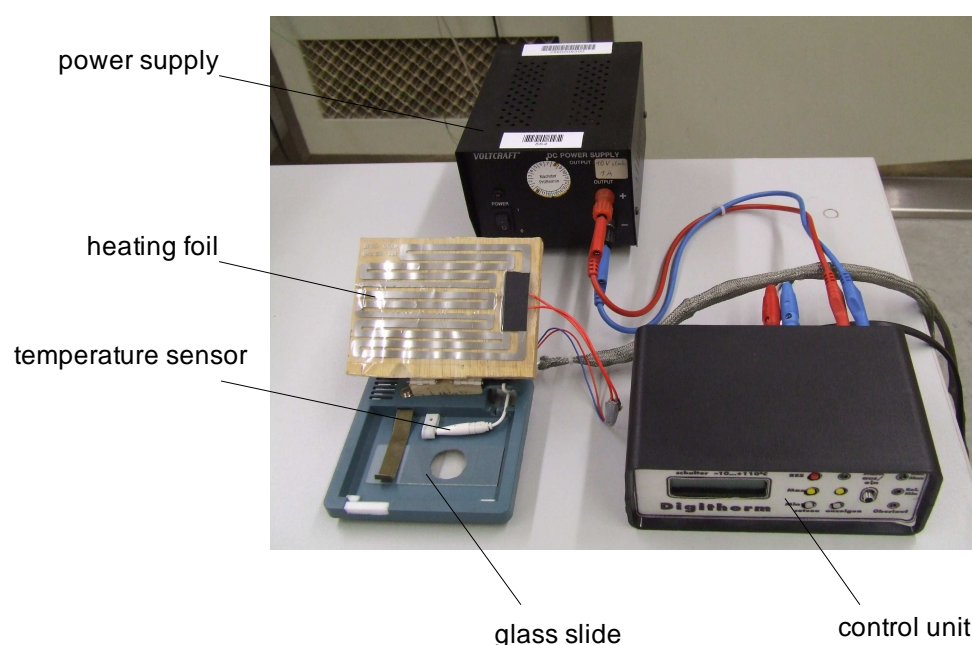

Fig. 3.3**: Set up of a simple temperature cell for fluorescence microscopy.** A temperature sensor next to the sample measured the actual temperature and provided information for the control unit, which compared actual temperature and user-defined set-point. A heating foil regulated by the control unit heated up the sample until the set-point was reached. Temperature range lasted from the actual room temperature up to about 45 °C.

Later a second, more elaborate temperature cell was planned and constructed in cooperation with Sebastian Stengl, an electrical engineering student from the University of Applied Sciences Lübeck. The actual cell consisted of an upper and lower part, which could be screwed together (Fig. 3.4). The upper part contained a hemispheric cavity, which could be covered with a glass slide at the bottom. A latex gasket (isodam, Sigma Dental Systems GmbH, Handewitt, Germany) was placed at the rim between glass and chamber to seal the

cavern. Now, the lower part of the cell was screwed to the upper part, fixing the position of the glass slide. An observation notch in the lower part fitted the microscope lens and allowed viewing the cavity from below. The sealed cavity could be filled with liquid solved samples from a lateral filling opening. The design of the cell was created with the 3D computer-aided design (CAD) solid modeling software Solid Edge V20 (Siemens PLM Software, Plano, TX, USA). The cell was manufactured according to my specifications by µ-Tec GmbH (Chemnitz, Germany).
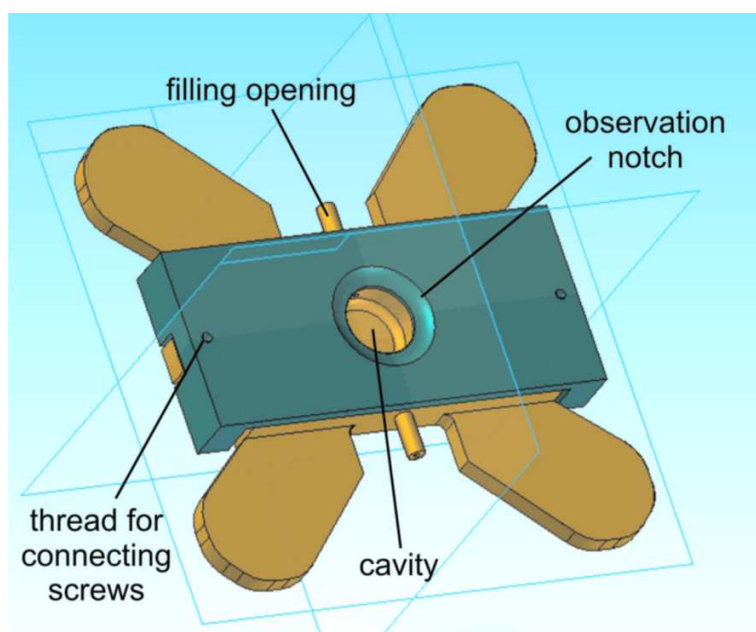

Fig. 3.4: **Construction sketch of the final temperature cell.** The illustration shows the bottom of the cell, which is pointed towards the lens of an inverse fluorescence microscope during experiments. The cavity in the upper (gold colored) part of the cell is thereby covered with a glass slide fixed between upper part and lower (green colored) part. An observation notch in the lower part of the cell allows for observation of the sample in the cavity.

The temperature cell could be actively heated and cooled in a temperature range between about 10 and 60 °C. To do so a sensor unit (PT1000, Conrad Electronic SE, Hirschau, Germany) measured the actual sample temperature and passed the value to a PC using an I/O card (PCI-6036E, National Instruments Germany GmbH, Munich, Germany). Here, a LabVIEW 7.1 (National Instruments Germany GmbH, Munich, Germany) based program, written by Sebastian Stengl, was used to compare the measured actual temperature with a user defined set-point. The software controlled a relay, which adjusted amperage and polarity of a direct current applied to a 27 W peltier element (7105, standard quality, Conrad Electronic SE, Hirschau, Germany). This peltier element was glued to the top of the upper part of the cell. Depending on the direction of current one side of the element became hot

while the other became cold or *vice versa*. By this, the sample chamber could be cooled or heated. Efficient cooling was only possible, when the waste heat was removed from the hot side of the peltier element. In the build device a water-cooling system (Kailon Nemesis 120 Retail, Aquatuning GmbH, Bielefeld, Germany) functioned as a heat sink (Fig. 3.5). Heat was transferred to water, which was flowing through a heat exchange unit on top of the peltier element.
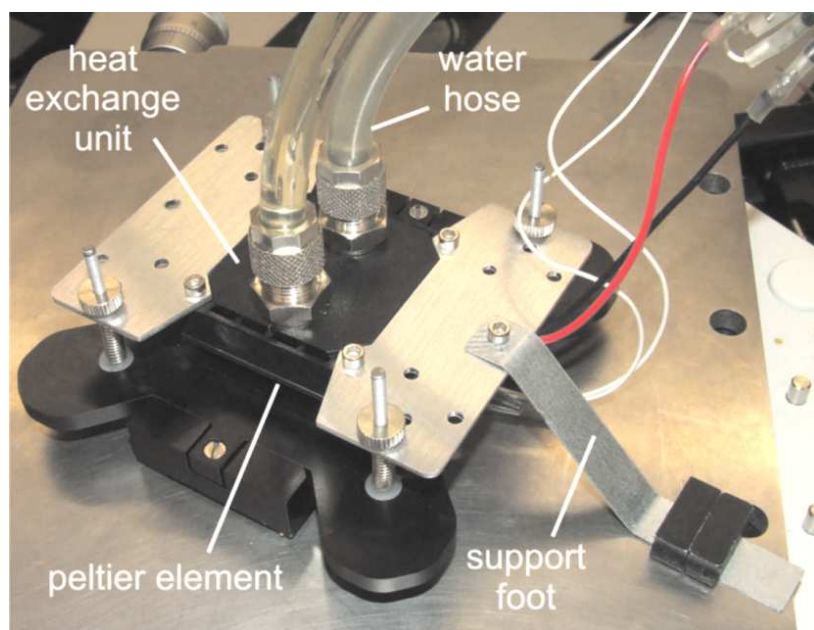
Fig. 3.5: **Setup of the final temperature cell.** The photography shows the temperature cell on top of the sample table of an Olympus IX 70 fluorescence microscope. For temperature control a peltier element was glued to the top of the cell. Excess heat or cold on the upper side of the peltier element was transferred to a heat exchange unit, which was perfused with water.

3.4 PMB-INDUCED FUSION OF VESICLES

One possible mechanism of interaction between lipid membranes and AMPs is peptide-induced fusion. GUVs were used to investigate the fusion inducing properties of the antibiotics PMB and PMBN. Because of their size, GUVs could be used to directly visualize the vesicle fusion and provide a proof of principle. The addition of PMB or PMBN to a mixture of GUVs, which were made of PE:PG 1:1 and either labeled with NBD-DHPE (green) or Rh-DHPE (red), led to the fusion of the vesicle membranes (Fig. 3.6). The mixing of separately prepared vesicles did not cause fusion of vesicle membranes, but showed discrete red or green vesicles (Fig. 3.6 A). However, the addition of PMBN (Fig. 3.6 B) as

well as the addition of PMB (Fig. 3.6 C) at a final peptide concentration of 26 µM was sufficient to induce membrane fusion. Fused GUVs appeared yellow, due to the mixing of the former separated fluorophors NBD and Rh and the superpositioning of their fluorescence. Comparison of PMB and PMBN showed that PMB had a higher activity, resulting in an almost complete aggregation of the vesicles with aggregates mostly 5 to 60 µm in size. PMBN generated only an incomplete fusion of the vesicles. Aggregates resembled those caused by PMB. Although the preceding electroformation has formed some aggregated vesicles too, these unichrome green or red aggregates could be clearly distinguished from the yellowish aggregates formed after addition of PMB or PMBN.
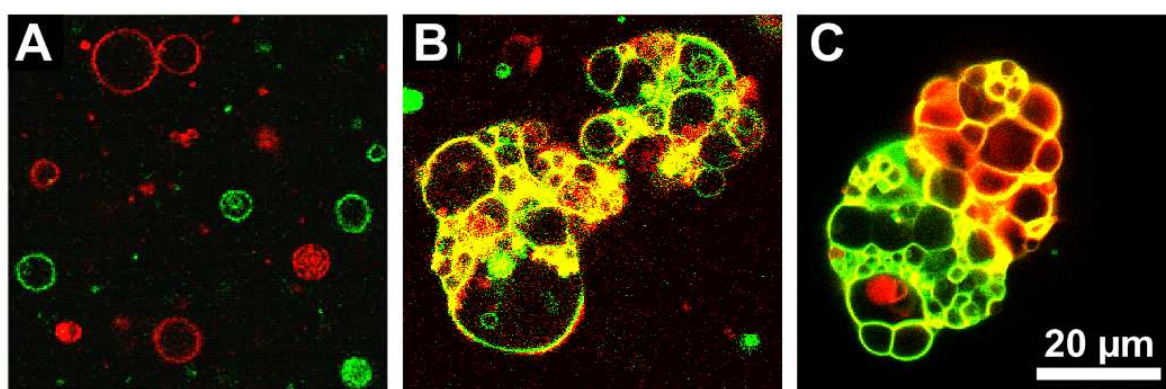

Fig. 3.6 **Addition of PMB or PMBN caused aggregation/fusion of GUVs made of PE:PG 1:1.**
(A): Mixture of equal amounts of 1:500 NBD-DHPE (green) and 1:500 Rh-DHPE (red) labeled vesicles as a control; (B): Addition of PMBN at a final concentration of 26 µM caused a bigger part of the vesicles to aggregate; (C): Addition of PMB in a final concentration of 26 µM to an independent vesicle mixture caused virtually all vesicles to aggregate. All measurements were performed in purified water at 21 °C using a Leica TCS SP1 confocal microscope. NBD and Rh were excited at 488 and 543 nm respectively; fluorescence emission was recorded from 500 to 550 nm or from 580 to 650 nm, respectively. Pictures of NBD and Rh fluorescence were merged for the final pictures. Scale bar is the same for all images. GUVs were prepared using electroformation protocol (i).

3.5 INVESTIGATION OF SM-CHOLESTEROL RICH DOMAINS IN GUVS

Membranes with certain concentrations of sphingomyelin (SM), cholesterol, and a low melting point lipid tend to form domains rich in SM and cholesterol. SM-cholesterol rich domains in artificial membranes are thought to resemble lipid rafts in natural cells (cf. paragraph 1.2.3). To establish a GUV model system for the observation of SM-cholesterol rich domains, GUVs with several lipid compositions have been prepared and observed by fluorescence microscopy. Depending on the used lipid composition SM-cholesterol rich domains did or did not appear in the membranes. Initially a composition of DOPC:bSM:chol

9:9:2 was used for the preparation of GUVs (Fig. 3.7). However, no domains were visible in GUVs, although small domains were observed by means of AFM in solid supported bilayers of this lipid composition (data not shown). In some preparations domains appeared sporadically in a few GUVs, but arose probably due to inhomogeneous lipid mixing. Either domains were too small for observation with an optical microscope or other parameters prevented their emergence.

Fig. 3.7**: GUVs made of 9:9:2 DOPC:bSM:chol did not show any SM-cholesterol rich domains at 21 °C.** GUVs labeled with Rh-DHPE in a molar ratio of 1:500 were prepared by electroformation using protocol (i). GUVs were suspended in purified water. Microscopy was performed using an Olympus IX 70 fluorescence microscope.

In contrast, mixtures with a high ratio of SM and cholesterol easily formed SM-cholesterol rich domains. Fig. 3.8 gives an example of such a preparation with DOPC:bSM:chol in a molar ratio of 3:5:2. In fluorescence microscopic images the SM-cholesterol rich domains appeared dark, because the lipid attached fluorophors were excluded from them. Due to the high rate of SM and cholesterol the dark SM-cholesterol rich domains were more extended, than in vesicles with other lipid compositions. Bright DOPC domains formed within the SM-cholesterol rich domains. Domains were mobile within the lipid matrix. Domain movement, fusions and separations of domains were observed.
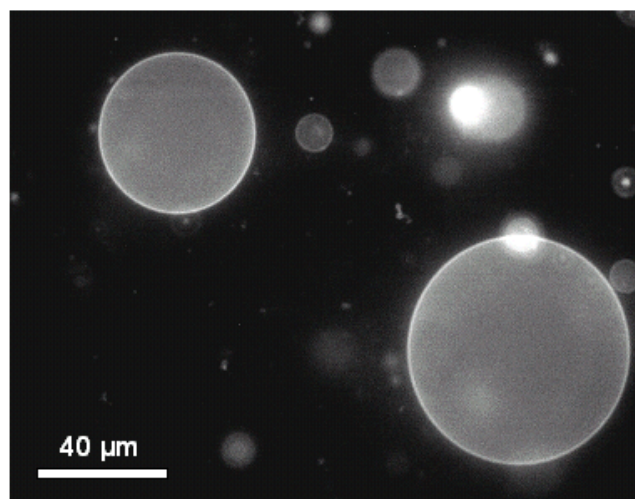
Fig. 3.8**: GUVs made of DOPC:bSM:chol 3:5:2 showed SM-cholesterol rich domains at 21 °C.** GUVs labeled with Rh-DHPE in a molar ratio of 1:500 were prepared by electroformation using protocol (i). GUVs were suspended in purified water. Microscopy was performed using an Olympus IX 70 fluorescence microscope. Fluorophors were excluded from the dark SM-cholesterol rich domains.

GUVs made of DOPC:bSM:chol 3:5:2 were basically suitable for a closer investigation of SM-cholesterol rich domains, but were dismissed because of their unnaturally high content of sphingolipids (van Meer et al., 2008). The domain formation in GUVs made of DOPC:bSM:chol 2:2:1 has been described before (e.g. Veatch and Keller 2003) and own experiments with this composition (Fig. 3.9) showed a good reproducibility. Because this mixture also mirrors the ratio of unsaturated lipids, sphingomyelins and cholesterol in plasma membranes to some extent, it was chosen as a standard for further experiments. Improvements in the preparation protocol also allowed preparing these GUVs in 10 mM Na-Ph-buffer instead of purified water.
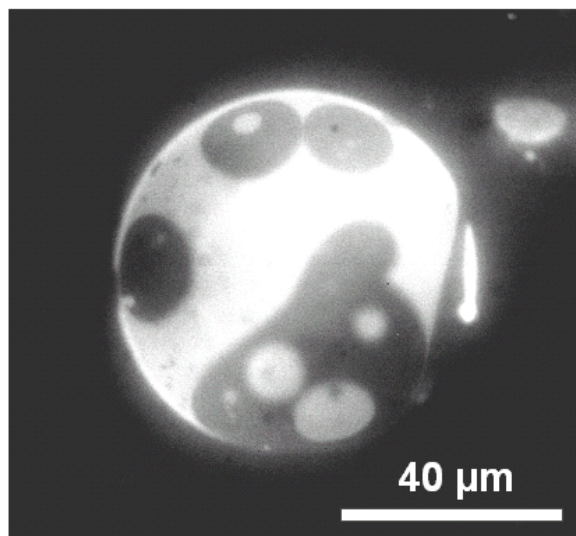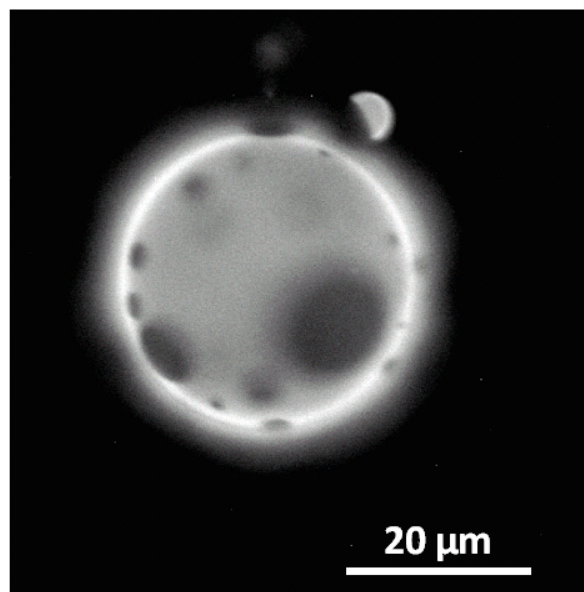
Fig. 3.9: GUVs made of DOPC:bSM:chol 2:2:1 showed SM-cholesterol rich domains at 21 °C.
GUVs labeled with Rh-DHPE in a molar ratio of 1:500 were prepared by electroformation using
protocol (ii). GUVs were suspended in 10 mM Na-Ph-buffer, preparations in purified water showed
no qualitatively different results. Microscopy was performed using an Olympus IX 70 fluorescence
microscope. Fluorophors were excluded from the dark SM-cholesterol rich domains.

After a basic biophysical model for the investigation of SM-cholesterol rich domains has
been set up, antimicrobial peptides were tested for their ability to bind to GUVs and possibly
alter the domain structure. As SM-cholesterol rich domains give a raw model for lipid rafts
in natural cells, substances, which are able to change these domains, could also possibly
interfere with lipid rafts. These raft-peptide interactions could have an dramatic effect on
cellular function, as lipid rafts are thought to be involved in many cellular processes like
sorting of membrane proteins and immune receptor signaling (Rajendran and Simons, 2005).
Therefore, non toxic substances, being able to prevent or induce lipid raft formation, could
be used as drugs with e.g. anti-inflammatory effects. Fig. 3.10 shows the formation of SM-
cholesterol rich domains in fluorescent GUVs made of DOPC:bSM:chol 2:2:1 and the
binding of different fluorescent AMPs to these vesicles. The simultaneous use of two
different types of fluorophors required the utilization of a Leica TCS SP1 confocal
microscope, which allowed discriminating between vesicle and peptide derived fluorescence.
Due to the low depth of field of this microscope, it was impossible to depict the entire
vesicle at once. Thus, a cross section through the spherical vesicles was recorded. In the
confocal images untreated GUVs appeared as open circles, because the lipid attached
fluorophors (either Rh or NBD) were excluded from membrane regions occupied by SM-
cholesterol rich domains (Fig. 3.10 A). The varying labeling of the vesicles with NDB or Rh
was necessary because the used AMPs were differently labeled with either NDB or Rh. Rh
labeled peptides were used with NDB labeled vesicle and *vice versa* to separate peptide and

vesicle related signals. Domains in the vesicles usually covered about an eighth to a third of the membrane. The addition of 10 µM LL32-NBD to the GUV solution led to a binding of the LL32 to the vesicle membrane, which was limited to areas outside the SM-cholesterol rich domains (Fig. 3.10 E, F). Binding of the LL32 occurred within seconds after addition and caused a minor part of the GUVs to collapse. Within 15 min bound LL32 did not cause any visible changes in the size and shape of the SM-cholesterol rich domains of intact GUVs (Fig. 3.10 D). Independent experiments with 2 µM NK-2-NBD, 10 µM hBD-3-l-Rh or 10 µM L-Pep 19.2-5-Rh provided similar results for these peptides (Fig. 3.10, G-I, overlay of NBD and Rh channels shown solely). NK-2 appeared to have a stronger effect on membranes of this lipid composition as compared to the other investigated AMPs. At 10 µM NK-2 destroyed all vesicles (data not shown), hence a concentration of 2 µM was used. In all experiments the added AMPs bound to regions of the GUV membrane outside the SM-cholesterol rich domains and destroyed a certain part of the GUVs. In intact GUVs no vanishing of the domains was observed.
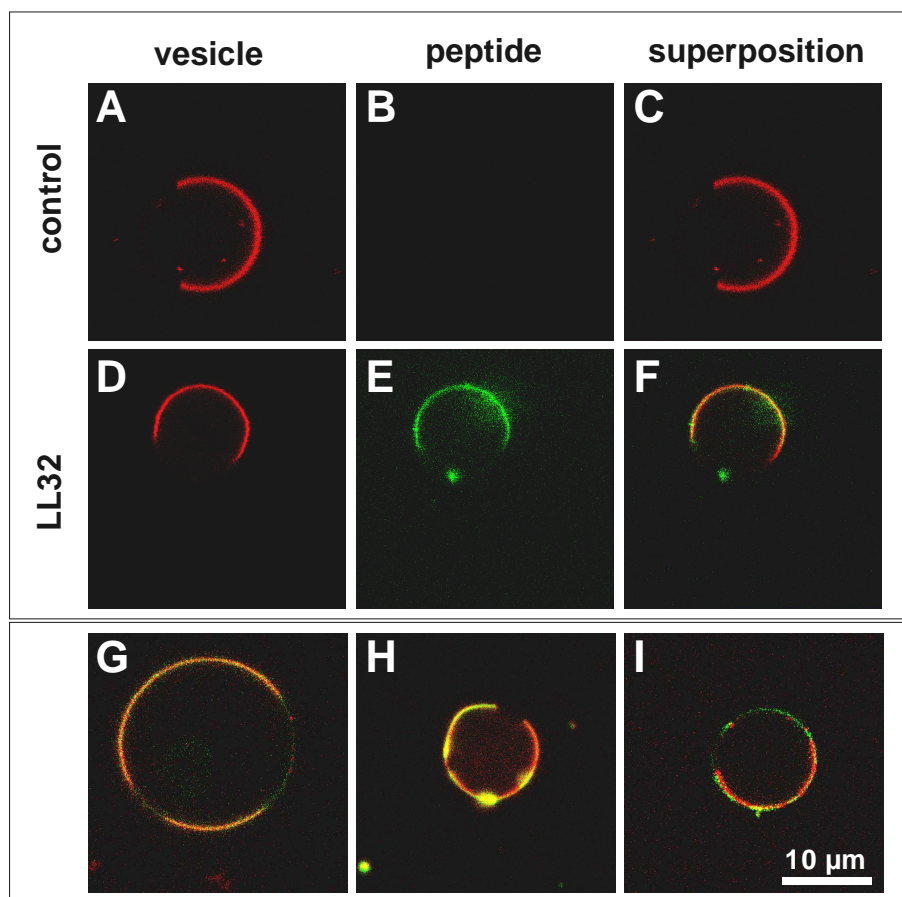
Fig. 3.10: **Different AMPs were able to bind to GUVs made of DOPC:bSM:chol 2:2:1 but did not cause any visible changes in the domain structure.** GUVs were labeled 1: 500 with either NBD-DHPE or Rh-DHPE. (A): Rh fluorescence of an untreated GUV exhibiting a SM-cholesterol rich domain at the left; (B): Channel of the fluorescent peptide, dark in the control measurement, where no peptide was added; (C): Superposition of A and B; (D): Rh fluorescence of an LL32-NBD treated GUV exhibiting a SM-cholesterol rich domain in the lower part; (E): Fluorescence of the added LL32-NBD; (F): Superposition of D and E illustrates that peptide binding was limited mostly to areas outside the SM-cholesterol rich domain; (G-I): Superposition of vesicle and peptide fluorescence of (G): NBD labeled GUVs with L-Pep 19.2-5-Rh; (H): Rh labeled GUVs with NK2-NBD; (I): NBD labeled GUVs with hBD-3-l-Rh; No changes in domain size or shape were observed after addition of the different peptides. All experiments were carried out at about 25 °C in 10 mM Na-Ph-buffer using a Leica TCS SP1 confocal microscope. Final AMP concentration was 10 μM except for NK-2 (2 μM). Scale bar is the same for all images. GUVs were prepared by electroformation protocol (ii).

3.6 LPS Containing GUVs and Asymmetric Vesicles

As shown before (Fig. 3.6 A) GUVs made of the bacterial lipid PE and PG could be prepared and used as a membrane model. To shift this model towards the LPS containing outer membrane of Gram negative bacteria (Fig. 1.6), GUVs made of PE, PG and LPS R45 in a ratio of 2:2:1 were prepared (Fig. 3.11). Preparations contained aggregated structures but also many intact GUVs, which possessed dark domains on their surface. These areas represented LPS domains, from which the lipid attached fluorophor Rh-DHPE was excluded. Domains were stable at room temperature as well as at 37 °C (data not shown). Although LPS containing GUVs could be prepared, this method was not extensively used for further experiments with AMPs, because in the meantime an even more promising model of asymmetric vesicles arose.
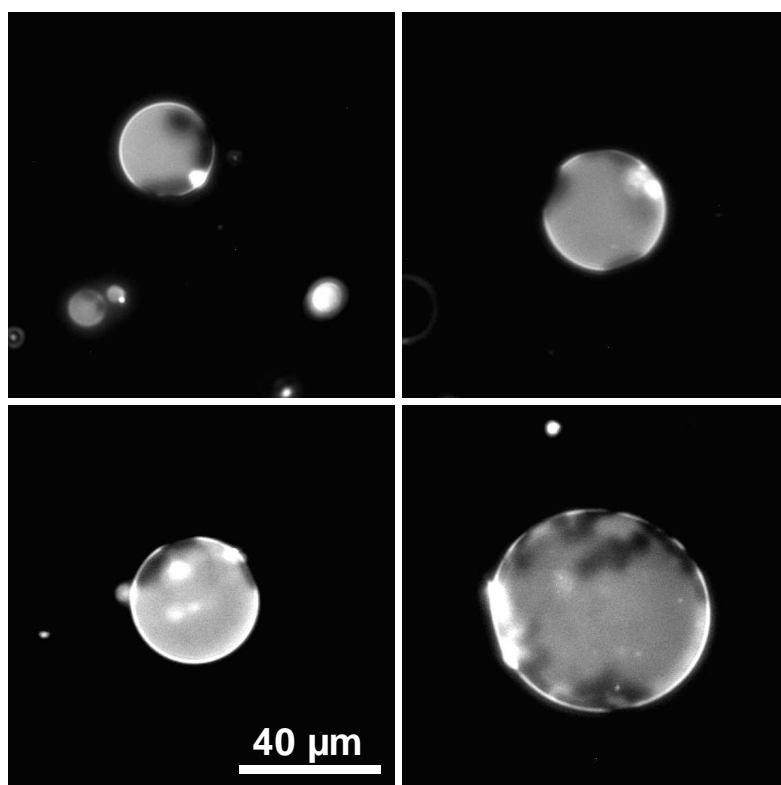

Fig. 3.11**: PE:PG:LPS R45 2:2:1 GUVs exhibited dark LPS domains.** Fluorescence microscopic images of 1:100 Rh-DHPE labeled GUVs in purified water using an Olympus IX 70 fluorescence microscope. GUVs were prepared by electroformation protocol (ii). Sample temperature was 20 °C. Scale bar is the same for all images.

While phospholipids and LPS formed lateral domains within the LPS containing GUVs, asymmetric vesicles consisted of an inner phospholipid monolayer (inner leaflet) and an outer LPS monolayer (outer leaflet). This setup resembled the outer membrane of Gram negative bacteria better. A method for the preparation of asymmetric phospholipid/phospholipid vesicles was first described by *Pautot et al., 2003*, adopted for the preparation of LPS/phospholipid asymmetric vesicles by my coworker Annemarie Brauser and later used and slightly modified by me. In the beginning of our work with asymmetric vesicles Annemarie Brauser and I developed an experiment, which proved the asymmetry of our vesicles. Asymmetric vesicles made of the LPS R45 on the outside leaflet and a phospholipid mixture of PE:PG:DPG 81:17:2 (w/w/w) (abbreviated PL for phospholipids) on the inside leaflet were prepared twice. In one preparation fluorescent FITC-R45 was added to the LPSs in the outer leaflet (Fig. 3.12 A, a). In the other preparation the fluorophor FITC-PE was mixed with the lipids, which later formed the inner PL leaflet (Fig. 3.12 C, c). During confocal microscopy the fluorescence quencher KI was added to the two samples. In case of outer leaflet labeling, KI was able to quench the fluorescence of the vesicles virtually completely (Fig. 3.12 B, b). The small insert in Fig. 3.12 (B) shows the presence of the vesicle in phase contrast, proving that it had not been destroyed by the quencher but lost its fluorescence. In case of inner leaflet labeled vesicles the fluorescence remained unquenched after the addition of KI (Fig. 3.12 D, d). Here, the external application of KI did not affect the fluorescence of the FITC in the inner leaflet, which was shielded by the outer leaflet. This experiment demonstrated that we were able to selectively place a lipid attached fluorophor into the inner or outer leaflet of a vesicle. It is reasonable to assume, that the evenly treated LPS and lipid molecules also attained defined positions in the inner or outer leaflet.
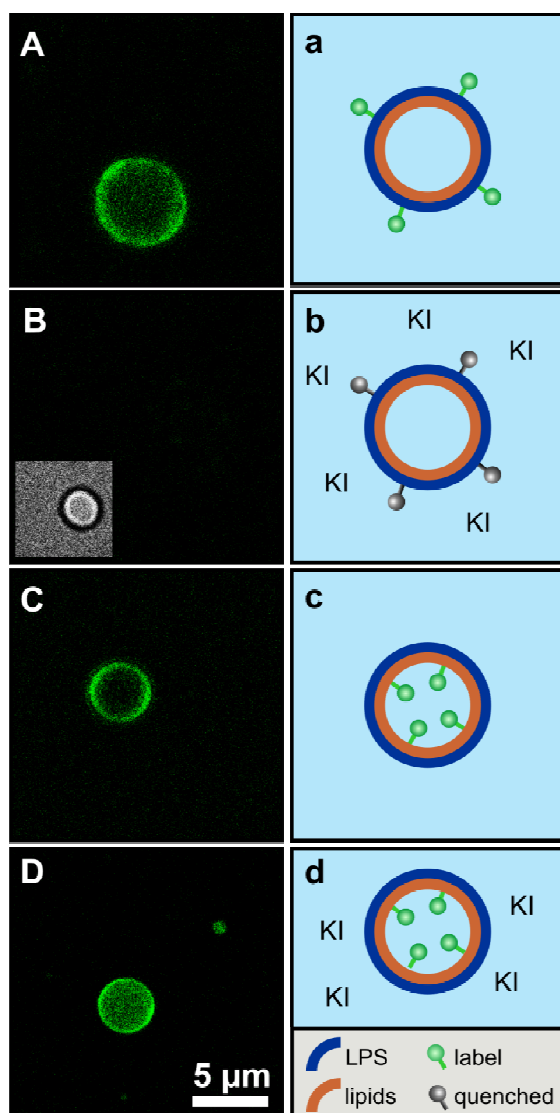
Fig. 3.12**: Addition of the fluorescence quencher KI demonstrated the asymmetry of differently labeled LPS R45/PL vesicles.** (A, a): Asymmetric vesicles with LPS R45 in the outer leaflet and PL (PE:PG:DPG 81:17:2 w/w/w) in the inner leaflet; 5 % (w/w) of the LPS R45 in the outer leaflet were fluorescent FITC-LPS R45; (B, b): Quenched fluorescence of the vesicles in (A) after the addition of KI. The small insert shows the vesicle in phase contrast; (C, c): Asymmetric vesicles with LPS R45 in the outer leaflet and PL in the inner leaflet; 2 % (w/w) of the PL in the inner leaflet were fluorescent FITC-PE; (D, d): Vesicles in (C) after the addition of KI. The fluorophors in the inner leaflet were protected from quenching. Experiments carried out at 25 °C in 100 mM KCl, 5 mM MgCl$_2$, 5 mM Hepes buffer (pH 7) using a Leica TCS SP1 confocal microscope. Final KI concentration was 0.83 M; Scale bar is the same for all images. Samples prepared and investigated in cooperation with Annemarie Brauser.

Further experiments involved the effect of AMPs on asymmetric vesicles as a model for the outer membrane of Gram negative bacteria. Asymmetric LPS R45/PL vesicles were labeled with FITC-PE on the inside leaflet and treated with fluorescent LL32-Rh at a final concentration of 38 nM. Additionally the FITC quencher KI was added to the medium. Fluorescence emission was recorded back-to-back on two channels; one for the FITC fluorescence (Fig. 3.13 A) and one for the Rh fluorescence (Fig. 3.13 B). Fig. 3.13 (A) and (B) pictured the same two vesicles, from which the one on the left possessed an average FITC fluorescence and an average Rh fluorescence. The right vesicle, on the contrary, showed a weak FITC fluorescence and a strong Rh fluorescence. This observation is best explained as follows; the left vesicle in Fig. 3.13 (A) and (B) has taken up some LL32-Rh but stayed undamaged, by which the FITC labels in the inner leaflet were still shielded from the KI. The right vesicle, however, has heavily taken up LL32-Rh, by which the membrane was permeabilized, allowing KI to enter the lumen of the vesicle and quench the FITC fluorescence of the inner leaflet. The super positioning of Fig. 3.13 (A) and (B) is shown in Fig. 3.13 (C). The cartoon in Fig. 3.13 (D) illustrates the setup.
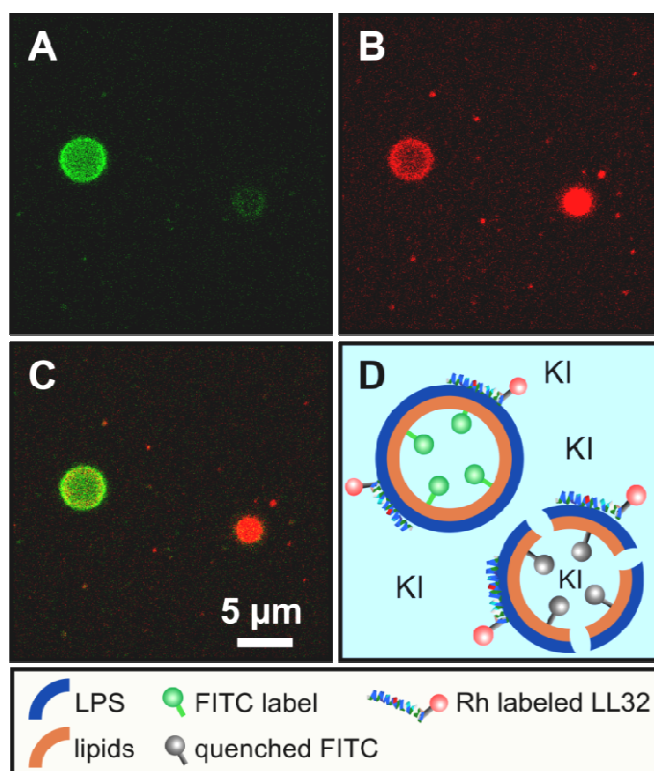
Fig. 3.13**: Asymmetric LPS R45/PL vesicles were partly permeabilized by 38 nM LL32.** For fluorescent labeling of the vesicles 2 % (w/w) of the PL in the inner leaflet were fluorescent FITC-PE. Images show the vesicles after incubation with 0.83 M KI and 38 nM LL32-Rh. (A): FITC fluorescence; (B): Rh fluorescence; (C): Superposition of A and B; (D): Illustration of the experiment. The left vesicle had taken up less LL32-Rh, remained intact and therefore exhibited unquenched FITC fluorescence from its inner leaflet. The right vesicle had taken up more LL32-Rh, was permeabilized and partly quenched by invading KI. Experiments were carried out at 25 °C in 100 mM KCl, 5 mM MgCl$_2$, 5 mM Hepes buffer (pH 7) using a Leica TCS SP1 confocal microscope. Scale bar is the same for (A), (B) and (C).

Besides the effect of LL32-Rh, also the AMPs LL32-4A-Rh and hBD-3-l-Rh were tested for their activity against LPS R45/PL asymmetric vesicles in an equivalent way. Fig. 3.14 (A) and (B) show the FITC and Rh fluorescence of an LPS R45/PL vesicle in presence of 38 nM LL32-4A-Rh and KI as a quencher. The unquenched green fluorescence in Fig. 3.14 (A) derived from the inner FITC labeled leaflet of the vesicle, indicating that the added LL32-4A-Rh had not permeabilized the bilayer. Fig. 3.14 (B) pictures the distribution of the fluorescent LL32-4A, which has bound evenly to the membrane of the vesicle. Thus, LL32-4A was able to bind to LPS R45, but did not permeabilize the membrane at the given concentration. Fig. 3.14 (C) and (D) show the FITC and Rh fluorescence of a LPS R45/PL vesicle in presence of 38 nM hBD-3-l-Rh and KI as a quencher. Here, the addition of the AMP destroyed virtually all vesicles in the sample, by which the FITC labels of the inner vesicle leaflet were exposed to the KI and quenched (Fig. 3.14 C). The fluorescent hBD-3-l

and vesicle fragments spread onto the glass slide, causing a fluorescent film in the background (Fig. 3.14 D).
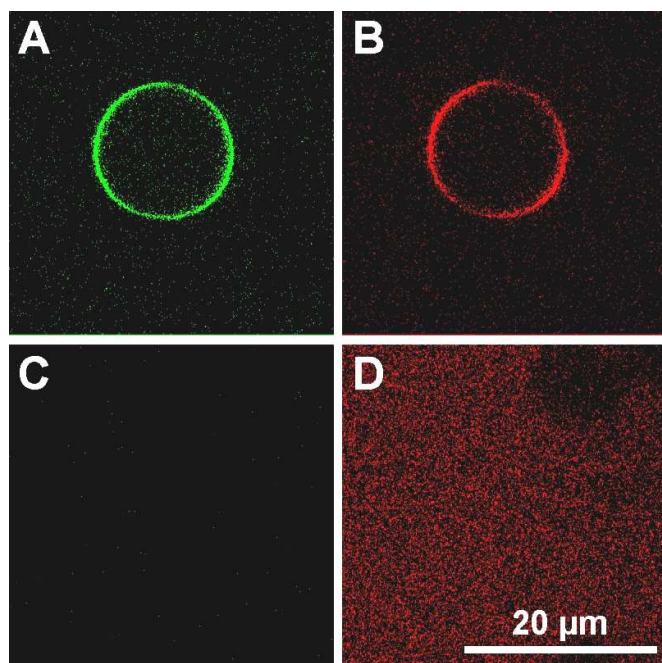
Fig. 3.14**: Asymmetric LPS R45/PL vesicles remained intact after LL32-4A treatment but were destroyed by hBD-3-l.** For fluorescent labeling of the vesicles 2 % (w/w) of the PL in the inner leaflet were fluorescent FITC-PE. (A): FITC fluorescence of LL32-4-A-Rh treated but still intact vesicles; (B): Rh fluorescence of LL32-4-A-Rh treated vesicles shows that the AMP has bound to the vesicle membrane; (C): Quenched FITC fluorescence of hBD-3-l-Rh treated vesicles. Virtually all vesicles in the sample were destroyed; (D): Disperse Rh fluorescence after hBD-3-l-Rh addition to vesicles. Experiments carried out at 25 °C in 100 mM KCl, 5 mM MgCl$_2$, 5 mM Hepes buffer (pH 7) using a Leica TCS SP1 confocal microscope. KI concentration: 0.83 M; LL32-4-A-Rh or hBD-3-l-Rh concentration: 38 nM. Scale bar is the same for all images.

3.7   INTER LEAFLET COUPLING IN SYMMETRIC AND ASYMMETRIC MEMBRANES

Besides the investigation of AMP effects, asymmetric vesicles were used as a novel tool for research on thermodynamic coupling between the inner and outer membrane leaflet. Our aim was to investigate the occurrence of gel/liquid-crystalline phase separations in one leaflet of a bilayer in dependence on the influence of the other leaflet. To gain a better understanding of the phase behavior of the used lipids and LPSs, their phase transition temperatures were measured by IR spectroscopy. Phase transitions were concluded from the absorption maxima

of the CH$_2$ symmetric stretching vibrations of the samples alkyl chains. Lipids and LPSs were prepared as SUVs by means of sonication. For LPSs it is, however, unlikely that the prepared structures constituted vesicles, as the extended alkyl chains probably triggered the formation of inverted structures. Furthermore, the sonication method did not allow creating defined compositions of outer and inner leaflet. It is assumed that the used molecules were distributed randomly between the vesicle leaflets. The phase transition of the PL (PE:PG:DPG 81:17:2 w/w/w) lipid mixture could not be determined directly, but the relatively high wavenumbers showed that the sample existed in a fluidic state over a broad range of temperatures (Fig. 3.15, black squares). LPS R45 showed a phase transition at 50 °C (Fig. 3.15, grey triangles), while PL:LPS R45 1:1 mixtures changed phase at about 40 °C (Fig. 3.15, dark-grey circles). Phase transition occurred where the graphs had the steepest increase in wavenumber. Results showed that the addition of fluidic PL changed the phase transition of LPS R45 from 50 °C to about 40 °C and also increased the overall fluidity of the sample. It was not jet possible to measure the phase transition of asymmetric LPS R45/PL vesicles as used in Fig. 3.12, because the preparation protocol provided only insufficiently low vesicle concentrations for IR spectroscopic measurements.
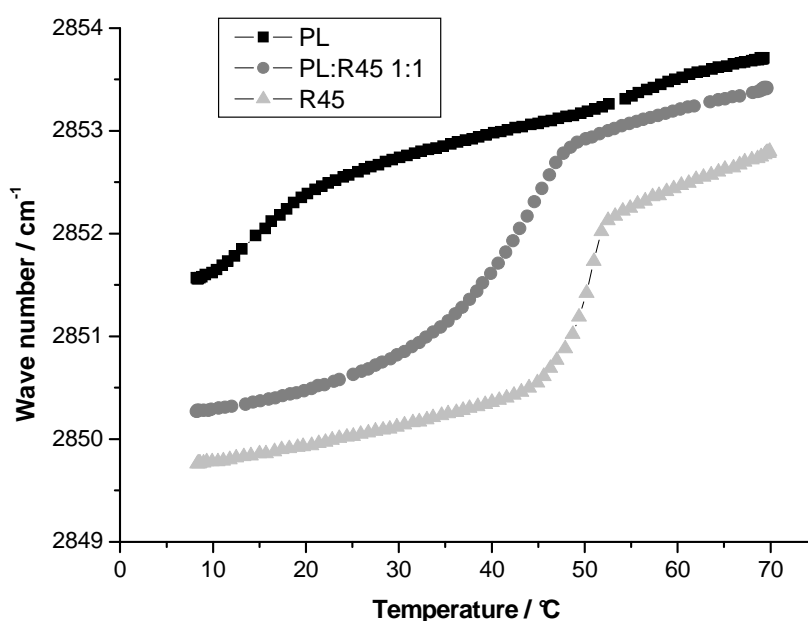
Fig. 3.15: **FTIR spectroscopy showed a shift in LPS R45 phase transition when mixed with phospholipids.** The absorption maximum of CH$_2$ symmetric stretching vibrations from the sample alkyl chains shifts to higher wavenumbers at elevated temperatures. LPS R45 showed a phase transition at 50 °C, which was altered to lower temperatures in PL:LPS R45 1:1 mixed samples due to the influence of fluidic PL. LPS and lipid concentrations were 20 mM; buffer: 100 mM KCl, 5 mM MgCl$_2$, 5 mM Hepes (pH 7).

The newly established preparation protocol for asymmetric vesicles allowed creating symmetric and asymmetric vesicles for the investigation of inter-leaflet coupling. Vesicles were fluorescently labeled with Rh-DHPE, a fluorophor that favors a fluid (liquid-crystalline) environment and is excluded from more ordered gel and liquid-ordered domains. The aim of these experiments was to figure out, if phase separations in one leaflet could be prevented by the influence of the other leaflet. Confocal microscope showed vesicles composed of LPS R45 in the outer and PL in the inner leaflet (LPS R45/PL) not exhibiting any domains (Fig. 3.16 A, a), while LPS R45/LPS R45 symmetric vesicles clearly showed stripe- and patch-shape domains (Fig. 3.16 B, b). This indicates that LPS R45 phase separates into a more solid and a more liquid phase at room temperature and that this phase separation can be prevented in the outer leaflet of asymmetric vesicles, when the inner leaflet consists of highly fluidic PL. These results were in agreement with data from collaborators derived from AFM measurements on solid supported bilayers (Fig. 4.1) and fluorescence microscopic investigations of planar lipid bilayer (Fig. 4.2) also showing a strong coupling between inner and outer leaflets of bilayers.
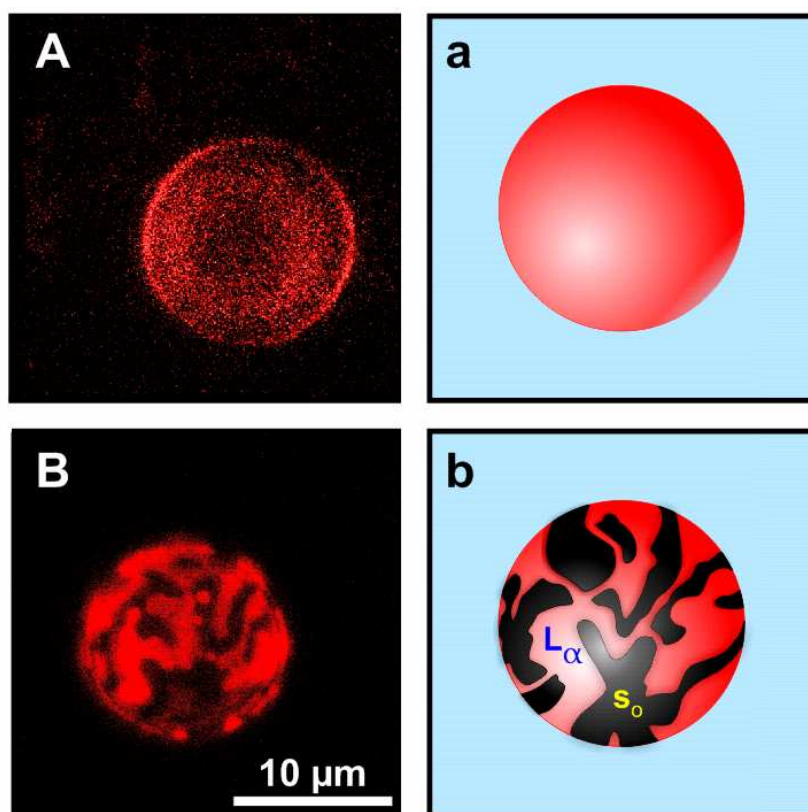
Fig. 3.16**: Phase separation of the outer leaflet of unilamellar vesicles was depending on the inner leaflet.** (A): In LPS R45+Rh-DHPE / PL asymmetric vesicles the outer LPS R45 leaflet was prevented from phase separation by interactions with the fluidic inner PL leaflet; (B): LPS R45+Rh-DHPE / LPS R45+Rh-DHPE symmetric vesicles were phase separated in the outer as well as in the inner leaflet, exposing stripe and patch shaped domains. L_α: liquid-crystalline phase; s_o: gel phase; All experiments were carried out at about 25 °C in 100 mM KCl, 5 mM $MgCl_2$, 5 mM Hepes buffer (pH 7) with a Leica TCS SP1 confocal microscope. Fluorescent leaflets contained 1:100 Rh-DHPE. Multiple confocal images of a z-stack were merged to generate the final pictures. Scale bar is the same for both images. All vesicles were prepared according to the preparation protocol for asymmetric vesicles.

3.8   THE ROLE OF TDM IN MEMBRANES

The major part of this work dealt with the properties of the mycobacterial glycolipid trehalose dimycolate (TDM). While a multitude of evidence for the connection between mycobacterial virulence and TDM exists (cf. paragraph 1.4.1), the biophysical basis of these findings is less well understood. Research in this work was focused on two aspects; the organization of TDM within lipid bilayers and the interactions of TDM with antimicrobial peptides. The biophysical results dealing with the setup of TDM layers and the incorporation of TDM into lipid bilayers led to new ideas about the possible organization of TDM within the mycobacterial outer membrane. For investigation of TDM-AMP interactions, several peptides were tested for their activities against mycobacteria mimicking structures. Results affirmed the peculiar role of TDM. Investigations dealt with pure TDM aggregate as well as with mixtures of TDM and DOPC or PE:PG. For research on the interactions of TDM with AMPs, the lipids PE and PG were most of the times favored over eukaryotic PC to form the lipid matrix, because of their occurrence in bacterial membranes (Epand and Epand, 2011).

3.8.1   STRUCTURAL PROPERTIES OF TDM

At the beginning of this thesis some experiments about the structural properties of TDM in monolayers had already been realized in our workgroup. Langmuir-Blodgett films of pure phospholipids or mixtures of phospholipids and TDM were prepared and investigated by AFM. By this, the topography of the sample was recorded, revealing height differences derived from the different sizes of TDM and phospholipids. The results of these measurements (Fig. 4.3) are discussed together with my own data in the Discussion section. I continued our research on the TDM structure by AFM experiment on solid supported bilayers. To prepare these bilayers, vesicles made of pure phospholipids or mixtures of phospholipids and TDM were spread onto a solid support by absorption from vesicle suspensions. While pure DOPC bilayer appeared plain (Fig. 3.17 A), mixed bilayers of DOPC:TDM in a ratio of 1:1 (w/w) showed stable TDM domains within the lipid matrix (Fig. 3.17 B; height profile b). TDM domains usually appeared to be about 5-7 nm higher when compared to the DOPC bilayer. With the DOPC bilayer considered to be about 4 nm thick (Lewis and Engelman, 1983), the overall thickness of the TDM domains was about 9 to 11 nm. Besides the basic height level of a single TDM bilayer, TDM domains were able to form multilayers with heights of over 20 nm over the level of the phospholipids. The great variation in the height profiles of these piled up domains indicated that these structures were not set up as defined lamellar layers, but were rather disordered above the basic bilayer. TDM domains were not only stable over time, but also did not dissolve when the sample was

heated up to 37 °C (simulated body temperature, data not shown) or even 41 °C (simulated fever, Fig. 3.17 C; height profile c). However, the amount of "excess" TDM piled up on top of the basic height level was reduced, when the sample was warmed up. This finding, again, promotes the idea that those TDM molecules located above the basic bilayer are rather disordered and loosely associated.
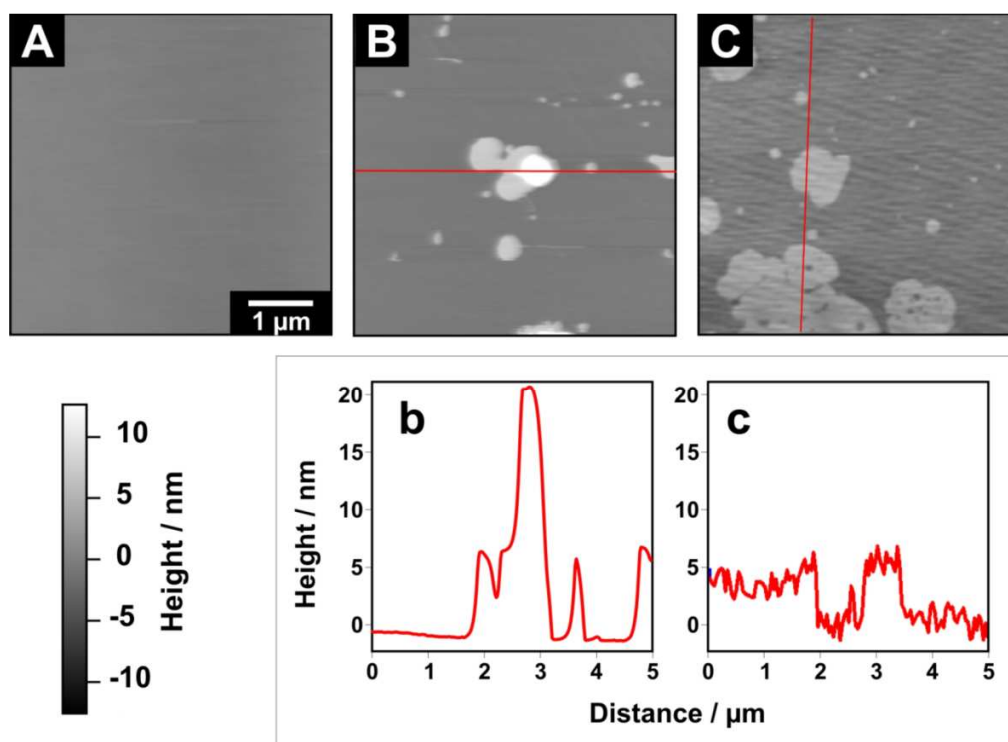
Fig. 3.17**: Topographical AFM images of a DOPC:TDM bilayers showed TDM domains at 20 ° C and 41 ° C.** (A): Plain DOPC bilayer; (B): DOPC:TDM 1:1 (w/w) bilayer with TDM domains at 20 °C; (C): DOPC:TDM 1:1 (w/w) bilayer with TDM domains at 41 °C. Ripples in image C were due to instrumental noise. Images taken in 100 mM KCl, 5 mM Hepes buffer (pH 7), scan speed 25 µm/s. Cantilever RC 800 PSA2, nominal spring constant 0.76 N/m. Scale bar is the same for all images.

Attempts to create planar TDM layers by spreading of pure TDM from vesicles/aggregates onto a solid support failed (data not shown). The recorded topography of mica, which was incubated with a solution of TDM aggregates, was not significantly different from untreated mica. This indicates that no TDM had spread on the surface. Attempts to create TDM multilayers by air drying of chloroform-solved TDM, as described in paragraph 2.11, led to the formation of incomplete films. AFM measurements in air showed that many closely located TDM spots with a height of up to about 70 nm had formed (Fig. 3.18). TDM spots appeared to be slightly leveled off, creating a plane fringe around each spot. In this area the

TDM might have spread as an ordered mono- or bilayer on top of the solid support. But after all the tendency to self aggregate prevailed, binding most of the TDM in the spots.
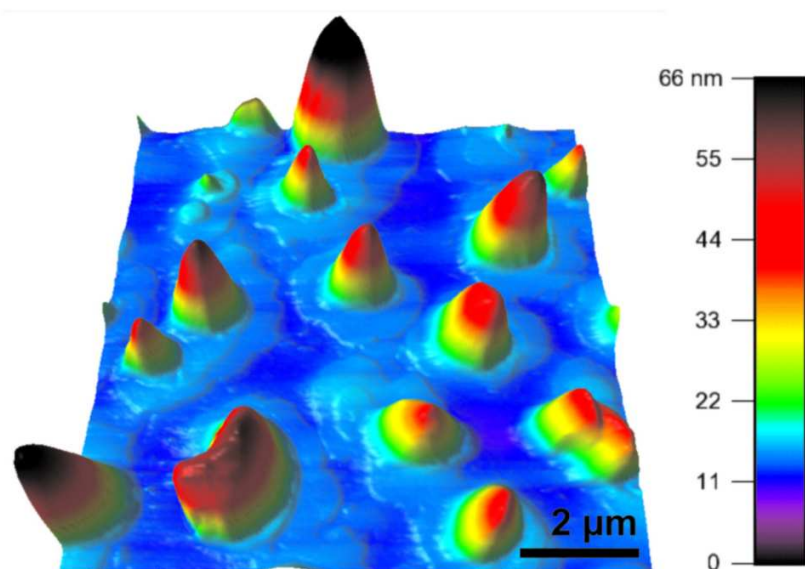
Fig. 3.18: Dried TDM did not form closed solid supported layers but aggregated structures.
TDM spread on mica by evaporation of a chloroform solution. Contact mode AFM measurement in air, temperature 20 °C; cantilever RC 800 PSA2, spring constant 0.48 N/m. Scan speed 25 µm/s.

For a determination of the respective phase transition temperatures, SUVs made of phospholipids, TDM and mixtures of phospholipids and TDM were prepared by sonication. The exact structure of small TDM agglomerations in solution is unknown. From the chemical structure of TDM, however, an existence as vesicles is rather unlikely, as the alky chains are relatively extended and previous experiments already showed its tendency to aggregate. It is therefore not clear, if the investigated TDM structures constituted SUVs, inverted structures or less ordered aggregates. For measurement of the phase transition temperature, the absorption maximum of the sample´s CH_2 symmetric stretching vibration was plotted against temperature (Fig. 3.19). From this data the highest point in the first derivative provided the phase transition, as listed in the following: PE:PG 1:1 (w/w) 8.9 °C; PE:PG:TDM (45:45:10) (w/w/w) 6.8 °C and 34.5 °C; PE:PG:TDM (25:25:50) (w/w/w) 33.7 °C; pure TDM 38.1 °C. Interestingly, the mixed system PE:PG:TDM (45:45:10) showed two phase transitions, one at 6.8 °C for the phospholipids and one at 34.5 °C for the TDM. In the other mixed system PE:PG:TDM (25:25:50) only one phase transition appeared at 33.7 °C. Results showed that TDM was able to shift the melting point of phospholipid mixtures towards higher temperatures. The phase transition temperature of pure TDM aggregates appeared to be at 38.1 °C, but it is unclear, if this value also applies for TDM on a solid support. If so, the pictured TDM domains at 41 °C in Fig. 3.17 (C) would be in the fluid

state as well as the surrounding phospholipids and domain formation could not be explained by a solid-fluid phase separation.
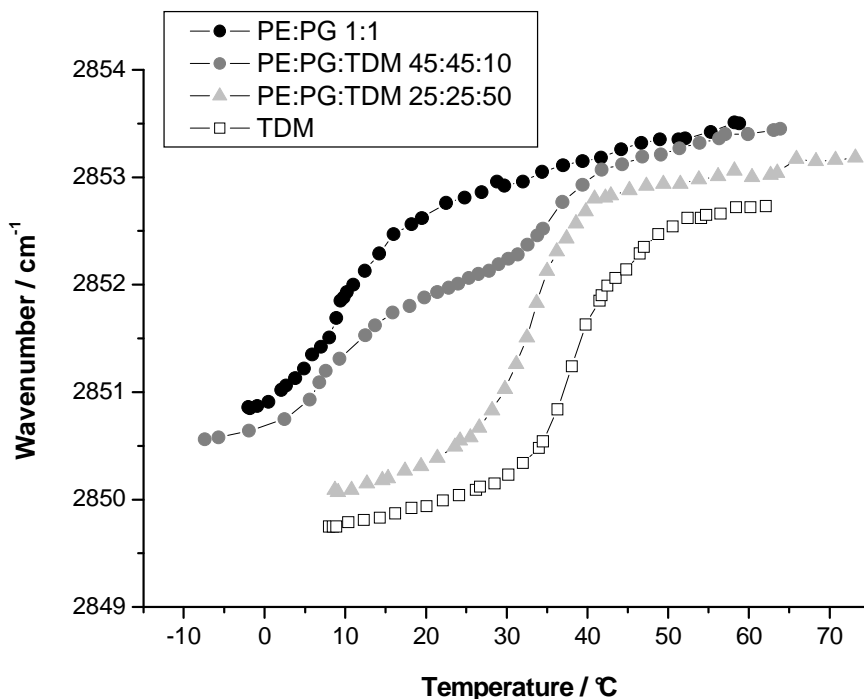
Fig. 3.19: **FTIR spectroscopy showed the phase transition temperatures of TDM, phospholipids, and mixtures thereof.** The absorption maximum of CH_2 symmetric stretching vibrations from the sample alkyl chains shifted to higher wavenumbers at elevated temperatures. The steepest increase in the graph indicates the phase transition temperature. Buffer 100 mM KCl, 5 mM Hepes (pH 7); sample concentration 20 mM.

Besides topographical images, also AFM force spectroscopic measurements were performed on DOPC:TDM bilayers. Force spectroscopy was carried out at various positions on the sample. Two representative curves are depicted in Fig. 3.20. Results showed that TDM domains had a higher mechanical stability compared to the phospholipids. By lowering the tip of the cantilever towards the mica, a significant higher force was needed to penetrate a TDM domain, compared to the force needed to penetrate the DOPC bilayer. A force graph recorded on the DOPC bilayer (black graph) showed an increase in force when the cantilever touched the bilayer, while a characteristic break trough kink appeared at about 4 nN. This kink came into being, when the movement of the cantilever was fist hindered by the surface of the bilayer and continued rapidly, when the cantilever penetrated the bilayer. In contrast to DOPC bilayers, the penetration of TDM domains occurred at a higher force of about 10

nN (red graph). After the penetration of the samples the cantilevers hit the solid support on which the samples rested, leading a massive increase in force. Thus, about 2.5 times higher forces are needed to penetrate the TDM domains compared to the DOPC bilayer. It has to be mentioned that the absolute force values depend on the tip geometry and can therefore only be compared within the same experiment. Force graphs in Fig. 3.20 also provided information about the thickness of the penetrated structures. These values can be taken from the x-axis, describing the separation between the tip of the cantilever and the solid support under the sample. Penetration break troughs indicated a thickness of about 4 nm for DOPC and 8 nm for TDM bilayers. This value of 8 nm for the TDM is slightly lower than the height of the TDM domains calculated from the topographies in Fig. 3.17 (about 9 to 11 nm). Differences in these values originated from different amounts of force applied to the sample and the fundamental inability to determine exactly where the surface of a solid body begins (cf. Fig. 2.10: Lennard-Jones potential).
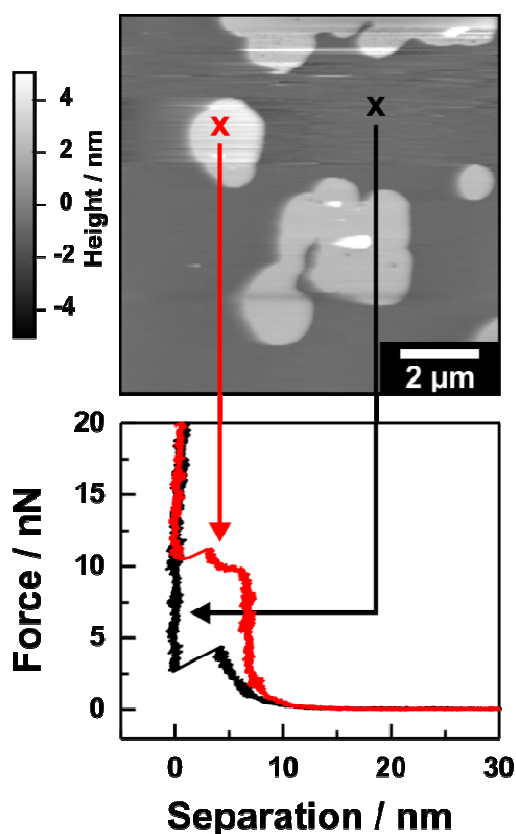
Fig. 3.20**: Force spectroscopy indicated that TDM domains had a higher mechanical stability than lipid bilayers.** Atomic force microscopic images of adsorbed bilayers composed of DOPC:TDM 1:1 (w/w) in 100 mM KCl, 5 mM Hepes buffer (pH 7). Red graph: force spectroscopic measurement on a TDM domain; black graph: measurement on the DOPC bilayer. Scan speed to record the upper topographical image was 25 µm/s; force graph pushing velocity 100 nm/s, sample rate 10 kHz; temperature 20 °C; cantilever RC 800 PSA2 with a spring constant of 0.34 N/m.

TDM domains were also observable by fluorescence microscopy using GUVs. While the lipid attached fluorophors had an isotropic distribution in GUVs made of egg PC (Fig. 3.21 A), GUVs made of egg PC:TDM 9:1 (w/w) showed dark TDM domains (Fig. 3.21 B). Domains appeared dark, because the fluorophor was excluded from them. This finding showed that the domain formation of TDM was not limited to solid supported model membranes. The exclusion of the lipid attached fluorophors from the TDM domains indicated that the TDM molecules tended to form a relative tightly packed lattice and separated themselves from phospholipids. This is in good agreement with the force spectroscopic measurements, which also showed the higher consistency of TDM domains. The emergence of TDM domains in GUVs also suggested that TDM had formed bilayers. The observed domains could not be set up as a TDM monolayer, because such a structure would not be stable in a vesicle membrane. Asymmetric domains, with TDM on one leaflet and lipids on the other, were generally imaginable, but would also allow the lipid attached fluorophors to enter the domains on the lipid side, leading to a weaker contrast between the domains and the surrounding lipid bilayer. The observed high contrast between domains and surrounding is best explained by TDM domains as symmetric bilayers. Unfortunately, the preparation of TDM containing GUVs was tricky and produced disperse samples, in which some GUVs showed domains, while others did not. Sometimes the preparation of GUVs failed completely for unknown reason. The problems preparing TDM containing GUVs were probably due to the high hydrophobicity of the TDM and its tendency to self-aggregate into non-lamellar structures (cf. Fig. 3.18).
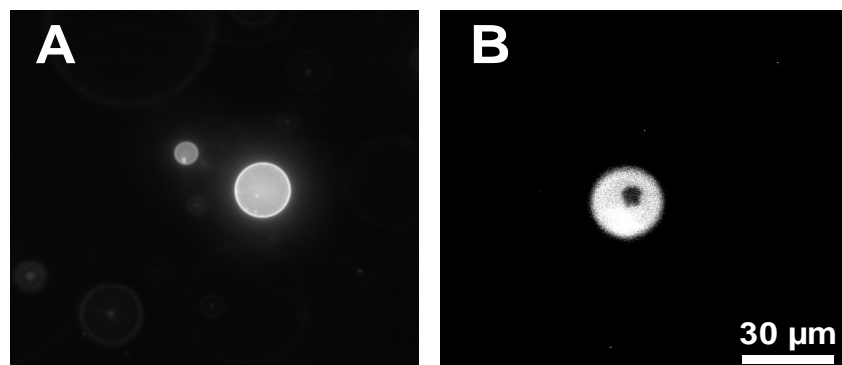
Fig. 3.21**: GUVs made of egg PC: TDM 9:1 (w/w) exhibited dark TDM domains.** Fluorescence microscopic images of 1:500 Rh-DHPE labeled GUVs in 10 mM Na-Ph-buffer (pH 7.4) using an Olympus IX 70 fluorescence microscope. (A): even fluorescence of egg PC GUVs; (B): dark domains in an egg PC:TDM 9:1 (w/w) GUV. Vesicles were prepared by electroformation using protocol (ii). Sample temperature was 20 °C. Scale bar is the same for both images.

3.8.2 TDM INTERACTIONS WITH ANTIMICROBIAL PEPTIDES

Besides the structural properties of TDM containing membranes, the focus of this thesis was placed on TDM interactions with AMPs. Biophysical experiments with several AMPs were carried out, on the one hand to get a deeper insight into the activity of the used peptides and on the other hand to investigate the role of TDM in resistance against antimicrobial substances. The general concept of the research described in this chapter was to test the abilities of the AMPs LL32, LL32-4A and hBD-3-l to bind and permeabilize model membranes with and without TDM. Artificial membranes made of TDM or PE:PG:TDM 25:25:50 (w/w/w) were used as a model for the mycobacterial outer membrane, while reconstituted PE:PG 1:1 (w/w) bilayers were used to mimic other bacterial membranes. Biophysical data derived from fluorescence spectroscopy, AFM, fluorescence microscopy and planar lipid bilayer experiments were later compared with *in vitro* data derived from experiments with mycobacteria. To obtain information about the binding of the different AMPs to TDM or PE:PG 1:1 (w/w) vesicles, binding studies with lipid SUVs, TDM aggregates and antimicrobial peptides were carried out using a fluorescent spectroscopy assay based on the phenomenon of FRET. The fluorescently-labeled antimicrobial peptide LL32-Rh was added to sample solutions labeled with NBD-DHPE. Binding of the peptides led to energy transfer from the donor labels in the vesicles/aggregates to the acceptor labels attached to the peptides and therefore to a decrease in donor fluorescence. The donor fluorescence was plotted against the peptide concentration (Fig. 3.22). Results showed that LL32 was able to bind to vesicles made of PE:PG, while binding to TDM aggregates was more limited. Qualitatively similar results have also been obtained for the addition of LL32-4A-Rh and hBD-3-l-Rh to TDM or PE:PG 1:1 (w/w) vesicles (data not shown).
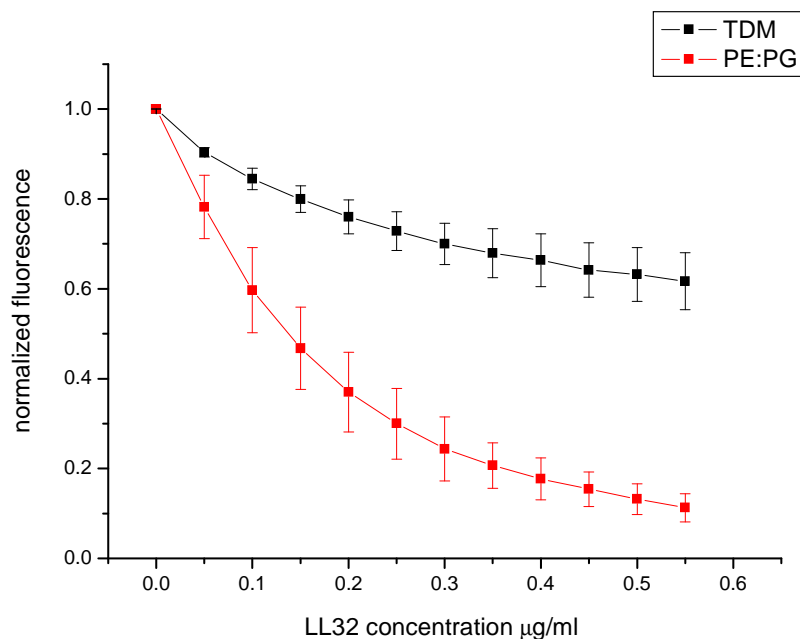
Fig. 3.22: **A FRET based binding assay showed the limited binding of LL32 to TDM.** Plot of normalized donor fluorescence against peptide concentration; addition of fluorescent LL32-Rh to TDM or PE:PG 1:1 (w/w) vesicles/aggregates labeled 1:500 with NBD-DHPE caused a quenching in NBD (donor) fluorescence due to resonance transfer of energy to the Rh (acceptor) labels. The decrease in donor fluorescence corresponds to the amount of peptide bound to the sample. Temperature 37 ˚C; buffer: 100 mM KCl, 5 mM Hepes (pH 7); excitation of the sample occurred at 470 nm; emission was recorded at 531 nm.

While the fluorescence spectroscopic assays were well suited to demonstrate the binding abilities of the peptides, they did not provide any information about the abilities of the AMPs to permeabilize membranes. For a closer investigation on this topic AFM measurements of solid supported bilayers were performed. Vesicles were spread onto a planar solid support and the topography of the sample was recorded. As aforementioned, pure TDM did not form bilayers, thus, a mixture of PE:PG:TDM 25:25:50 (w/w/w) was used as a model membrane roughly mimicking the mycobacterial outer membrane. AMP effects on membranes of this mixture were compared with the effects on PE:PG 1:1 (w/w) bilayers to glean the influence of TDM. Fig. 3.23 shows the effects of LL32, LL32-4A, hBD-3-l, LL32+hBD-3-l and LL32-4A+hBD-3-l in a final concentration of 5 µg/ml on PE:PG bilayers spread from vesicle suspensions. An untreated PE:PG bilayer (control) appeared relatively plain, with only very few higher spots. These were probably caused by excess lipids on top of the bilayer and were not present in all samples. Addition of hBD-3-l led to the formation of peptide domains, which varied in lateral extension between about 100 nm and 2 µm.

Domains were between 0.5 and 5 nm higher than the phospholipid bilayer. Addition of LL32 caused small and cloudy peptide domains within the bilayer, which can also be considered as a blurring of the sample (see also chapter 3.9: A Closer Look on AMP Effects). LL32 domains did not show a well defined transition between domain and surrounding, by which their lateral size could not be determined exactly. Domains were mostly between about 100 nm and 500 nm wide and up to 0.8 nm higher than the phospholipid bilayer. In contrast, addition of LL32-4A led to the formation of relative big, sharply bounded domains. LL32-4A domains were between 50 nm and 1 µm wide and up to 2 nm higher than the phospholipids. When LL32 was added first and hBD-3-l afterwards, the domain structure became cloudier as compared to the hBD-3-l treated sample. The observed domains were between 100 nm and 1.5 µm wide and up to 3 nm higher than the phospholipid bilayer. Domains were less well bounded as pure hBD-3-l domains. Similar results were observed when LL32-4A was added first and hBD-3-l afterwards.

Fig. 3.23**: Topographical AFM images showed the effect of different AMPs on solid supported PE:PG bilayers.** PE:PG 1:1 (w/w) bilayers were investigated in 100mM KCl, 5mM Hepes (pH 7) at 20 °C. Samples were either untreated (control) or treated with the AMPs indicated in the images. AMPs were added to the buffer above the bilayer in a final concentration of 5 µg/ml. Scan speed 25 µm/s; cantilever RC 800 PSA2, nominal spring constant 0.76 N/m. Scale bar is the same for all images.

Equivalent experiments as shown in Fig. 3.23 have been accomplished with PE:PG:TDM 25:25:50 (w/w/w) bilayers spread from vesicle suspensions (Fig. 3.24). Shown is the topography of the samples with and without the addition of AMPs in a final concentration of 5 µg/ml. In the untreated control sample the domain size varied with different sample preparation, but in all cases more or less extended TDM domains were visible. Similar to the observation in previous experiments (Fig. 3.17), µm-sized TDM domains were about 5 nm higher than the phospholipid bilayer and showed piled up excess TDM on top of the basic domain. Addition of hBD-3-l to the sample triggered shape changes in the TDM domains,

blurred the height difference between TDM and lipids, but did not cause a complete vanishing of the domains. Additionally many towering small spots were observed. These spots were up to 10 nm higher than the basic height level of the phospholipids and consisted probably of hBD-3-l, TDM of mixtures thereof. Addition of LL32 caused broad changes in the TDM domain structure, by which a clear discrimination between TDM and lipid occupied areas became impossible. Several higher spots, up to 3 nm above the basic height level, were visible and might have consisted of TDM or LL32. The addition of LL32 first and hBD-3-l afterwards caused domains, which were between 300 nm and 1.5 µm wide and up to 7 nm higher than the basic height level. In my opinion the mayor part of these domains was most likely made of hBD-3-l. In contrast to the sample treated with hBD-3-l alone, the highest domains were larger but also less clearly bordered. The global sample appeared blurry, an effect caused probably by the prior addition of LL32. Treatment of the PE:PG:TDM bilayer with LL32-4A resulted in an altered TDM domain structure similar to the hBD-3-l treated sample. Some higher spots were visible. These spots could be made of LL32-4A as to a larger amount observed in the LL32-4A treated PE:PG sample (Fig. 3.23). Finally, a PE:PG:TDM bilayer was treated with LL32-4A first and hBD-3-l afterwards. The addition of these two AMPs caused a blurring of the TDM domains and many small holes in the membrane. These holes were partially a measurement artifact caused by a so called double-tip (AFM cantilever had two tips instead of only one, by which elements of the sample were erroneously recorded and pictured twice), but did also indicate, that the bilayer was heavily damaged and had probably started to detach from the solid support.
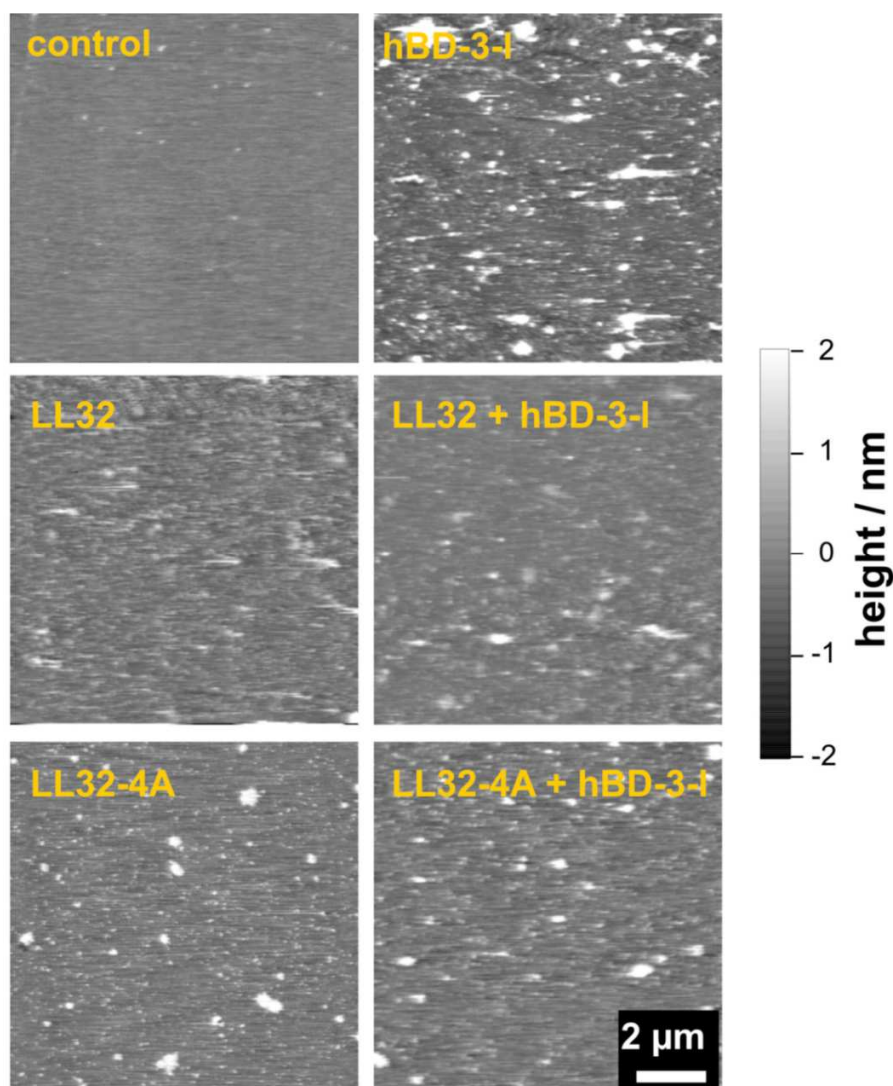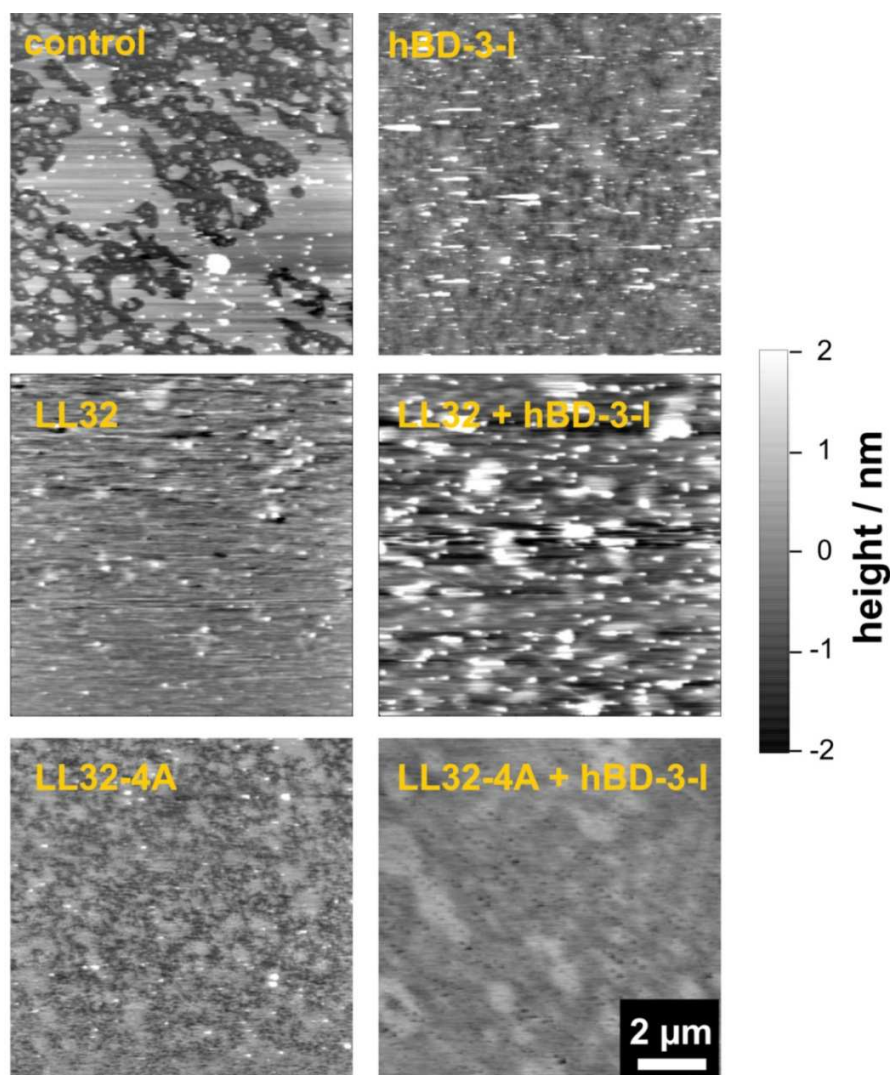
Fig. 3.24: **Topographical AFM images showed the effect of different AMPs on solid supported PE:PG:TDM bilayers.** PE:PG:TDM (25:25:50) bilayers were investigated in 100mM KCl, 5mM Hepes (pH 7) at 20 °C. Samples were either untreated (control) or treated with the AMPs indicated in the images. AMPs were added to the buffer above the bilayer in a final concentration of 5µg/ml. Scan speed 25 µm/s; cantilever RC 800 PSA2, nominal spring constant 0.76 N/m. scale bar is the same for all images.

Besides AFM, also planar lipid bilayer experiments were carried out to further characterize the AMP effect on lipid bilayers. These experiments were performed by Thomas Gutsmann and are further dealt with in the Discussion section (Fig. 4.6). Biophysical data were compared with data derived from experiments with real mycobacteria. These experiments were carried out by our collaborators and are described and interpreted in the Discussion section (Fig. 4.7).

3.9 A CLOSER LOOK ON AMP EFFECTS

Besides the described experiments with reconstituted PE:PG and PE:PG:TDM membranes, also membranes made of DOPC were treated with AMPs. This simple model with only one phospholipid was well understood and easy to handle. It allowed for a closer investigation of the used AMPs LL32 and hBD-3-l by AFM, as shown in Fig. 3.25. A pure DOPC bilayer, which was spread from vesicles onto a solid support, appeared very smooth and plain (Fig. 3.25 A). Addition of LL32 to the bilayer made the whole structure blurry and somewhat uneven. Hardly any clearly bounded peptide domains were visible (Fig. 3.25 B). Addition of hBD-3-l, however, led to the formation of many small peptide domains, which were about 0.3 µm wide and up to 5 nm higher than the pure bilayer (Fig. 3.25 C).
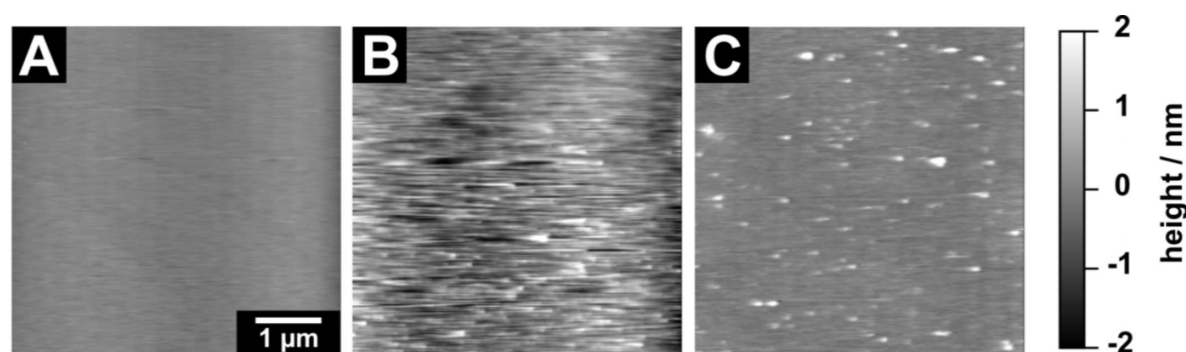
Fig. 3.25: **Topographical AFM images of AMP treated DOPC bilayers showed the different effects of LL32 and hBD-3-l.** (A): Untreated DOPC bilayers appeared plain; (B): LL32 treated DOPC bilayers appeared blurry; (C): hBD-3-l treated DOPC bilayers showed many small hBD-3-l spots. Images taken in 100 mM KCl, 5 mM Hepes buffer (pH 7), temperature 20 °C; scan speed 25 µm/s. Final AMP concentration in (B) and (C) was 5 µg/ml. AMPs were added to the buffer above the bilayer. Cantilevers RC 800 PSA2 with a nominal spring constant 0.76 N/m were used. Scale bar is the same for all images.

Besides recordings of the membrane topography, also force spectroscopic experiments on untreated and AMP treated DOPC bilayers were carried out to obtain further information on the peptides. Fig. 3.26 shows representative force curves taken on a DOPC bilayer before (black graph) and after (red graph) LL32 addition. The black graph shows the characteristic break through kink of a DOPC bilayer (cf. Fig. 3.20), while the red graph describes an even penetration of the bilayer. This indicates that the LL32 did not reside on top of the DOPC bilayer, but was incorporated into the membrane. This incorporation has somehow changed the packing of the phospholipids and altered the stiffness of the membrane into a more malleable state. The two graphs in Fig. 3.26 have been recorded with an identical cantilever, allowing for direct comparison of the integrals of the graphs, which represents the work needed to push the cantilever through the sample. This amount of work was higher in the

LL32 treated sample compared to the untreated. Thus, a general softening of the bilayer due to LL32 cannot be concluded.
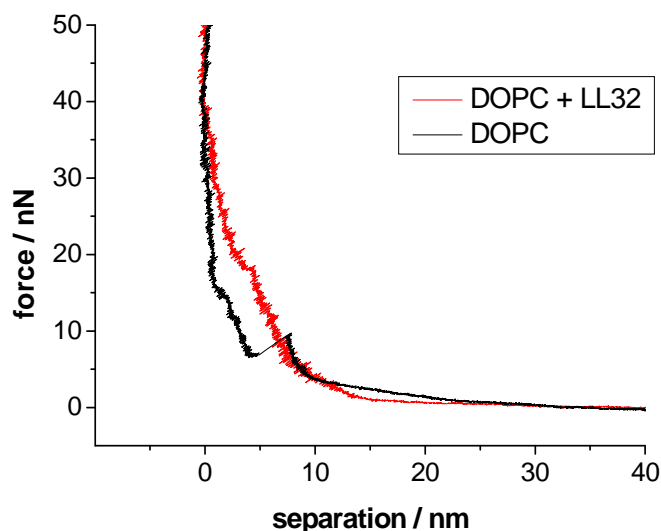
Fig. 3.26**: AFM force curves revealed LL32 incorporation in DOPC bilayers.** Black graph: force spectroscopic measurement on a DOPC bilayer. Red graph: measurement on a DOPC bilayer after the addition of LL32 in a final concentration of 5 µg/ml. Same cantilever RC 800 PSA2 with a spring constant of 0.65 N/m was used to record both curves at a velocity of 100 nm/s. Buffer: 100 mM KCl, 5 mM Hepes (pH 7), temperature 20 °C.

As shown in Fig. 3.25 (C), hBD-3-l gathered into peptide domains when added to a DOPC bilayer. Fig. 3.27 shows representative force curves recorded on such a domain (red graph) and on the DOPC bilayer next to the domain (black graph). The black graph looked similar to other force graphs recorded on various DOPC membranes before, indicating that the added hBD-3-l had not caused any major changes in this part of the bilayer. The red graph however, which was recorded on an hBD-3-l domain, showed a rather even penetration, indicating that the properties of the bilayer have been altered at this position. The graph indicates that hBD-3-l did not pile up onto the bilayer but was located within. Akin to LL32 the bilayer was altered to a more malleable state, while a general softening cannot be concluded.
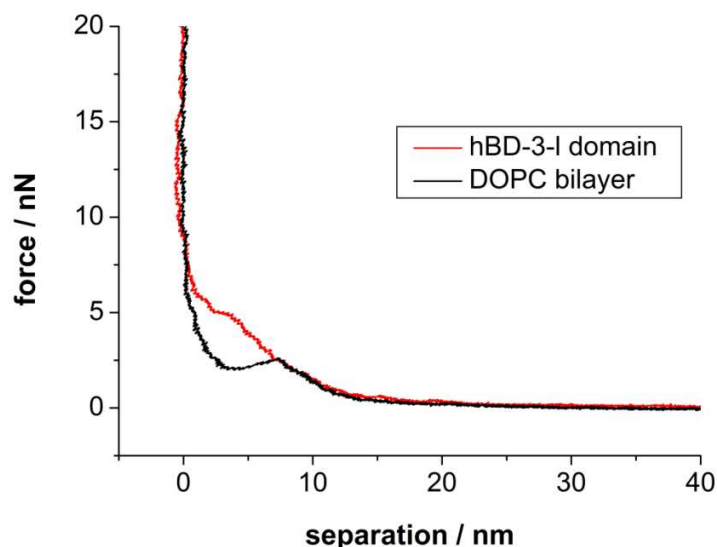
Fig. 3.27**: AFM force curves provided information about the hBD-3-l incorporation in DOPC bilayers.** Black graph: force spectroscopic measurement on a DOPC bilayer. Red graph: measurement on an hBD-3-l domain after the addition of hBD-3-l in a final concentration of 5 μg/ml. Same cantilever RC 800 PSA2 with a spring constant of 0.56 N/m was used to record both curves at a velocity of 100 nm/s. Buffer: 100 mM KCl, 5 mM Hepes (pH 7), temperature 20 °C.

Although the recorded force graph contained further information about e.g. sample thickness and absolute stiffness, they were here only evaluated in a qualitative and restrained way. This approach was necessary, because of variation in the graphs, especially when AMP treated samples were investigated. The increase in variation after AMP addition was probably due to inhomogeneous peptide incorporation or ongoing reorganization processes within the membrane during the measurement. Furthermore, unbound peptide could possibly interact with the cantilever and bias the results. It was therefore impossible to generate reliable force graphs for AMP treated TDM containing membranes as well as for LL32-4A or LL32+hBD-3-l treated samples.

4 DISCUSSION

As every living cell contains some kind of membrane, membranes constitute an obvious object of interests when structure and properties of cells are investigated. The complexity of natural membranes, however, sometimes prevents understanding of cellular processes, while membrane models provide a simplified and better controllable alternative. Membrane models of the cell membrane of human macrophages, the outer membrane of Gram negative bacteria and the outer membrane of mycobacteria were reconstituted in this thesis. The prepared membrane mimics allowed for research on the activity of antimicrobial substances as well as on the biophysical properties of the model membranes themselves. As many experiments were based on GUVs, this membrane system is initially characterized and discussed in the following. Afterwards the results of the respective applications of GUVs are contemplated. This includes (i) interaction of AMPs with GUVs exhibiting SM-cholesterol rich domains as a model for lipid rafts in macrophages, (ii) investigation of the membrane fusing properties of the antibiotics PMB and PMBN on GUVs mimicking bacterial lipid membranes and (iii) studies of LPS containing GUVs. The latter were used as a model for the outer membrane of Gram negative bacteria and were also prepared as asymmetric vesicles with LPS in the outer membrane leaflet and phospholipids in the inner. Besides binding and permeabilization studies with AMPs, asymmetric vesicles were also used for the investigation of thermodynamic inter leaflet coupling in membranes. In addition to the mentioned topics this thesis involved research on mycobacteria mimicking membranes. Here, the structural properties of TDM and its interactions with AMPs were investigated in various membrane systems.

4.1 GUVs AS A MEMBRANE SYSTEM

Cell-sized giant unilamellar vesicles (GUVs) are usually used to study membrane properties, but have also been shown to form microreactors for chemical reactions (Noireaux and Libchaber, 2004), vessels for protein crystallization (Yamashita et al., 2002) and might someday even form a membrane for an artificial living cell (Luisi et al., 2006). For reviews on GUVs see *Walde et al., 2010* and *Dimova et al., 2006*. While a general preparation of GUVs is not so difficult to archive, the adaptation of the membrane system to certain scientific questions remains challenging and is therefore discussed in the following. The main advantage of the GUV membrane system is the size of the vesicles. In own preparations GUVs showed diameters between 1-80 µm (e.g. Fig. 3.1) and were therefore well above the resolution limit of optical microscopy. This allowed for imaging without the

need of sub-diffraction microscopy. The possibility for direct visualization of GUVs also allowed for a more straight-forward interpretation of the results, while results produced by indirect methods are partly difficult to interpret and more prone to unidentified artifacts. A GUV preparation usually contained many hundreds, maybe several thousands of GUVs, and therefore also included a sufficiently high number of GUVs with a cell-sized diameter of about 40 µm. The cell-like size of GUVs leads to a natural membrane curvature to mimic eukaryotic cells, while the curvature is way too high in SUVs with an about 500 fold smaller radius. While curvature is too high in SUVs it is unnaturally low in solid supported bilayers, where the membrane is stabilized by a planar support. As the membrane curvature adds to the Gibbs energy of a system (Helfrich, 1973), SUVs, GUVs and planar bilayers can behave differently in experiments. Furthermore, membrane curvature itself seems to play a crucial role for certain biological processes. A curvature related sorting of membrane lipids between liquid-ordered and liquid-crystalline phases has been observed in GUVs and is suggested to be involved in membrane budding in early endosomes and the Golgi apparatus (van Meer and Vaz, 2005; Roux et al., 2005). Even bigger problems arise when the volume of SUVs or GUVs is important for an experiment (e.g. in dye release assays). Because the volume scales with the third power of the radius, GUVs and SUVs clearly differ in this parameter. Disadvantages, which arise by using GUVs, are their fragile nature and problems involving their preparation. GUVs are usually free floating in solution but tend to attach and spread to solid surfaces like glass slides. This limited the time span for GUV microscopy in own experiments to several minutes. Furthermore, GUVs could not be stored for longer time spans than about 10-20 hours after preparation. After longer storage GUVs in the preparations were aggregated or spread to the chamber. Stirring or shaking of GUVs solutions was equally impossible as exchange of buffer. Replacement of buffer or addition of high concentrations of soluble substances will cause a difference in osmolarity between the GUV lumen and the outside medium, by which GUVs will collapse or burst.

GUVs are best prepared by rehydration of dried lipids under the influence of an alternating electric field, a procedure known as electroformation (Angelova and Dimitrov, 1986). Other preparation methods (e.g. so called gentle hydration or solvent evaporation methods) are more likely to produce multilamellar vesicles with a more heterogeneous size distribution (Rodriguez et al., 2005; Bagatolli et al., 2000). Own experiments using a solvent evaporation method (Moscho et al., 1996) also produced only low vesicle yields and mainly GUVs with defects (data not shown). Preparation of GUVs by electroformation is, however, slow and standard protocols failed for certain lipids or if salt containing buffer solutions were used as medium. Although the electroformation method is widely used, the underlying physical principle is not fully understood, which limits the potential for optimization by theoretical evaluations. During this thesis, I established different types of GUVs as membrane mimics for different types of membranes. The individual protocols were developed by literature search as well as by trial and error. Time-consuming fine tuning of several preparation parameters like temperature, incubation time, frequency, voltage and ionic strength of the medium allowed me adjusting the preparation also for charged lipids like PG and the use of

10 mM Na-Ph-buffer (pH 7.4) instead of purified water. Experiments in buffer enabled controlling the pH value, while experiments in purified water were prone to fluctuation in pH when substances were added. For the used Na-Ph-buffer a pH value within the range of the blood pH (7.35 to 7.45) (Waugh and Grant, 2007) was used. I finally established different types of GUVs as membrane mimics for different membranes:

- GUVs made of sphingomyelin (SM), cholesterol and a low melting point lipid (e.g. DOPC:bSM:chol in a molar ratio of 2:2:1 resembled the plasma membrane of human macrophages. Artificial membranes showed SM-cholesterol rich domain, which are thought to possess similarities to lipid rafts in natural cells. The results of experiments with GUVs of this type and different AMPs are discussed in paragraph 4.2.

- GUVs made of certain bacterial phospholipids (PE:PG 1:1) or phospholipids and LPS (PE:PG:LPS R45 2:2:1) resembled bacterial lipid membranes or the LPS containing outer membrane of Gram negative bacteria. The effect of antimicrobial substance on these membrane models and their further use are discussed in paragraphs 4.3 and 4.4.

- GUVs made of phospholipids and TDM (egg PC: TDM 9:1 w/w) resembled the outer membrane of mycobacteria in a simplified way. Preparations of GUVs with incorporated TDM were problematic due to the high hydrophobicity of the molecule. TDM was either bound to the electrodes and did not distich during electroformation or did not integrate into the lamellar GUV bilayer due to the formation of non-lamellar phases. TDM containing GUVs contributed to the research on the architecture of the outer membrane of mycobacteria in paragraph 4.7 but were not used to characterize the interaction with AMPs.

Establishment of GUVs as membrane models dealt not only with the preparation of GUVs but also with improvements for their observation by fluorescence microscopy. Here, suitable fluorophors had to be chosen and incorporated into the vesicles. Experiments showed that labeling was done best by mixing lipid attached fluorophors with the other lipids prior to preparation in chloroform. Head group NBD or Rh conjugated PE was suited for all experiments. By this, NBD appeared to be more prone to photobleaching as compared to Rh. Furthermore, a temperature cell (cf. paragraph 3.3) was developed, enabling also fluorescence microscopic experiments at elevated temperatures (e.g. 37 °C simulated body temperature or 41 °C simulated fever).

4.2   INVESTIGATION OF SM-CHOLESTEROL RICH DOMAINS IN GUVS

GUVs made of certain ratios of SM, cholesterol and a lipid with a low melting point show a temperature dependent phase separation into a liquid-crystalline phase rich in the low melting point lipid and a liquid-ordered phase rich in SM and cholesterol (cf. paragraph 1.2.2 and 1.2.3). Model membranes exhibiting these domains were used to mimic lipid rafts in cell membranes. After a preparation protocol for GUVs with SM-cholesterol rich domains has been established, observation of these domains by fluorescence microscopy was possible. To do so, the vesicles were labeled with NBD-DHPE or Rh-DHPE, fluorophors that are excluded from liquid-ordered domains (Baumgart et al., 2007). Therefore, SM-cholesterol rich domains appeared dark in fluorescent microscopic images, while the surrounding liquid-crystalline areas appeared bright. GUVs made of DOPC:bSM:chol 3:5:2 and 2:2:1 showed SM-cholesterol rich domains (Fig. 3.8 and Fig. 3.9) at room temperature. The existence of SM-cholesterol rich domains in GUVs made of DOPC:bSM:chol 2:2:1 has been reported before (Veatch and Keller, 2003). Domains were mobile within the membrane and tended to aggregate and form fewer but bigger domains over time. The coalescence of domains and their mostly round shape are indication of an entropy driven process, in which the system strives to minimize the boundary between domains and surrounding. In contrast, GUVs made of DOPC:bSM:chol 9:9:2 did not show any domains (Fig. 3.7), although domains were observed by AFM in solid supported bilayers of the same lipid composition (data not shown). This indicates that domains in GUVs were either too small to be resolved by optical microscopy, or that in solid supported bilayers the influence of the solid support or the missing membrane curvature promoted a phase separation not present in the fluid GUV bilayer. From these results the importance of the used membrane system is emphasized, and it is shown that results obtained by different systems are not directly comparable. The emergence of SM-cholesterol rich domains in GUVs of certain lipid compositions is triggered by interactions between SM and cholesterol (Rietveld and Simons, 1998), while at other compositions entropy driven random distribution prevails. Formation of liquid-ordered domains in artificial model membranes is widely accepted and has been investigated extensively for many lipids (e.g. Veatch and Keller, 2005). While a liquid-ordered / liquid-crystalline phase separation in model membranes leads to stable micrometer-sized domains, equivalent phase separation in natural cell membranes is thought to trigger the formation of lipid rafts. This kind of domains is based on the same chemical interactions between cholesterol and sphingolipids as in SM-cholesterol rich domains. Lipid rafts are, however, regarded to be transient and small structures (<200 nm in size) eventually stabilized to bigger and more enduring forms by interactions with membrane proteins (Pike, 2006; Kusumi et al., 2004). Furthermore, lipid rafts in cells appear to be rather non-equilibrium fluctuations in the lipid distribution unless stabilized, while SM-cholesterol rich domains in model membranes are in thermodynamic equilibrium. Because of these differences, results obtained by the investigation of SM-cholesterol rich domains in model membranes cannot be directly assigned to natural cells. This difficulty to combine biophysical and biological data

is not always sufficiently regarded by other authors, leading to occasionally improper terminology, e.g. found in a review with the title "Giant unilamellar vesicles - a perfect tool to visualize phase separation and lipid rafts in model systems" (Wesołowska et al., 2009). With a lipid raft defined as a structure in natural cell membranes their visualization in model membranes is inherently impossible as working with models is inherently connected to the use of a reduced copy of reality. Furthermore, GUVs are mostly connected to the use of optical (fluorescence) microscopy where structures of the size of lipid rafts cannot be resolved due to the Abbe diffraction limit, unless sub-diffraction microscopy is used. Despite all the uncertainties in the field of lipid rafts, research with SM-cholesterol rich domains can provide information about the *in vivo* situation, but careful consideration of the data is necessary. In my own research I tested the effects of different AMPs on the structure of SM-cholesterol rich domains, as a biophysical counterpart for lipid rafts in macrophages and monocytes. Rafts in these cells are thought to be involved in the regulation of CD14 (Schmitz and Orsó, 2002) and TLR4 (Triantafilou et al., 2002) receptors. These receptors play an important role in the recognition of LPSs from cell membranes of Gram negative bacteria and the subsequent induction of inflammatory processes. From this medical relevance of lipid rafts arises by eventually preventing inflammation in patients by giving of pharmaceuticals, which act on the lipid raft structure. Such a treatment would be especially beneficial for the treatment of patients suffering from sepsis or septic shock (cf. paragraph 1.3.1) where an overreaction of the immune system to LPSs eventually causes a life threatening drop in blood pressure. As the results in Fig. 3.10 show, all tested AMPs (LL32, L-Pep 19.2-5, NK2 and hBD-3-l) were able to bind to GUVs made of DOPC:bSM:chol 2:2:1, but none of the peptides caused any visible changes in size or shape of the present SM-cholesterol rich domains. As lipid rafts in cell membranes are thought to be naturally transient but possibly stabilized by proteins, they might interact differently as the relatively stable SM-cholesterol rich domains in model membranes. AFM measurements, which were carried out in our lab by my colleague Yani Kaconis, showed a vanishing of small SM-cholesterol rich domains in AMP treated solid supported bilayers (data not shown). In these experiments LL32, hBD-3-l and L-Pep 19.2-5 were able to alter the structure of nanometer-sized SM-cholesterol rich domains after more than 30 minutes of peptide incubation. The inability to observe changes in the size of domains in GUVs has several possible reasons. First of all are nanoscopic changes not resolved in fluorescence microscopy and the observation time in the experiments was limited to about 15 minutes due to sample desiccation. The different fluidity and membrane curvature of the two membrane systems might also influence domain stability. In the results shown in Fig. 3.10, AMPs were used as conjugates with the fluorophors Rh or NBD to be able to observe them by fluorescence microscopy. The chemical connection of a fluorophor to the peptide might influence its activity; however, the used fluorescent peptides did not show significant differences compared to unlabeled forms in killing experiments with Gram negative bacteria (data not shown). We therefore assume that labeling of the peptides did not affect their activity in an important way. AFM experiments did not provide any information about the localization of the AMPs on the membrane, but as fluorescence microscopy in Fig. 3.10 showed, was AMP

binding limited to DOPC areas outside the SM-cholesterol rich domains. Binding in this area was based mostly on hydrophobic interactions, as the DOPC lipids are of neutral charge, only slightly polar and do therefore not apply for strong electrostatic interactions. I assume that the inability of all tested AMPs to bind to SM-cholesterol rich domains was caused by the high cholesterol content of the domains. A general reduction of the activity of different AMPs by cholesterol has been described before (Zasloff, 2002; Matsuzaki, 1995), but the exact mechanism is unclear. The combined results of AFM and fluorescence microscopy indicate that AMPs bind initially to areas outside of the SM-cholesterol rich domains and probably act on the fringe of the domains. Nanometer-sized domains, as observed in AFM experiments, possess a much more extended boundary relative to their surface area as compared to micrometer-sized domains in GUVs. Small SM-cholesterol rich domains are therefore more likely to be destabilized by AMPs. As lipid rafts are considered to be also nanometer-sized, the tested AMPs might act on them although much larger SM-cholesterol rich domains in GUVs were not affected.

4.3 PMB-INDUCED FUSION OF VESICLES

One mode of action of antimicrobial agents is the induction of membranes fusion, which is described here for the peptide antibiotics PMB and PMBN. Bacterial membranes were reconstituted as GUVs made of PE and negatively charged PG, lipids also found in bacterial membranes (Osborn, et al., 1972). The preparation of GUVs with incorporated charged lipids was tricky and produced not only spherical GUVs but also multilamellar vesicles and aggregated structures, in which several vesicles had fused and formed an unordered compound. These problems with the preparation were unsurprising as similar difficulties have been reported before (Morales-Penningston, 2010). I assume that charged lipids somehow interfere differently with the electric field during electroformation as compared to uncharged lipids and hinder the ordered detachment of bilayers. Preparation artifacts were not critical for the later fluorescence microscopic experiments, as also sufficient high numbers of intact GUVs came into being. As shown in Fig. 3.6, an untreated control sample contained a mixture of separately prepared either red (Rh labeled) or green (NBD labeled) GUVs. After addition of PMB or PMBN also orange and yellow aggregates appeared, caused by a fusion of the former separated Rh and NBD vesicles and superposition of the fluorescence. Both antimicrobials induced the fusion of vesicles, however, PMB had a more pronounced fusion activity as compared to PMBN. The observed membrane fusing activities of PMB and PMBN were in agreement with a FRET based fusion assay, while the fusion related increase in aggregate size could be affirmed by dynamic light scattering (DSL) (data not shown). FRET and DSL experiments were carried out by Malte Hammer, a former PhD student in our lab, and were evaluated in cooperation with Thomas Gutsmann and me. In

summary, our results showed that both PMB and PMBN were able to fuse negatively charged lipid membranes. Furthermore, they were both able to increase the size of small LPS aggregates in DSL experiments, while only PMB but not PMBN was able to fuse these LPS aggregates. Fusion of bacterial membranes is considered as the mode of action for PMB under *in vivo* conditions. The lower activity of PMBN is due to its chemical structure, which lacks the fatty acid residue present in PMB. By this, PMBN has a lower hydrophobicity and reduced tendency to incorporate into membranes. The described experiments were carried out at the beginning of my thesis. At this time the preparation of cell-sized asymmetric vesicles (cf. paragraph 2.8) has not yet been established in our lab. For further research on PMB and PMBN it is now possible to repeat the experiments shown in Fig. 3.6 with LPS/PE:PG asymmetric vesicles and directly visualize the PMB-induced fusion of LPS vesicles for the first time.

4.4 LPS CONTAINING GUVS

Gram negative bacteria are causative for a vast number of diseases, from which medical interest in these organisms arises. When testing the activity of membrane active substances (e.g. AMPs) against Gram negative bacteria, the utilization of membrane models can extend the knowledge obtained from real microorganisms. Working with artificial membranes instead of real bacteria removes the risk of infection and often allows for a better experimental control and a deeper insight into the underlying mechanisms of the results. To create a membrane model mimicking the outer membrane of Gram negative bacteria, LPS containing GUVs were prepared by electroformation. These GUVs contained the phospholipids PE and PG, as well as the deep rough mutant LPS R45 from the bacterium *Proteus mirabilis* strain R45. GUVs made of PE:PG:LPS R45 in a molar ratio of 2:2:1 are shown in Fig. 3.11. At room temperature the incorporated LPSs formed domains within the phospholipid matrix. These domains appeared dark because the lipid attached fluorophor Rh-DHPE, which was used for labeling of the vesicles, was excluded from the domains. The formation of LPS domains was due to a phase separation between LPSs in the gel phase and phospholipids in the liquid-crystalline phase. Those phase separations are well known for phospholipids with different melting points (e.g. van Dijck et al., 1977) and do also occur between phospholipids and LPSs. As shown by FTIR spectroscopy the main phase transition of PE:PG 1:1 (w/w) vesicles took place at about 9 °C (Fig. 3.19), while the phase transition temperature was about 50 °C for LPS R45 (Fig. 3.15). For IR measurements LPS R45 was used at a relatively high concentration of 20 mM in an aqueous environment and probably formed inverted (inverse hexagonal or cubic) phases, while LPS R45 was in lamellar phase in the observed GUVs. Because of this, the phase transition temperature of LPS R45 in GUVs probably differs from the value measured by IR spectroscopy shown in Fig. 3.15. It

is, nevertheless, likely that LPS R45 was below its phase transition in gel phase at room temperature, while the PE:PG lipids were clearly above and in liquid-crystalline phase. The existence of LPS domains in phospholipid GUVs has recently also been shown by another group using Rh-DHPE as well as a fluorescent marker. These authors likewise explained the formation of domains by a gel / liquid-crystalline phase separation (Kubiak et al., 2011). The nominal LPS rate in my preparations was 20 mol % and as LPS head groups are more extended than phospholipid head groups, one would expect more than 20 % of the membrane surface covered by LPS. The dark areas in the domains are, however, estimated to cover about 10 to 15 % of the surface only, indicating that not all of the applied LPSs have been incorporated into GUVs. Despite this finding, obtained results are considered as success, as the incorporation of LPS into model membranes is generally problematic (Dijkstra et al., 1988). It has also been reported that LPS rates of more than 25 mol % for rough-form LPS are unlikely to be achieved anyway (Kubiak et al., 2011). The problems preparing LPS containing GUVs are related to the formation of non-lamellar phases. LPS in these phases interferes with the ordered detachment of lipid bilayers during electroformation of GUVs. The tendency of a molecule to form micelles, lamellar bilayers or inverted structures is connected to its molecular geometry and can be rationalized by the critical packing parameter P_c (Israelachvili et al., 1976; Israelachvili, 1985):

$$P_c = \frac{V}{A_0 * l_{alkyl}}$$
(Equation 8)

P_c: critical packing parameter; V: volume of the hydrophobic part of the molecule; A_0: surface area of the hydrophilic head group; l_{alkyl}: length of the unpolar (alky) chain in fluid state.

The critical packing parameter is the ratio between the volume of the hydrophobic part of the molecule that favors the formation of inverted structures and the product of head group area and chain length promoting the formation of micelles. While phospholipids usually possess P_c values around 1 and therefore apply for lamellar phases, LPSs possess much higher values and favor inverted structures. The induction of inverted structures has also been reported for deep rough mutant LPS in PE:PG lipid mixtures (Urban et al., 2006). The observed existence of not inverted but lamellar LPS domains in own preparations of LPS containing GUVs can be explained as follows: during preparation LPSs and phospholipids are mixed uniformly in chloroform. This solution is then dried out to form multiple stacked bilayers (cf. paragraph 2.6). The LPS concentration in the sample is low enough to obtain a lamellar orientation for LPSs surrounded by lipid molecules, which already naturally favor lamellar phases. This process is probably promoted by the low water content of the sample, while the low lateral mobility prevents a lateral phase separation and clustering of LPSs. During electroformation

90

the sample is fully rehydrated and the lamellar bilayers pinch off from the electrodes and form GUVs. Due to the rehydration and the assembly as unilamellar structures, mixed lipids and LPSs obtain a higher lateral mobility and phase separate. In the now emerging domains high local LPS concentrations come into being. LPS in domains would, according to their P_c value, favor the formation of inverted structures, but once "trapped" in lamellar structures and bordered by an aqueous environment on both sides the inversion of the LPSs is prevented by hydrophobic interactions. Besides the reflection of LPS containing GUVs from a more physical point of view, also the biological relevance of the system should be evaluated. While the lack of sterols (cholesterol) in bacterial membranes would generally allow LPS in gel phases, the actual membrane architecture seems to be different. To my knowledge the existence of LPS domains within a fluid lipid matrix has not been reported for any bacterial membrane. While the inner membrane of Gram negative bacteria does not contain LPSs, the outer membrane consists of an inner phospholipid leaflet and an outer LPS leaflet (Fig. 1.6). Here, areas covered by LPSs and phospholipids are not laterally separated but oppose each other across the bilayer. Because of this, we consider LPS containing GUVs rater useful for the biophysical investigation of LPS / lipid interactions, while their potential to resemble Gram negative bacteria is limited. To generate a better membrane mimic for the outer membrane of Gram negative bacteria, the preparation of asymmetric vesicles with phospholipids in the inner leaflet and LPSs in the outer leaflet was established (see next paragraph).

4.5 ASYMMETRIC VESICLES

Membranes, which contain different molecules in their inner and outer leaflet, are considered asymmetric. While a slight asymmetry is probably found in most membranes, certain membranes possess a marked asymmetry, worth to be reflected in membrane mimics for these membranes. Eukaryotic plasma membranes, for example, possess more SM and PC in the outer leaflet, while the inner leaflet is richer in PE and phosphatidylserine (PS) (Zachowski, 1993). Furthermore, asymmetry can also be found in the outer membrane of Gram negative bacteria (Osborn et al., 1972). Here, the outer leaflet consists of LPSs, while the inner leaflet is made of phospholipids, often PE, PG and also DPG. To establish a membrane model for the outer membrane of Gram-negative bacteria my coworker Annemarie Brauser and I used a protocol for the preparation of asymmetric phospholipid / phospholipid vesicles (Pautot et al., 2003) and subsequently adopted it for the preparation of asymmetric LPS / phospholipid vesicles [n.b. syntax for the description of asymmetric vesicles in this thesis is "outer leaflet / inner leaflet". An e.g. LPS R45/DOPC asymmetric vesicle would consist of LPS R45 in the outer leaflet and DOPC in the inner leaflet]. Fig. 3.12 shows a preparation of asymmetric vesicles with LPS R45 in the outer leaflet and a

phospholipid (PL) mixture of PE:PG:DPG 81:17:2 (w/w/w) in the inner leaflet. A lipid composition of PE:PG:DPG 81:17:2 (w/w/w) has been reported to be present in the lipidic leaflet of the outer membrane of Gram negative bacteria (Osborn et al., 1972). The FITC-KI fluorescence quenching assay shown in Fig. 3.12 proved the asymmetry of the created vesicles. Here, fluorescence of FITC labels located in the inner leaflet of the vesicles remained intact after the external addition of the fluorescence quencher KI, because the molecules were shielded by the outer leaflet. Addition of KI to vesicles with labeled outer leaflets, however, caused a quenching of FITC fluorescence. Asymmetric vesicles usually showed a size distribution between 1 and 20 µm in diameter and were therefore slightly smaller than GUVs. Their size still allowed for direct observation by optical microscopy, while membrane curvature was only a little too low for a bacteria mimicking model. We assume that the successful preparation of asymmetric LPS / phospholipid vesicles under physiological buffer conditions (100 mM KCl, 5mM Hepes, 5 mM $MgCl_2$; pH 7) and their observation by fluorescence microscopy are new to science and have been archived in our lab for the first time. While basically a potent membrane system, the not so straight-forward preparation protocol could limit the use of asymmetric vesicles. Furthermore, own attempts to use LPS WBB01 instead of LPS R45 for the preparation of the outer leaflet failed for unknown reasons. Future work will reveal, if the described protocol is generally limited to certain LPSs or if it can be extended to a more encompassing form. Prospective preparations of asymmetric vesicles could also use different buffers in the lumen of the vesicles and the surrounding, eventually creating a transmembrane potential across the bilayer. By this, the model would gain additional biological relevance.

Experiments with asymmetric vesicles and AMPs were carried out to test the membrane permeabilizing abilities of the peptides LL32, LL32-4A and hBD-3-l (Fig. 3.13 and Fig. 3.14). To do so, the inner leaflet of LPS R45/PL vesicles was fluorescently labeled with FITC and the quencher KI was added to the external medium together with one of the AMPs. While the FITC fluorescence was protected from the quencher in undamaged vesicles, membrane permeabilization allowed entering of the quencher to the vesicle lumen and quenching of the fluorescence. By this, the reduction in fluorescence can be seen as a measure for the permeabilization activity of an AMP. Comparing this approach to assays, in which AMPs are simply added to phospholipid vesicles, we are able to kill two birds with one stone; fist of all the model of asymmetric vesicles is a better mimic for Gram negative bacteria as it exhibits LPSs on the outside, and furthermore the selective labeling of only the inner leaflet allows for the described permeabilization assay. Results of the AMP experiments showed that a final concentration of 38 nm LL32 caused a partial permeabilization of asymmetric LPS R45/PL vesicles (Fig. 3.13). In equivalent experiments LL32-4A showed only binding but no permeabilization activity (Fig. 3.14 A, B) while hBD-3-l caused a virtually complete permeabilization of all vesicles (Fig. 3.14 C, D). These experiments demonstrate the possibility to investigate AMP-related permeabilization of LPS / phospholipid vesicles as a proof of principle. A more detailed quantitative characterization of AMP activities is planned for the future but does still require some further groundwork.

Especially a quantification of the amount of quenched fluorescence would be desirable and could probably be archived by performing the permeabilization assays in a fluorescence spectrometer rather than under a fluorescence microscope. Future adjustment of the preparation protocol could be pushed towards the production of high yields of small (<1µm) asymmetric vesicles suited for fluorescence spectroscopy, where no direct visualization is needed. Such vesicles would provide a superior membrane model, not only because of their reflection of natural asymmetry and membrane curvature but also because of their high rate of LPS. Generic SUV or multilamellar vesicle models, in contrast, are reported to contain often not more than around 2 mol % LPS (Dijkstra et al., 1988; Nakhla et al., 1996). Problems in preparing LPS containing SUVs are probably connected to the formation of non-lamellar (inverted) LPS phases, whose occurrence is promoted at high LPS concentrations. Modification of the temperature while preparing the asymmetric vesicles might help preparing vesicles of various compositions because one could choose a temperature above the phase transition temperatures of the individual components. Interestingly, our adapted preparation protocol did not only allow for the preparation of large LPS / phospholipid vesicles with a high LPS content, but was later also used to prepare symmetric vesicles made almost solely of LPS (Fig. 3.16 B). To our knowledge this is the most sophisticated, if not the only, protocol capable in producing unilamellar micrometer-sized LPS vesicles without suffering from the emergence of non-lamellar phases.

4.6 Inter Leaflet Coupling in Symmetric and Asymmetric Membranes

As shown in the previous paragraph, we were able to prepare asymmetric vesicles with LPS in the outer leaflet and phospholipids in the inner leaflet. The described protocol was, however, also suited to create other types of symmetric and asymmetric vesicles. By this, my coworker Annemarie Brauser and I started to investigate the coupling between inner and outer leaflet of lipid bilayers. The properties of interactions between two leaflets combined to a lipid bilayer by hydrophobic interactions are an old biophysical question in the scientific community as well as in our laboratory group. Within this context we decided to investigate, whether an inner phospholipid leaflet in liquid-crystalline phase is able to alter the phase of an outer LPS leaflet between gel and liquid-crystalline phase. Some experiments with asymmetric solid supported mono- and bilayer and asymmetric free standing bilayers had already been carried out by members of our laboratory group. Fig. 4.1 shows AFM data of lipid or LPS mono- and bilayers prepared by the Langmuir-Blodgett technique (cf. paragraph 2.9). The sample topography of an LPS R45 monolayer showed higher (grey) and lower (white) domains (Fig. 4.1 A, a) at room temperature. This indicates a phase separation, as lipids (Tristram-Nagle et al., 2002; Kucerka et al., 2005) and LPSs (Roes et al., 2005) are reported to be more extended in gel phases than in the liquid-crystalline phase. A gel/fluid

phase separation has also been observed in unsupported LPS R45 monolayers (Fig. 4.2 A) and symmetric LPS R45 vesicles (Fig. 3.16 B) at room temperature but has not been fully understood yet. Coexistence of gel and liquid-crystalline phases in lipid bilayers with only one lipid species has been occasionally reported before (Bagatolli and Gratton, 1999) but was limited to a narrow temperature range around the main phase transition temperature. Eventually the greater structural variation within the used LPS R45 samples extended this region of coexistence. Furthermore, the phase transition temperature of LPS R45 in monolayers and GUVs is unknown, leaving the vague possibility of measuring incidentally near the phase transition temperature. While AFM measurements of solid supported LPS R45 monolayers revealed a phase separation, PL (PE:PG:DPG 81:17:2 w/w/w) monolayers showed an even sample topography, indicating that all lipids were in the same phase (Fig. 4.1 B, b). IR measurement of this sample (Fig. 3.15) revealed that PL was relatively fluid at room temperature and existed in the liquid-crystalline phase. When the fluidic PL monolayer was combined with the rigid LPS R45 monolayer to form a common solid supported bilayer, a lateral phase separation within the LPS layer was undetectable by AFM. By this, it did not matter if the LPS R45 monolayer formed the upper (Fig. 4.1 C, c) or the lower (Fig. 4.1 D, d) leaflet of the new bilayer. These findings suggest that the PL leaflet had an influence on the phase of the LPS R45 layer, but it remained unclear if this influence caused a stabilization of a gel or a liquid-crystalline phase. As the PL itself was fluidic, an increase in fluidity within the LPS R45 leaflet appeared more likely but could not be proven on the basis of this data set.
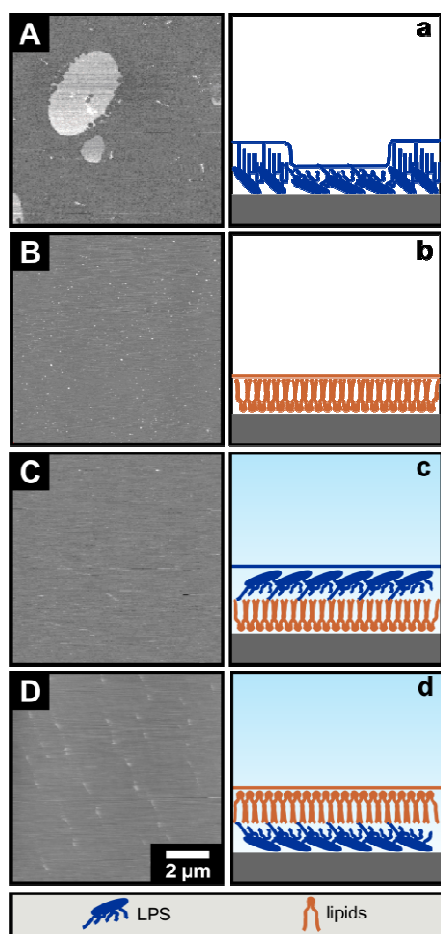
Fig. 4.1: **Fluid PL leaflets prevented LPS R45 leaflets from phase separation in Langmuir-Blodgett films.** AFM measurements of (A, a): an LPS R45 monolayer in air; (B, b): a PL monolayer in air; (C, c): a PL/LPS R45 bilayer with the PL adsorbed to the solid support and the LPS oriented to the buffer; (D, d): an LPS R45/PL bilayer with the LPS adsorbed to the solid support and the PL oriented to the buffer. Only the LPS R45 monolayer showed a phase separation. Buffer in (C) and (D): 100 mM KCl, 5 mM MgCl$_2$, 5 mM Hepes (pH 7); temperature 21 °C; lateral pressure of the monolayers 20 mN/m. Scale bar is the same for all images. Data by courtesy of Thomas Gutsmann, published in *Roes et al., 2005*.

Experiments with free standing mono- and bilayers formed across a small hole in a Teflon foil (cf. paragraph 2.16) provided similar results as obtained by AFM. Planar LPS R45 monolayers showed an uneven distribution of an incorporated fluorophor (NBD-DHPE), when observed with a fluorescence microscope (Fig. 4.2 A, a). As the lipid attached fluorophor is known to be preferably located in the liquid-crystalline phase (Baumgart et al., 2007), the dark domains could be identified as gel phases. In contrast to LPS R45 monolayers, NBD-DHPE labeled planar PL monolayers appeared uniformly and did not show any signs of phase separation (Fig. 4.2 B, b). Furthermore, planar LPS R45/PL asymmetric bilayers, in which the LPS R45 leaflet was labeled with NBD-DHPE, appeared

uniformly too (Fig. 4.2 C, c). Again, the influence of the PL leaflet had hindered phase separation in the LPS R45 leaflet. The vanishing of the dark domains and the then isotropic distribution of the NBD-DHPE labels indicate that the LPS R45 leaflet was probably in liquid-crystalline phase when combined with a PL leaflet.
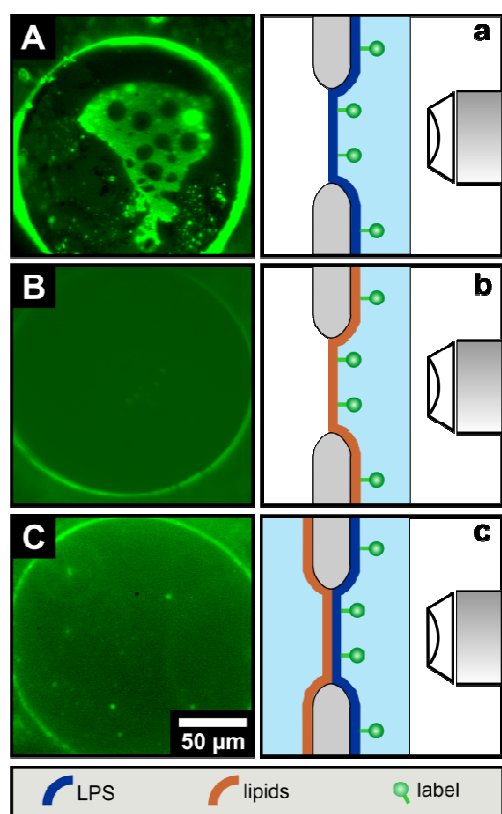
Fig. 4.2: **Fluid PL leaflets prevented LPS R45 leaflets from phase separation in free standing bilayers.** Fluorescence microscopic images of (A): a free standing LPS R45 monolayer, (B): a free standing PL monolayer and (C): an LPS R45/PL planar bilayer, all reconstituted over an aperture by the Montal-Mueller technique. Buffer: 100 mM KCl, 5 mM MgCl$_2$, 5 mM Hepes (pH 7), temperature 37 °C. Fluorescent leaflets were labeled 1:100 with NBD-DHPE. Images taken with a partly home built fluorescence microscope, described in paragraph 2.16. Scale bar is the same for all images. Data by courtesy of Thomas Gutsmann.

To contribute to this project, I prepared Rh-DHPE labeled LPS/PL and LPS/LPS vesicles using the preparation protocol for asymmetric vesicles. In agreement with the aforementioned experiments, a phase separation was also prevented in LPS R45/PL vesicles (Fig. 3.16, A) while it was clearly observable in LPS R45/LPS R45 vesicles (Fig. 3.16, B). Like NBD-DHPE the used Rh-DHPE labels have also been reported to gather in liquid-crystalline phases (Baumgart et al., 2007), rendering gel-like domains dark. The addition of the fluorophor to both leaflets in LPS R45/LPS R45 vesicles in Fig. 3.16 (B) revealed that

the observed gel domains were equally present in both leaflets, i.e. spanned the whole bilayer. Interestingly, the dark domains exhibited a stripe and patch shaped form, while the domains observed in solid supported bilayers (Fig. 4.1, A) and free-standing planar bilayers (Fig. 4.2, A) were rather round. Stripe and patch shaped domains are characteristic for gel/fluid phase separation in vesicles and have been reported before (e.g. Bagatolli and Gratton, 2000; Li and Cheng, 2006). Differences in domain shape between the used membrane models might be due to different membrane curvatures, the solid support or the exposure of the monolayers to air. To support the performed imaging experiments the phase transition temperatures of PL, LPS R45 and a PL:LPS R45 1:1 mixture were measured by IR spectroscopy (Fig. 3.15). Here, the LPS R45 phase transition was determined to be at about 50 °C, but as aforementioned this value might be of little relevance as it is derived from inverted LPS R45 structures differing from the lamellar setup of LPS R45 in vesicles and planar mono- or bilayers. Isolated consideration of the IR data in Fig. 3.15 was, however, possible and showed that the mixed system PL:LPS R45 1:1 did not exhibit two independent phase transitions, one for the phospholipids and one for the LPSs, but only one phase transition at about 40 °C. This is in agreement with the other experiments and points out that PL and LPS R45 interact when mixed together. This interaction leads to an increase in fluidity as compared to pure LPS R45. To avoid working with samples in unknown and possibly inverted conformation, prospective IR measurements with samples prepared by the asymmetric vesicle protocol are planned. By this, the phase transitions of LPS R45/PL and LPS R45/LPS R45 vesicles could be measured directly, eventually confirming the proposed fluidization of LPS R45 leaflets by PL leaflets. The actual preparation protocol provides only vesicle concentrations too low for IR spectroscopy. Higher vesicle concentration would also enable fluorescence spectroscopic investigation of the vesicles' phase behavior. Here, individual leaflets of asymmetric vesicles could be labeled with the environment sensitive fluorophor 6-dodecanoyl-2-dimethylamine-naphthalene (laurdan) (Parasassi et al., 1990), which is able to reveal the phase state of membranes by shifts in its fluorescence emission maximum. I already used laurdan to successfully investigate the phase behavior of symmetric phospholipids and LPS vesicles/aggregates by fluorescence spectroscopy (data not shown), whereas the use of the fluorophor in fluorescence microscopy is impaired by the low photostability of the molecule.

Results obtained so far in this project exhibit consistently that a fluidic PL leaflet is able to prevent phase separation in an opposing LPS R45 leaflet by increasing the LPS fluidity. A similar prevention of lipid domains in one leaflet by interactions with lipids of the other leaflet has been reported by another group (Collins and Keller, 2008) based on experiments with asymmetric planar bilayers. Domains in their work were due to a liquid-ordered / liquid-crystalline phase separation in cholesterol containing bilayers and therefore not directly comparable to the gel / liquid-crystalline phase separation observed in our experiments. But the results of *Collins and Keller, 2008* also elucidate the possibility of interactions between the leaflets of a bilayer. As shown in Fig. 3.16 (B), lateral gel domains in LPS R45/LPS R45 vesicles were symmetric in both leaflets, an indication that the system

strives to avoid the facing of gel and fluid alkyl chains across the leaflets. A gel domain in one leaflet therefore sorts the lipids of the other leaflet, locally gathering a gel domain as its counterpart. In LPS R45/PL vesicles this architecture of opposing gel phases cannot be archived, because the fluidic PL leaflet includes lipids in the liquid-crystalline phase only. Thus, the alkyl chains of LPSs in gel phase have to interact with fluidic alkyl chains from the phospholipids of the opposing leaflet, by which the formation of gel phase domains is abolished. An increase in LPS fluidity makes sense with respect to the *in vivo* situation. Many LPSs, extracted from the outer membranes of Gram negative bacteria, possess melting points way above 40 °C, but gel phases have not been reported to exist in bacteria at room temperature. As membrane fluidity in bacteria cannot be increased by cholesterol, which is only present in animal membranes, another mechanism needs to be present. I suggest that the regulation in LPS fluidity in the outer leaflet of the outer membrane of Gram negative bacteria might be achieved by interactions with fluid phospholipids from the inner leaflet of the outer membrane. Fluidity is probably transferred from the phospholipid leaflet to the LPS leaflet by interactions of the opposing alky chains in the center of the bilayer. In an ongoing attempt to better understand inter leaflet coupling, besides LPS R45/PL vesicles, also other lipid combinations have already been tested (data not shown) and further experiments based on fluorescence microscopy, fluorescence spectroscopy and also molecular dynamic simulations are planned to follow.

Besides further work with asymmetric LPS / phospholipid vesicles, the preparation protocol could also be used to create and investigate asymmetric mimics of human cell membranes in future. As mentioned at the beginning of the previous paragraph, higher rates of SM are found in the cholesterol rich outer leaflet of human and animal cell membranes as compared to the inner leaflet. As SM is known to cluster with cholesterol and eventually forming lipid rafts, these structures should be more extended in the outer leaflet than in the inner. This assumption, however, leads to the question, whether lipid rafts are usually asymmetric or symmetric in both leaflet or if symmetric and asymmetric rafts co-exist simultaneously. Maybe inclusion of the natural asymmetry of cell membranes could help to fix some of the contradictions in the field of lipid rafts, which are partly derived from studies of SM-cholesterol rich domains in symmetric model membranes. Akin to the asymmetric LPS / phospholipid arrangement in Gram negative bacteria the MOM can be thought as an asymmetric TDM / phospholipid bilayer, although this model is less precise than in Gram negative bacteria. Therefore prospective experiments could also involve asymmetric TDM vesicles.

4.7 STRUCTURAL PROPERTIES OF TDM

The major part of this thesis focused on investigations of the mycobacterial glycolipid TDM. The corresponding results are discussed in two paragraphs. In the present paragraph the structural properties of TDM are discussed, while the next paragraph deals with the effects of AMPs on TDM containing membranes. Model membranes were used to create a membrane mimic for the MOM (cf. paragraph 1.4 and Fig. 1.8), where larger amounts of TDM are present *in vivo*. Experiments were carried out to contribute to the ongoing discussion of the architecture of the MOM, for which several partly conflicting models have been suggested by different authors. Understanding the setup of this membrane is crucial for the development of anti-mycobacterial substances, as the MOM constitutes the outermost barrier of mycobacteria. At the beginning of this work some experiments about the structural properties of TDM in monolayers had already been realized in our research group. Langmuir-Blodgett films of pure phospholipids or mixtures of phospholipids and TDM were prepared and investigated by AFM. By this, the topographies of the samples were recorded, revealing height differences derived from the different molecule sizes of TDM and phospholipids. While pure DOPC monolayers appeared smooth and plain with height differences only in the picometer range (Fig. 4.3 A), DOPC:TDM monolayers showed higher TDM domains (Fig. 4.3 B and C, height profiles b and c). These domains had a basic height level of about 2.5 nm above the level of the phospholipids. Domains showed multiple higher spots of piled up TDM, when larger amounts of the glycolipid were used for the preparation (Fig. 4.3 C, height profile c).
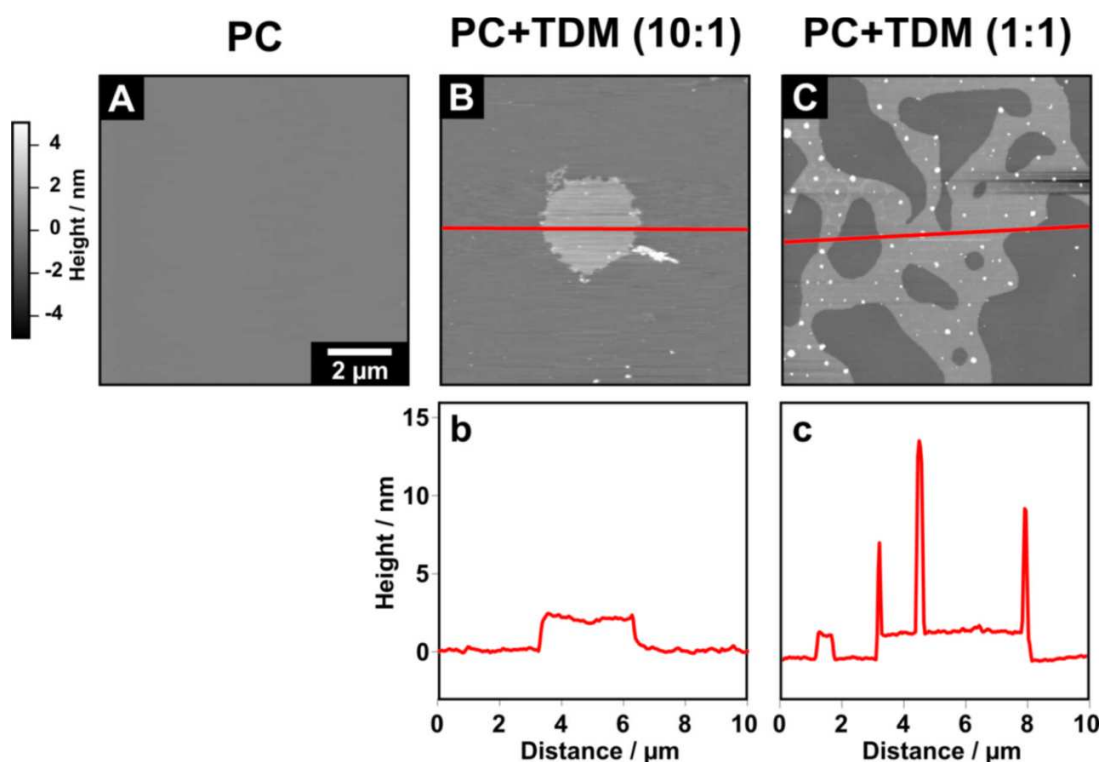
Fig. 4.3: **AFM on DOPC:TDM Langmuir-Blodgett monolayers revealed TDM domains.** (A): plain DOPC monolayer; (B, b): DOPC:TDM 10:1 (w/w) monolayer with a higher TDM domain in the middle; (C, c): DOPC:TDM 1:1 (w/w) monolayer with a higher stripe shaped TDM domain. Further TDM was piled up on the domain. Height profiles are given below the images. Buffer during monolayer preparation: 100 mM KCl, 5 mM HEPES (pH 7). Films were transferred at a lateral pressure of 20 mN/m. AFM measurements performed in air at 20 °C. Cantilever: NSG 11, spring constant 5 N/m. Scale bar is the same for all images. Figure by courtesy of Thomas Gutsmann.

I contributed to this project by preparation of TDM containing membranes, also revealing the domain forming properties of TDM in solid supported PC bilayers (Fig. 3.17 B, C and Fig. 3.20) as well as in GUVs made of PC and TDM (Fig. 3.21). Investigations showed a height difference between TDM domains and surrounding phospholipids of 2.5 nm in solid supported monolayers (Fig. 4.3 B, height profile b) and about 5 nm in solid supported bilayers (Fig. 3.17 B, height profile b). Height differences were derived from the different alkyl chain length of phospholipids and TDM. Results indicate that TDM domains in lipid bilayers, which were spread from vesicle suspensions, consist of a TDM bilayer. Embedded TDM monolayers would have caused a lower height difference between TDM and phospholipids, while TDM multilayers would have caused a higher difference. Furthermore, the finding that the height difference in bilayers is twice the difference in monolayers is a hint for the formation of symmetric TDM bilayers. Each of the two TDM monolayers in the bilayer evokes a height difference of 2.5 nm, which sums up to a total of 5 nm. A symmetric TDM bilayer is also the most likely explanation for the observed dark domains in phospholipid GUVs (Fig. 3.21). TDM molecules formed domains, from which the lipid

attached fluorophors were excluded due to a phase separation. Domains could not be set up as a TDM monolayer, because such a structure would expose its hydrophobic alkyl chains to the polar medium and would therefore be unstable. A mixed TDM/phospholipid bilayer with TDM in one leaflet and lipids in the other is generally thinkable, but would also contain fluorophors on the lipid side. Incorporated labels, however, would illuminate the TDM domains causing a weaker contrast between domains and surrounding as observed. In conclusion, TDM domains are thought as symmetric TDM bilayers with no or only few lipid inclusions. Force spectroscopy on TDM domains (Fig. 3.20) showed an about three times higher mechanical stability compared to the phospholipids. This domain stiffness suggests an ordered conformation of TDM in a gel-like phase and promotes the idea of TDM as a stabilizing element within the MOM. TDM domains appeared stable over time and were not destabilized, when the sample was heated up to 41 °C (Fig. 3.17 C), providing a further hint for domain stability. As the phase transition temperature for TDM in solid supported bilayers is unknown, the influence of the phase state on the formation of TDM domains within a lipid matrix remains unclear. I assume that TDM domains do not only exist due to a phase separation between gel-like TDM and fluidic phospholipids, but once established are further stabilized by intermolecular H-bonds and/or van-der-Waals interactions. Phase transition temperatures of TDM, PE:PG and mixed systems were determined by IR spectroscopy (Fig. 3.19). While the used lipids were most likely set up as lamellar bilayers in SUVs, TDM containing elements could also have formed micelles, aggregates or inverted structures leading to eventually altered phase transition temperatures. The measured phase transition temperature of about 38 °C for TDM can therefore not be directly transferred to TDM in lamellar conformation. Despite this uncertainty in conformation, the IR measurements showed that TDM was able to increase the order in mixed TDM:PE:PG SUVs, leading to an elevated phase transition temperature as compared to PE:PG vesicles. The increase in order was more pronounced as one might expect from the pure mixing of ordered TDM with unordered PE:PG, indicating an effect of TDM on the lipids. While TDM has an ordering effect on lipids, lipids are thought to influence the conformation of TDM as well, promoting the formation of lamellar structures. While planar lipid bilayers made of lipid and nominal 50 % (w/w) TDM could be prepared by spreading of vesicles (Fig. 3.17 B, C), preparations of planar bilayers made of pure TDM failed. Not only spreading of TDM aggregates in buffer (data not shown) but also spreading of chloroform-solved TDM in air (Fig. 3.18) led to the formation of aggregates instead of lamellar structures. As Fig. 3.18 shows, most of the TDM was aggregated, while only a small portion on the fringe of the aggregates had formed lamellar-like structures on the solid support.

The finding of symmetric gel-like TDM domains with a thickness of about 8 to 10 nm (Fig. 3.17 B, Fig. 3.20) allows commenting on the length and conformation of the TDM molecules. As shown in Fig. 1.9 in the Introduction section, TDM consists of a trehalose sugar connected to two mycolic acids with two alkyl chains each. These chains constitute the biggest part of the lengths of TDM and are at a first glance thought to exist in a basically elongated and ordered conformation, characteristic for gel phases. But how long are the alkyl

chains exactly in their extended conformation? It is known that carbon (C) atoms in alkyl chains exhibit sp3-hybridized bonds with bond angles of about 109.5° (Bent, 1961). To be precise, an angle of 109.5° is only exactly true, if all substituents of the carbon atom are of the same type (as e.g. in methane). In alkyl chains each carbon is, however, bound to two other carbons and two hydrogens. The resulting divergence in the bond angle is small and therefore neglected in the following. With the known bond length of an sp3-hybridized C-C single bond to be 0.154 nm (Fox and Whitesell, 1995), a simple formula for calculation of the length (L) of straight alkyl chains can be developed using a trigonometric function. It applies:

$$L = \frac{(n-1)}{2} * 2l \sin(\frac{\theta}{2}),$$ *(Equation 9)*

which can be shortened to

$$L = (n-1) * l \sin\left(\frac{\theta}{2}\right)$$ *(Equation 10)*

$$L \approx (n-1) * 0.126 \text{ nm}$$ *(Equation 11)*

L: maximal length of the alkyl chain; n: number of carbons in the chain; Θ: bond angle (109.5°); l: bond length (0.154 nm)

To use this formula, the number of carbons in the TDM alkyl chains needs to be determined; TDM samples, used for experiments in this thesis, varied in alkyl chain length and had an average atomic mass of 2749 u measured by mass spectrometry. This value is in agreement with the published atomic mass of TDM, which is 2874.9 ± 140.3 u (equals ± 10 CH_2) (Noll et al., 1956). With 510.3 u being derived from the trehalose sugar and the mycolic acids, 2238.7 u of our TDM would fall upon the alky chains. To obtain the number of carbon atoms in the chains a slightly simplified chemical structure is assumed, in which the alkyl chains only consist of a number of repetitive methylene, more precisely methanediyl [-CH_2-], groups. Natural TDM alkyl chins do also contain a methyl [-CH_3] group at the end of the chains and eventually very few cyclopropane rings, which, however, do not bias results much and can be neglected. With the known mass of a methylene group of 14 u, a mass of 2238.7 u corresponds for about 160 methylene groups in the alky chains. Distributed among two longer meromycolic chains (about 70 % of lengths) and two shorter chains (about 30 % of lengths) the meromycolic chains of the used TDM contained about 56 carbons each, while the short chains contained about 24 carbons each. These values are in agreement with published data about mycolic acids from another mycobacterial species with similarities to *M. tuberculosis. Mycobacterium bovis* BCG mycolic acids have been reported to possess 49

to 61 carbon atoms in their main (meromycolic) chain (Steck et al., 1978) and 20 to 26 carbons in the short chain (Zuber et al., 2008). Results are also in agreement with the resolved chemical structure of TDM from *M. tuberculosis* (Noll et al., 1956). Application of these calculated values to *equation 10* gives a length of about 6.9 nm for meromycolic chains and 2.9 nm for short chains.

With the approximately determined alkyl chain length of TDM and the measured thickness of TDM mono- and bilayers, statements about the structural conformation of TDM are possible. Although several models for the orientation of TDM molecules within a bilayer are imaginable (Fig. 4.4), our results are able to point out the need for a folded configuration of TDM alkyl chains.
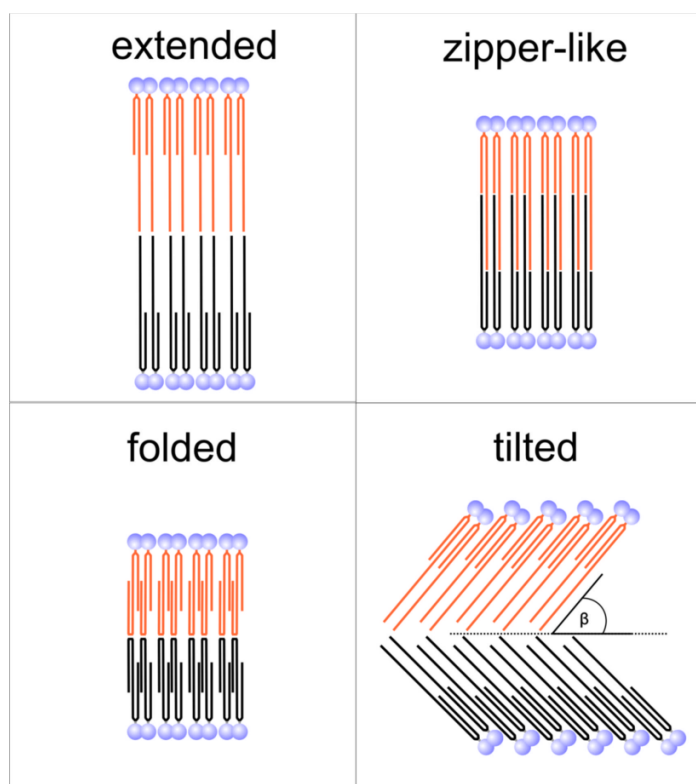
Fig. 4.4: **Possible setups of symmetric TDM bilayers.** Besides an extended TDM alkyl chain conformation, a zipper-like intercalation of meromycolic and short alkyl chains, a folding of meromycolic chains or a tilt of the TDM molecules are imaginable. The combined consideration of the results discussed in this paragraph indicates a folded configuration of TDM meromycolic chains. Alkyl chains of TDM molecules from the upper leaflet are colored orange for better visualization.

Opposing extended meromycolic chains of TDM in a bilayer would cause a membrane thickness of about 13.8 nm plus the thickness of the TDM head groups and are therefore unable to fit the measured thickness of TDM bilayers (8-10 nm). TDM in this orientation would furthermore not be able to fit the measured thickness of the MOM. Although older models suggest a thicker ($\geq$10 nm) membrane (Minnikin, 1982; Brennan and Nikaido, 1995; Chatterjee, 1997) more recent models based on results obtained by cryo-electron tomography and electron microscopy of ultrathin cryo sections propose a MOM with lipids distributed over both leaflets and a thickness of about 8 nm (Hoffmann et al., 2008), or 7.5 $\pm$ 0.8 nm (Zuber et al., 2008). A zipper-like setup, in which long meromycolic chains of TDM molecules from the outer leaflet of the MOM interdigitate with mycolic acids from the inner leaflet, was suggested by *Tonge, 2000* and is shown in Fig. 1.8. While such a setup is generally possible, assumed mycolic acids with suitable lengths exist in the inner leaflet of the MOM, interdigitation is not suited to explain the height of TDM bilayers. As aforementioned, the height of a TDM bilayer equals approximately the height of two monolayers (Fig. 3.17 b, Fig. 4.3 b). This doubling of the domain thickness in planar bilayers compared to monolayers indicates that the opposing alkyl chains of both leaflets did not interdigitate significantly, which would otherwise have led to a thinner bilayer. Furthermore, the thickness of the MOM (8 nm) and the thickness of our artificial TDM bilayers (8-10 nm) do not match the thickness of TDM molecules in a zipper-like interdigitation well. Here, the added chain lengths of meromycolic and short chain would lead to an about 9.8 nm thick membrane to which the thickness of the TDM head groups still needs to be added. A tilted alignment of the TDM molecules as shown in Fig. 4.4 could allow for bilayers of variable thickness depending on the angle between alkyl chains and plain of the bilayer. However, the transition between tilted TDM molecules and straight phospholipids on the domain borders of a common membrane remains unclear for this setup. Furthermore, small-angle X-ray scattering (SAXS) experiments with solid supported TDM multilayers, indicate a rather perpendicular orientation between TDM alkyl chains and the plain of the bilayer (data not shown). To fit the measured membrane thickness a folding of the TDM meromycolic chains is therefore most likely, and has already been suggested by other authors (Zuber et al., 2008). A folding of the alkyl chains could also promote the formation of H-bonds and van-der-Waals interactions between the chains and correspond to the observed about three times higher mechanical stability of TDM domains (Fig. 3.20). The essence of the results on the structure of TDM in solid supported monolayers, solid supported bilayers and GUVs is illustrated in Fig. 4.5. With respect to the *in vivo* situation our investigations suggest that the high mechanical stability and hydrophobicity of the MOM are connected to the presence of TDM. TDM was shown to be able to form domains with a symmetric distribution of TDM on both leaflets in model membranes, by which its meromycolic chains were folded. Folded chains are also likely for TDM *in vivo* to fit the thickness of the MOM.
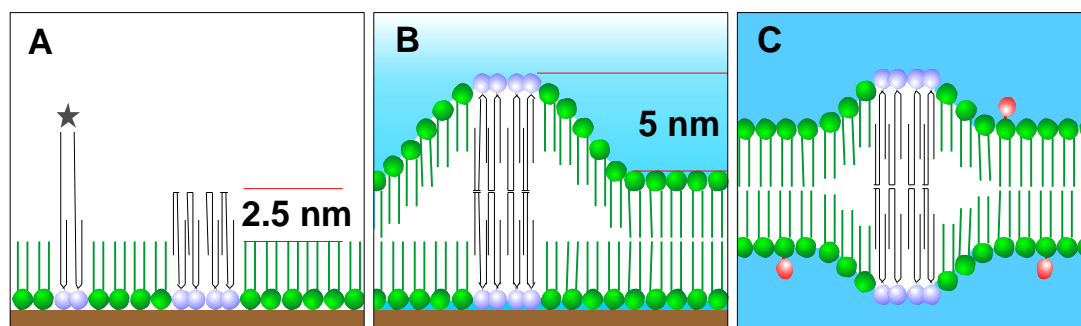
Fig. 4.5: **Setup of TDM domains in planar monolayers, planar bilayers and GUVs.** (A): Solid supported monolayer in air: Lipid (green) and TDM (purple) head groups are oriented towards the solid support, while the alkyl chains point upward. TDM meromycolic chains are folded leading to a height difference of 2.5 nm between lipids and TDM. The grey asterisk indicates a hypothetical TDM with elongated chains. TDM in this configuration was not found in the samples. (B): Solid supported bilayer in buffer: Lipids and TDM molecules form bilayers. TDM domains consist of two symmetric leaflets, exhibiting folded meromycolic chains and leading to a height difference of 5 nm compared to the lipid bilayer. White areas represent a more hydrophobic environment. To avoid hydrophobic mismatch the lipids next to the TDM domains form a relatively sharp transition area, in which the bilayer grows thicker. (C): GUV bilayer in buffer: Lipid attached fluorophors (red) are excluded from symmetric TDM domains, which appear dark in fluorescence microscopic images. Hydrophobic mismatch is prevented by swelling of the bilayer next to TDM domains. Dimensions of the molecules are approximately drawn in scale.

Another aspect, which is worth to be mentioned, is the observation of excess TDM on top of the ordered TDM domains in planar lipid bilayers (Fig. 3.17 B). In contrast to the basic TDM bilayer, this TDM was soft, only loosely associated and did not form structures of defined heights. At higher temperatures this TDM easily disconnected from the membrane (Fig. 3.17 C). Excess TDM in membrane mimics might be a simple preparation artifact but could also resemble natural excess TDM produced by mycobacteria. This form of TDM is thought to exist as cylindrical micelles with extended meromycolic chains and a diameter of 12.3 ± 1.6 nm (Retzinger et al., 1981). Remarkably, this value fits our calculated lengths of 13.8 nm for two opposing TDM molecules in extended conformation. The excess TDM was not further investigated, because it was too soft to be properly imaged by AFM and too small to be observed by fluorescence microscopy. Future work will deal with the configuration of TDM in solution involving SAXS experiments.

4.8   AMP EFFECTS ON TDM CONTAINING MEMBRANES

Besides the structural properties of TDM, also its interactions with AMPs were investigated. Within this context experiments were carried out to characterize the role of TDM in mycobacterial AMP resistance and possibly identify new active AMPs. As fluorescence spectrometric experiments showed, was the ability of different AMPs (LL32, HBD-3-l and LL32-4A) to bind to TDM generally lower as compared to the binding to PE:PG vesicles (Fig. 3.22). Before discussing this finding, a comment on the supramolecular structures of the samples is necessary. While the preparation of PE:PG vesicles for fluorescence spectrometric experiments in solution could be realized, the structure of TDM compounds in solution is unclear. As mentioned at the end of the previous paragraph, an older publication reports the existence of TDM as cylindrical micelles in solution (Retzinger et al., 1981), however, the imbalance in size between the four long alkyl chains and the relatively small trehalose head group suggests the formation of inverted structures. In both cases the direct comparability between TDM and phospholipids in lamellar phase (e.g. in SUVs) is complicated. Despite the differences in conformation the lower ability of AMPs to bind TDM compared to phospholipids is caused by different numbers of charges per molecule. As the used AMPs possess a positive net-charge, they are suited to bind to negatively charged PE:PG vesicles by electrostatic interactions. PE:PG vesicles were used to mimic negatively charged bacterial membranes, to which AMPs usually bind. TDM, in contrast, is uncharged and does not provide significant potential for electrostatic interactions. Although the trehalose head group of TDM contains hydroxyl (-OH) groups, which make this part of the molecule polar, their influence on the binding of AMPs appears minor. The existence of TDM in the MOM reduces the negative charge of this membrane and contributes to the resistance of mycobacteria against several AMPs active on other bacteria. Reduction of negative charges is known as a common strategy in different bacteria to obtain AMP resistance (Roy et al., 2009; Peschel et al., 1999). Besides the lower charge, also the higher mechanical stability of TDM compounds compared to phospholipids (cf. previous paragraph) possibly contributes to a reduced AMP binding.

Further conclusions on TDM-AMP interactions were drawn from experiments with planar bilayers, either attached to a solid support or formed as free standing bilayers. Solid supported bilayers with and without TDM were treated with different AMPs and investigated by AFM. From the observed changes in membrane topography conclusions on the peptides´ mode of action and the role of TDM were drawn. At first, the effects of LL32, hBD-3-l and LL32-4A were tested on PE:PG and PE:PG:TDM bilayers (Fig. 3.23 and Fig. 3.24). A mixture of PE, PG and TDM was used to mimic the MOM, because these types of molecules have also been found in the MOM (Tonge, 2000). Whereas PE:PG gave a general model for bacterial lipid membranes. A combined consideration of the results indicates that LL32 acted evenly on the PE:PG or PE:PG:TDM membranes and caused a blurring of TDM domains. This peptide exhibited a carpet-like mode of action and did not form any defined

pores, present in the toroidal-pore or the barrel-stave model. LL32 had a high tendency to bind membranes. hDB-3-l and LL32-4A, however, acted more isolated, forming peptide spots within the membranes but did not cause as pronounced changes in the membrane topography as LL32 did. For these peptides a carpet-like mode of action is also most likely, because the observed peptide spots or domains were too big and unshaped to constitute defined pores. The self aggregation of hDB-3-l and LL32-4A into peptide domains is interesting, because it created areas with a very high local peptide concentration while the overall peptide concentration in the sample was much lower. hDB-3-l and LL32-4A had a minor effect on the TDM domain structure as compared to LL32 and did not fully dissolved the domains. With respect to a possible use of AMPs as drugs against mycobacteria it is questionable, if a dissolving of TDM domains in the MOM would cause damage to the bacterium or would only trigger a reorganization of the membrane. Areas covered by membrane lipids could serve as a better target for attacking AMPs than TDM domains. Because of their higher charge, lower hydrophobicity and weaker mechanical stability phospholipid parts might constitute the weak point of the MOM. Further AFM experiments were carried out to investigate the effects of LL32 and hBD-3-l with respect to the formation of peptide domains by hBD-3-l. Because these domains were too mobile in PE:PG membranes to perform force spectroscopic experiments, DOPC was used as the lipid matrix instead. This lipid is rather common in eukaryotic membranes and was not a good model for bacterial membranes but allowed for some basic conclusions. As shown in Fig. 3.25, were the effects of LL32 and hBD-3-l on DOPC bilayers similar to those on PE:PG bilayers. LL32 caused a widespread reorganization of the membrane topography, while hBD-3-l created peptide domains. Force spectroscopic measurements on LL32, hBD-3-l and untreated DOPC bilayers (Fig. 3.26 and Fig. 3.27) showed that the addition of AMPs altered the bilayers towards a more viscid state. Thereby, LL32 treatment affected the whole membrane, while the effect of hBD-3-l was rather restricted to the hBD-3-l domains.

Conductivity experiments (cf. paragraph 2.16) with planar lipids bilayers were carried out by Thomas Gutsmann, to generate further data about the activity of LL32 and hBD-3-l. This method allowed measuring the permeabilization of a membrane, while the described AFM measurements could provide information about the binding of AMPs and reorganization processes within the membrane. A further advantage of planar lipids bilayers based experiments is the possibility to simulate a transmembrane potential across the free standing planar bilayer. This adds to the quality of the model, because the ability of AMPs to bind membranes *in vivo* is also influenced by the transmembrane potential of the cell (Matsuzaki et al., 1995). Cell membranes possess an inside-negative transmembrane potential, which is more distinct in bacteria and is thought to promote the incorporation of positively charged peptides into membranes. Therefore, AMP-cell interactions are not only based on electrostatic and hydrophobic interaction. For the planar lipid bilayer experiments shown in Fig. 4.6, PE:PG 1:1 (w/w) or PE:PG:TDM 25:25:50 (w/w/w) bilayers were formed across a small hole in a Teflon foil. For the actual measurements an electrical voltage was applied between the two sides of the chamber, by which the electrical resistance of the membrane

could be measured. AMP related changes in membrane permeability were recorded as changes in conductivity. Addition of LL32 to PE:PG bilayers led to a rupture of the membrane (Fig. 4.6 A), which can be seen from the dramatic increase in current after 25 seconds. Addition of LL32 to a PE:PG:TDM membrane, however, led to fluctuations, but no rupture of the membrane was observed even on longer timescales (Fig. 4.6 B). The recorded fluctuations are thought to resemble the LL32 triggered alterations in the TDM domain structure observed by AFM (Fig. 3.24, compare control and LL32 treated sample). Addition of hBD-3-l, in contrast, caused a rupture of PE:PG:TDM bilayers (Fig. 4.6 C) as well as of PE:PG bilayers (data not shown). This distinct activity might be related to the ability of hBD-3-l to form peptide domains outside of TDM domains and establish a high local hBD-3-l concentration in these domains. Interestingly, hBD-3-l lost its activity even at high concentrations, when the membrane had been incubated with LL32 before (Fig. 4.6 D). This aspect is especially interesting, as it indicates that LL32 rescues TDM containing membranes from permeabilization by hBD-3-l. We assume that this effect is related to the disruption of TDM domains by LL32 leading to a more equal distribution of TDM. Membrane permeabilization of PE:PG:TDM bilayers by hBD-3-l probably starts from peptide domains located outside of the more stabilized TDM domains. Addition of LL32 destroys TDM domains in PE:PG:TDM bilayers and causes a mixing of TDM with the lipids. For a subsequent hBD-3-l application the permeabilization of the membrane is now hindered, because the hBD-3-l comes into contact with TDM in all parts of the membrane. We suggest, therefore, that hBD-3-l is only active against mimics of the MOM, as long as it is able to act on TDM-free membrane areas. If TDM and phospholipids are mixed, hBD-3-l activity is impaired either by a TDM associated stabilization of the phospholipid or by direct TDM-hBD-3-l interactions. The potential of TDM to alter the organization of lipids has already been discussed in the previous paragraph and was demonstrated by IR spectroscopy, where TDM was able to increase the order in mixed TDM:PE:PG SUVs (Fig. 3.19). A third possible mechanism for the differential hBD-3-l activity could involve the transition areas between TDM domains and phospholipids. As described previously, TDM domains are thicker than the lipid bilayer and areas next to the bilayer need to be swollen to avoid hydrophobic mismatch (Fig. 4.5 B). In this transition area next to the domains the bilayer is tensed and locally stressed, by which a destabilization by AMPs is promoted. The observed hBD-3-l activity could take place in these areas and would be impaired after LL32 addition when the transition regions vanish together with the TDM domains.
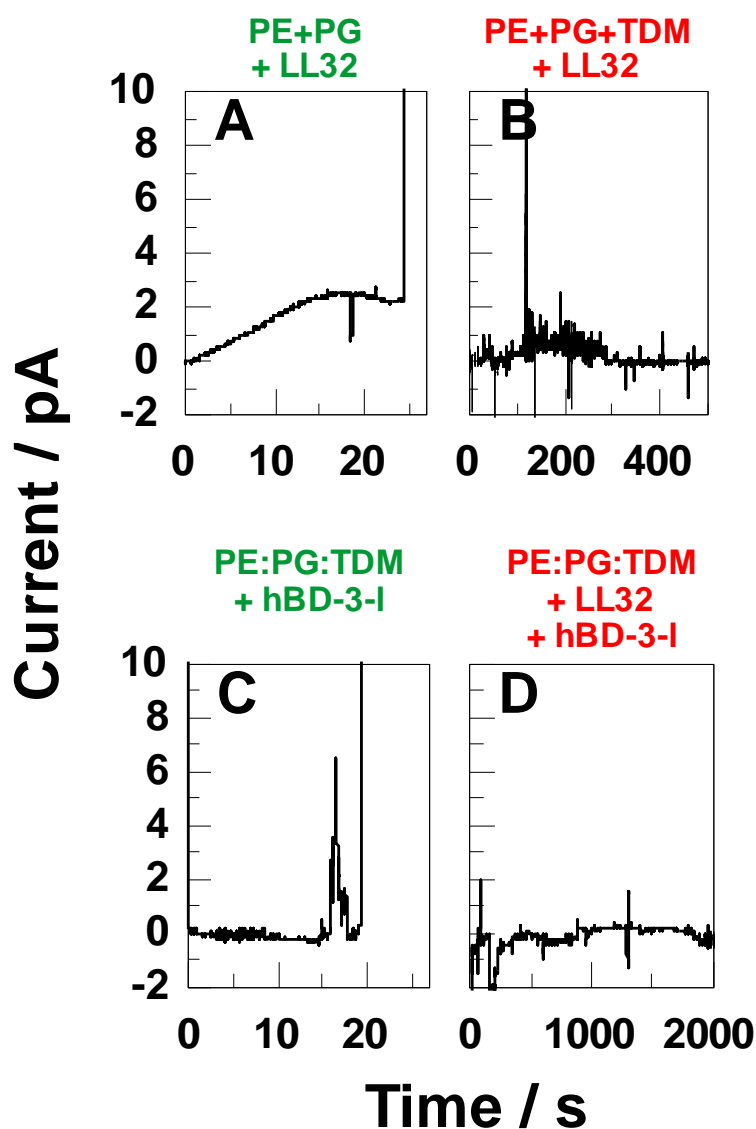
Fig. 4.6: **Influence of LL32 and hBD-3-l on the permeability of reconstituted planar membranes.** (A): Addition of LL32 to a PE:PG 1:1 (w/w) membrane caused a rupture of the bilayer; (B): Addition of LL32 to a PE:PG:TDM 25:25:50 (w/w/w) membrane caused fluctuations but no rupture of the bilayer. (C): Addition of hBD-3-l to a PE:PG:TDM 25:25:50 (w/w/w) membrane caused a rupture of the bilayer. Final peptide concentrations for the respective experiments were 1.7 µg/ml. (D): Adjustment of 1.7 µg/ml LL32 (at t = 60 s) and additionally 1.7 µg/ml hBD-3-l (at t = 660 s) and 8.5 µg/ml hBD-3-l (at t = 1260 s) caused no rupture of the bilayer. Buffer: 100 mM KCl, 5 mM $MgCl_2$, 5 mM Hepes (pH 7). Clamp voltage U = -20 mV. Figure by courtesy of Thomas Gutsmann.

To complete the research about AMP activity against mycobacteria mimicking membranes, the gathered biophysical data were compared with data derived from experiments with mycobacteria. This part of the project was implemented in collaboration with Ulrich Schaible from the Research Center Borstel and Sam Willcocks from the London School of Hygiene and Tropical Medicine in London, who did the practical work. Fig. 4.7 shows the number of colony forming units (CFUs) of an *M. tuberculosis* culture after 24 hours of incubation with AMPs. A value of 100 % on the y-axis represents the number of CFUs of an untreated control culture, while the pictured columns indicate the bacterial growth relative to this control. Interestingly, addition of LL32 had no inhibitory effect on mycobacterial growth, but led to more than 2.5 fold increased number of CFUs compared to the control. The reason for this finding is unknown. The addition of the AMPs LL32-4A and hBD-3-l, however, caused a reduced growth and about 50 % fewer CFUs after 24 hours. The two peptides can, therefore, be considered as active against mycobacteria within the scope of this experiment. In case of hBD-3-l this activity was nullified, when the bacteria had been treated with LL32 before. In this case the CFU count topped the untreated control and reached almost the value of an LL32 treated sample. This indication of an antagonistic effect of LL32 on hBD-3-l activity fits nicely to the conductivity experiments with TDM containing bilayers (Fig. 4.6). When the two active peptides LL32-4A and hBD-3-l were applied one after another, the LL32-4A and hBD-3-l effects added up, leading to a CFU count of about 25% relative to the control.
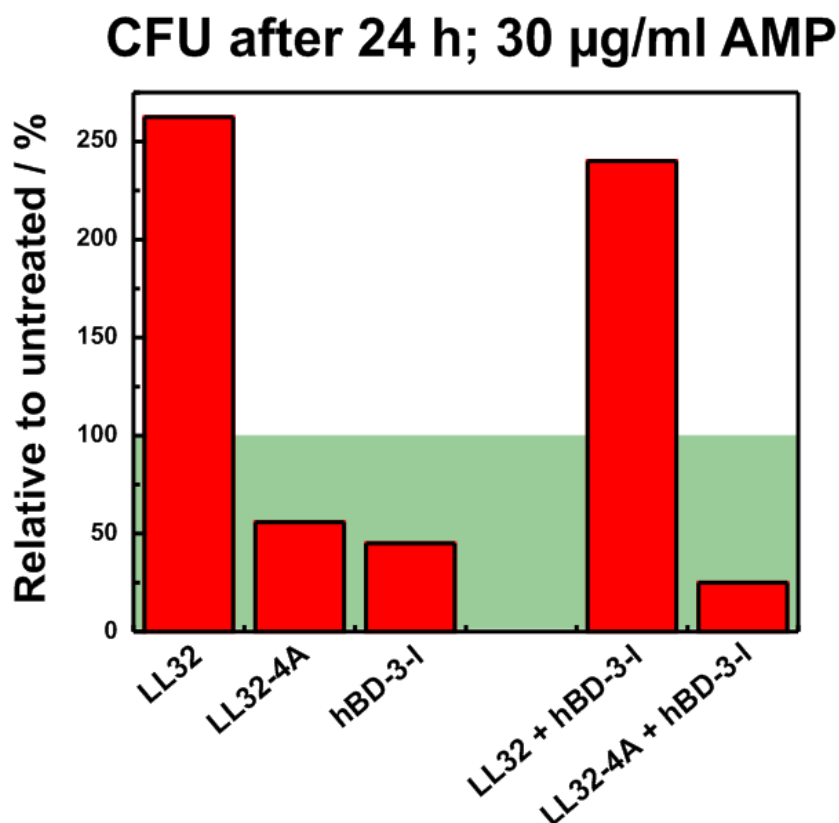
Fig. 4.7: **Effect of AMPs on mycobacterial growth.** Number of CFUs of *M. tuberculosis* cultures after 24 h of growth relative to an untreated control. While the bacterial growth was reduced by LL32-4A, hBD-3-l or a combination of LL32-4A and hBD-3-l, the addition of LL32 caused more CFUs. The inhibitory effect of hBD-3-l was abolished, when the bacteria have been treated with LL32 before. Figure by courtesy of Sam Willcocks.

A combined evaluation of the data discussed in this section concurs to the importance of TDM in the MOM. TDM did not only limit the binding activity of the tested AMPs but also saved membranes from permeabilization by LL32. hBD-3-l was able to permeabilize TDM containing membranes by formation of peptide domains with a high local peptide concentration. Permeabilization was, however, only possible, when the bilayer had not been treated with LL32 before. In LL32 treated bilayers TDM was rather evenly distributed and not organized in domains. We assume that the permeabilization activity of hBD-3-l is limited to lipid covered membrane areas outside of TDM domains and is hindered when TDM gets spread across the lipid bilayer. The comparison of the biophysical data with biological experiments involving *M. tuberculosis* bacilli shows a qualitative agreement. This indicates that the used membrane model made of PE:PG:TDM has biological relevance and can be used as a mimic for the MOM. This and similar membrane models could help out

scientists in the field of mycobacteria to carry out certain prospective experiments in a normal laboratory instead of having to work in a safety level three laboratory with potential dangerous bacilli. Furthermore, our results confirm the importance of TDM for mycobacterial drug resistance and even suggest a new mechanism for AMP resistance. Further research will reveal, if mycobacteria are able to use certain naturally occurring human AMPs to protect themselves from other AMPs or mechanisms of the immune system. If so, this sheds a new light on coevolution between man and human pathogenic microorganisms.

5 SUMMARY AND OUTLOOK

This thesis deals with the architecture of eukaryotic, Gram negative and mycobacterial membranes, their role in infection as well as their interactions with antimicrobial substances, especially antimicrobial peptides (AMPs). Experiments were carried out using different membrane models as mimics of natural membranes. In summary, the results showed three different activities of the tested antimicrobial agents: (i) weakening of SM-cholesterol rich domains, which were used as a model for lipid rafts in macrophages; (ii) induction of membrane fusion in vesicles mimicking bacterial lipid membranes and (iii) permeabilization of asymmetric LPS containing vesicles, used as a model for the outer membrane of Gram negative bacteria. Initially, two standard protocols for the preparation of giant unilamellar vesicles (GUVs) were adopted and established in our laboratory. GUVs were utilized to investigate the medical relevant complex of sepsis and septic shock. In this disease lipopolysaccharides (LPSs) from a local infection with Gram negative bacteria cause a severe inflammatory condition of the whole body and eventually lead to a life threatening drop in blood pressure. The observed strong immune reactions in patients are initially based on the recognition of LPSs by macrophages and other cells of the immune system. By this, the functionality of the involved receptor complex has been reported to be connected to localization within special membrane areas called lipid rafts. This allows for eventually preventing LPS recognition and inflammation by alternation of the lipid raft structure in macrophage membranes. Sphingomyelin(SM)-cholesterol rich domains in GUVs have been reconstituted as artificial mimics of lipid rafts and were treated with different AMPs to test for the induction of domain alteration. Results showed that all tested AMPs initially bound outside of SM-cholesterol rich domains to the membrane and probably started to dissolve the domains beginning from their boundary. Changes in domain size were, however, in the nanometer-range and only observable by atomic force microscopy (AFM) but not by fluorescence microscopy. Further experiments utilized GUVs, which were made of the bacterial phospholipids phosphatidylethanolamine (PE) and phosphatidylglycerol (PG) plus eventually LPSs, as mimics for bacterial membranes. At this, the membrane fusing properties of the antibiotic polymyxin B (PMB) and its nonapeptide (PMBN) on PE:PG GUVs were demonstrated. Results suggest that membrane fusion is also the mode of action for PMB *in vivo*. Furthermore, LPS containing GUVs provided a membrane model for outer membranes of Gram negative bacteria and could even be prepared as asymmetric vesicles with LPSs in the outer membrane leaflet and phospholipids in the inner leaflet. This membrane model reflected the natural asymmetry of Gram negative outer membranes and was used for probing the permeabilization activity of different AMPs as a proof of principle. The established membrane model provided the groundwork for more systematic testing of AMP activities in prospective experiments. Besides AMP related experiments, asymmetric vesicles were also used to study thermodynamic interactions between the two leaflets of a

bilayer. Here, we were able to show that an inner lipid leaflet in the liquid-crystalline phase was able to increase fluidity in an outer, more gel-like LPS leaflet. Inter leaflet coupling could constitute a new mechanism for the regulation of membrane fluidity in outer membranes of Gram negative bacteria, allowing to prevent gel phases in the outer LPS leaflet. Further research dealt with the outer membrane of *Mycobacterium tuberculosis*, the causative agent of tuberculosis in humans. As the mycobacterial outer membrane (MOM) plays an important role in mycobacterial virulence and resistance to antibiotics, this membrane was reconstituted as planar bilayers and GUVs. Membrane models contained the particular important mycobacterial glycolipid trehalose dimycolate (TDM), whose structural properties and interactions with AMPs were investigated. Results showed that TDM in lipid matrices gathered into stable domains of symmetric TDM bilayers and was also able to stabilize lipid membranes. When incorporated into lipid membranes the long alky chains of TDM were folded, possibly promoting H-bonds and van-der-Waals interactions with neighboring molecules. These findings indicate - in agreement with other authors - that TDM contributes to the mechanical stability of the MOM. In addition, experiments with AMPs revealed the peculiar role of TDM in mycobacterial AMP resistance. Results showed that the active human AMP hBD-3-l was able to permeabilize TDM containing bilayers by binding to lipid areas and formation of peptide domains with a very high local peptide concentration. Interestingly, the hBD-3-l activity was nullified, when the membranes had been treated with another human AMP called LL32 before. LL32 was by itself unable to permeabilize TDM containing bilayers but caused a partial vanishing of the TDM domains. In a subsequent hBD-3-l addition this peptide was now unable to act on TDM-free membrane areas, as TDM and lipids were mixed. hBD-3-l activity was impaired either by direct interaction with TDM molecules or by TDM mediated stabilization of the lipid bilayer. An LL32 triggered inhibition of hBD-3-l activity was not only found in model membranes but was also demonstrated by our collaboration partners using *Mycobacterium tuberculosis* bacilli. Further research will be necessary, but results obtained so far indicate a possibly new mechanism of bacterial resistance, in which mycobacteria utilize human AMPs, indented to remove them from the host, to alter their outer membrane and gain protection against other AMPs. For a further investigation of TDM, small-angle X-ray scattering experiments are planned and have partially been carried out already. By this, the TDM conformation in solution, in planar lipid bilayers and planar lipid multilayers is examined. Furthermore, AMP interactions with these structures are investigated. Prospective experiments will also deal with the promising membrane system of asymmetric vesicles. Here, the preparation of asymmetric TDM / phospholipid vesicles and their use for permeabilization experiments with AMPs are planned. Asymmetric vesicles could also mimic the natural asymmetry of eukaryotic cell membranes, which would allow for an investigation of lipid raft asymmetry. To be able to use asymmetric vesicles for fluorescence spectroscopy and IR spectroscopy, prospective work will include improvements in the preparation protocol. Spectroscopy could then reveal the phase behavior of asymmetric vesicles of different compositions and contribute to a better understanding of thermodynamic coupling between the two leaflets of a bilayer.

6 LITERATURE

Ahmed S.N., D.A. Brown, E. London (1997) On the origin of sphingolipid/cholesterol-rich detergent-insoluble cell membranes: physiological concentrations of cholesterol and sphingolipid induce formation of detergent-insoluble, liquid-ordered lipid-phase in model membranes. Biochemistry 36:10944-10953.

Alberts B., A. Johnson, J. Lewis, M. Raff, K. Roberts, P. Walters (2002) Molecular Biology of the Cell; Fourth Edition. New York and London: Garland Science.

Albrecht O., Gruler H., Sackmann E. (1978) Polymorphism of phospholipid monolayers. J Phys. 39:301-313.

Almeida P.F., A. Pokorny, A. Hinderliter (2005) Thermodynamics of membrane domains. Biochim Biophys Acta 1720:1-13.

Angelova M.I. and D.S. Dimitrov (1986) Liposome electroformation. Faraday Discuss. Chem. Soc. 81:303-311.

Armitige L.Y., C. Jagannath, A.R. Wanger, S.J. Norris (2000) Disruption of the genes encoding antigen 85A and antigen 85B of Mycobacterium tuberculosis H37Rv: effect on growth in culture and in macrophages. Infect Immun. 68:767-778.

Arreaza G. and D. A. Brown (1995) Sorting and intracellular trafficking of a glycosylphosphatidylinositol-anchored protein and two hybrid proteins with the same ectodomain in MDCK kidney epithelial cell. J. Biol. Chem. 270:23641-23647.

Bagatolli L.A. and E. Gratton (2000) Two photon fluorescence microscopy of coexisting lipid domains in giant unilamellar vesicles of binary phospholipid mixtures. Biophys. J. 78:290-305.

Bagatolli L.A. and E. Gratton (1999) Two-Photon Fluorescence Microscopy Observation of Shape Changes at the Phase Transition in Phospholipid Giant Unilamellar Vesicles. Biophys. J. 77:2090-2101.

Bagatolli L.A., T. Parasassi, E. Gratton (2000) Giant phospholipid vesicles: comparison among the whole sample characteristics using different preparation methods. A two-photon fluorescence microscopy study. Chem. Phys. Lipids 105:135-147.

Baird B., E.D. Sheets, D. Holowka (1999) How does the plasma membrane participate in cellular signaling by receptors for immunoglobulin E? Biophys. Chem. 82:109 -119.

Baumgart T., G. Hunt, E.R. Farkas, W.W. Webb, G.W. Feigenson (2007) Fluorescence probe partitioning between Lo/Ld phases in lipid membranes. Biochim Biophys Acta 1768:2182-2194.

Behling C.A., R.L. Perez, M.R. Kidd, G.J. Staton, R.L. Hunter (1993) Induction of pulmonary granulomas, macrophage procoagulant activity, and tumor necrosis factor-alpha by trehalose glycolipids. Ann Clin Lab Sci. 23:256-266.

Bent H.A. (1961) An Appraisal of Valence-bond Structures and Hybridization in Compounds of the First-row elements. Chemical Reviews 61:275-311.

Benz R. and K. Bauer (1988) Permeation of hydrophilic molecules through the outer membrane of gram-negative bacteria. review on bacterial porins. European Journal of Biochemistry 176:1-19.

Binnig G. and C.F. Quate (1986) Atomic Force Microscope. Phys. Rev. Lett. 56:930-933.

Binnig G. and D.P.E.Smith (1986) Single-tube three-dimensional scanner for scanning tunneling microscopy. Rev. Sci. Instrum. 57:1688-1689.

Blasie J.K. and C.R. Worthington (1969) Planar liquid-likearrangement of photopigment molecules in frog retinal receptor disk membranes. J. Mol. Biol. 39:417-439.

Bloch H. (1950) Studies on the virulence of tubercle bacilli: Isolation and biological properties of a constituent of virulent organisms. J Exp Med. 91:197-219.

Bloch H. (1955) Virulence of Mycobacteria. Adv Tuberc Res. 6:49-61.

Bloch H. and H. Noll (1955) Studies on the virulence of tubercle bacilli. The effect of cord factor on murine tuberculosis. Brit J Exp Path. 36:8-17.

Bloch K. (1991) Cholesterol: evolution of structure and function. In Biochemistry of Lipids, Lipoproteins and Membranes. D. E. Vance and J. E. Vance, editors. Elsevier, Amsterdam, The Netherlands. 363-381.

Blodgett K.B. and I. Langmuir (1937) Built-up films of barium stearate and their optical properties. Phys.Rev. 51:964-982.

Boman H.G. (1995) Peptide antibiotics and their role in innate immunity. Annu. Rev. Immunol. 13:61-92.

Boman H.G. (1998) Gene-encoded peptide antibiotics and the concept of innate immunity: An update review. Scand. J. Immunol. 48:15-25.

Boon J.M. and B.D. Smith (2002) Chemical control of phospholipid distribution across bilayer membranes. Med. Res. Rev. 22:251-281.

Brennan P.J. and H. Nikaido (1995) The envelope of mycobacteria. Annu. Rev. Biochem. 64:29-63.

Brogden, K. A. (2005) Antimicrobial peptides: pore formers or metabolic inhibitors in bacteria. Nature Reviews Microbiology 3:238-250.

Brown D.A. and E. London (1998). Functions of lipid rafts in biological membranes. Annu. Rev. Cell Dev. Biol. 14:111-136.

Brown D.A. and E. London (2000) Structure and function of sphingolipid- and cholesterol-rich membrane rafts. J. Biol. Chem. 275:17221-17224.

Cajal Y., J. Ghanta, K. Eswaran, A. Surolia, M.K. Jain (1996) Specificity for the Exchange of Phospholipids Through Polymyxin B Mediated Intermembrane Molecular Contacts. Biochemistry 35 5684 -95.

Cederlund A., G.H. Gudmundsson, B. Agerberth (2011) Antimicrobial peptides important in innate immunity. FEBS Journal 278:3942–3951.

Chamberlain L.H., R.D. Burgoyne, G.W. Gould (2001) SNARE proteins are highly enriched in lipid rafts in PC12 cells: implications for the spatial control of exocytosis. Proc. Natl. Acad. Sci. USA 98:5619-5624.

Chan Y.-H.M., S.G. Boxer (2007) Model membrane systems and their applications, Curr Opin Chem Biol. 11:581-587.

Chatterjee D. (1997) The mycobacterial cell wall: structure, biosynthesis and sites of drug action. Curr. Opin. Chem. Biol. 1:579-588.

Coin I., M. Beyermann, M. Bienert (2007) Solid-phase peptide synthesis: from standard procedures to the synthesis of difficult sequences. Nature Protocols 2:3247-3256.

Collins M.D. and S.L. Keller (2008) Tuning lipid mixtures to induce or suppress domain formation across leaflets of unsupported asymmetric bilayers Proc. Natl. Acad. Sci. USA 105:124-128.

Cone R.A. (1972) Rotational diffusion of rhodopsin in the visual receptor membrane. Nature New Biol. 15:39-43.

Cotran R.S. (1998) Robbins Pathologic Basis of Disease. Philadelphia: W.B Saunders Company.

Darnell J., H. Lodish, A. Berk, L. Zipursky, P. Matsudaira (1999) Molecular Cell Biology. W.H.Freeman & Co Ltd, 4Rev Ed.

Darnell J., H. Lodish, D. Baltimore (1986) Molecular Cell Biology, Scientific American Books Inc., New York.

Daugelavicius R., E. Bakiene, D.H. Bamford (2000) Stages of Polymyxin B Interaction With the Escherichia Coli Cell Envelope. Antimicrob. Agents and Chemother 44:2969-2978.

Dijkstra J., J.L. Ryan, F.C. Szoka (1988) A procedure for the efficient incorporation of wild-type lipopolysaccharide into liposomes for use in immunological studies. J Immunol Methods 114:197-205.

Dimitrov D. and M. Angelova (1988) Lipid swelling and liposome formation mediated by electric fields. Bioelectrochemistry and Bioenergetics 19:323-336.

Dimova R., S. Aranda, N. Bezlepkina, V. Nikolov, K.A. Riske, R. Lipowsky (2006) A practical guide to giant vesicles. Probing the membrane nanoregime via optical microscopy. Journal of Physics-Condensed Matter 18:1151-1176.

Edidin, M. (2003) The state of lipid rafts: from model membranes to cells. Annu. Rev. Biophys. Biomol. Struct. 32:257-283.

Engel C., F.M. Brunkhorst, H.G. Bone, R. Brunkhorst, H. Gerlach, S. Grond, M. Gruendling, G. Huhle, U. Jaschinski, S. John, K. Mayer, M. Oppert, D. Olthoff, M. Quintel, M. Ragaller, R. Rossaint, F. Stuber, N. Weiler, T. Welte, H. Bogatsch, C. Hartog, M. Loeffler, K. Reinhart (2007) Epidemiology of sepsis in Germany: results from a national prospective multicenter study. Intensive Care Med. 33:606-18.

Engelman D.M. (2005) Membranes are more mosaic than fluid. Nature 438:578-580.

Epand R.M. and R.F. Epand (2011) Bacterial membrane lipids in the action of antimicrobial agents, J. Pept Sci. 17:298-305.

Estes D. and M. Mayer (2005) Giant liposomes in physiological buffer using electroformation in a flow chamber. Biochimica et Biophysica Acta 1712:152-160.

Fairbanks G.,T.L. Steck, D.F.H. Wallach (1971) Electrophoretic analysis of the major polypeptides of the human erythrocyte membrane. Biochem. 10:2606-2617.

Field K.A., D. Holowka, B. Baird (1997) Compartmentalized activation of the high affinity immunoglubulin E receptor within membrane domains. J. Biol. Chem. 272:4276-4280.

Fischer K., D. Chatterjee, J. Torrelles, P.J. Brennan, S.H. Kaufmann, U.E. Schaible (2001) Mycobacterial lysocardiolipin is exported from phagosomes upon cleavage of cardiolipin by a macrophagederived lysosomal phospholipase A2. J Immunol. 167:2187-92.

Förster T. (1948) Zwischenmolekulare Energiewanderung und Fluoreszenz. Ann. Physik (Leipzig) 437:55-75.

Fox M.A. and J.K. Whitesell (1995) Organische Chemie. Spektrum Akademischer Verlag.

Franz V., S. Loi, H. Müller, E. Bamberg, H.J. Butt (2002) Tip penetration through lipid bilayers in atomic force microscopy. Colloids and Surfaces B: Biointerfaces 23:191-200.

Freire E. and B. Snyder (1978) Estimation of the lateral distribution of molecules in two-component lipid bilayers, lipid mixtures, Biochemistry 17:3934-3939.

Frohm Nilsson M., B. Sandstedt, O. Sörensen, G. Weber, N. Borregaard, M. Stahle-Bäckdahl (1999) The human cationic antimicrobial protein (hCAP18), a peptide antibiotic, is widely expressed in human squamous epithelia and colocalizes with interleukin-6. Infect Immun. 67:2561-2566.

Frye L.D. and M. Edidin (1970) The rapid intermixing of cell surface antigens after formation of mouse-human heterokaryons. J. Cell Sci. 7:319-335.

Galanos C., O. Luderitz, O. Westphal (1969) A new method for the extraction of R lipopolysaccharides. Eur. J. Biochem. 9:245-249.

Galbiati F., B. Razani, M.P. Lisanti (2001).Emerging themes in lipid rafts and caveolae. Cell 106:403- 411.

Gkantiragas I., B. Brugger, E. Stuven, D. Kaloyanova, X.-Y. Li, K. Lohr, F. Lottspeich, F.T. Wieland, J.B. Helms (2001) Sphingomyelinenriched microdomains at the Golgi complex. Mol. Biol. Cell 12:1819-1833.

Glickman M.S. and W.R. Jacobs (2001) Microbial pathogenesis of Mycobacterium tuberculosis: dawn of a discipline. Cell 104:477:85.

Goren M.B. and P.J. Brennan (1979) Mycobacterial lipids: chemistry and biologic activities. In: Tuberculosis (Youmans GP, Ed), Saunders, Philadelphia. pp 63-193.

Griffiths P.R. and J.A. de Haseth. (1986) Fourier Transform Infrared Spectrometry. John Wiley and Sons; New York. p. 45.

Gudmundsson G.H. and B. Agerberth (1999) Neutrophil antibacterial peptides, multifunctional effector molecules in the mammalian immune system. J. Immunol. Methods 232:45-54.

Hanada K., M. Nishijima, Y. Akamatsu, R.E. Pagano (1995) Both sphingolipids and cholesterol participate in the detergent insolubility of alkaline-phosphatase, a glycosylphosphatidylinositol-anchored protein, in mammalian membranes. J. Biol. Chem. 270:6254-6260.

Hancock J.F. (2006) Lipid rafts: contentious only from simplistic standpoints. Nat Rev Mol Cell Biol. 7:456-462.

Hancock R.E. (1997) Peptide antibiotics. Lancet. 349:418-422.

Hancock R.E. and M.G. Scott (2000) The role of antimicrobial peptides in animal defenses. Proc. Natl. Acad. Sci. USA 97:8856-8861.

Hanekom W.A., S.D. Lawn, K. Dheda, A. Whitelaw (2010) Tuberculosis research update. Trop Med Int Health 15:981-9.

Harder T., P. Scheiffele, P. Vekade, K. Simons (1998) Lipid domain structure of the plasma membrane revealed by patching of membrane components. J. Cell Biol. 141:929 -942.

Harland C.W., D. Rabuka, C.R. Bertozzi, R. Parthasarathy (2008) The Mycobacterium tuberculosis virulence factor trehalose dimycolate imparts desiccation resistance to model mycobacterial membranes. Biophys. J. 94:4718-24.

Hasday J.D. (2000) The role of fever in the infected host. Microbes and Infection 2:1891-1904.

Helfrich W. (1973) Elastic Properties of Lipid Bilayers - Theory and Possible Experiments. Z. Naturforsch, C. 28:693-703.

Hoffmann C., A. Leis, M. Niederweis, J.M. Plitzko, H. Engelhardt (2008) Disclosure of the mycobacterial outer membrane: cryo-electron tomography and vitreous sections reveal the lipid bilayer structure. Proc. Natl. Acad. Sci. USA 105:3963-3967.

Hunter R.L., M.R. Olsen, C. Jagannath, J.K. Actor (2006) (I) Multiple roles of cord factor in the pathogenesis of primary, secondary, and cavitary tuberculosis, including a revised description of the pathology of secondary disease. Annals of Clinical and Laboratory Science 36:371-386.

Hunter R.L., N. Venkataprasad, M.R.Olsen (2006) (II) The role of trehalose dimycolate (cord factor) on morphology of virulent M. tuberculosis in vitro. Tuberculosis (Edinburgh) 86:349-356.

Hutter J.L. and J. Bechhoefer (1993) Calibration of atomic-force microscope tips." Rev. Sci. Instrum. 64:1868-1873.

Huttner W.B. and J. Zimmerberg (2001) Implications of lipid microdomains for membrane curvature, budding and fission. Curr. Opin. Cell Biol. 13:478-484.

Huwiler A., T. Kolter, J. Pfeilshifter, K. Sandhoff (2000) Physiology and pathophysiology of sphingolipid metabolism and signaling. Biochim. Biophys. Acta. 1485:63-99.

Ikonen E. (2001) Roles of lipid rafts in membrane transport. Curr. Opin. Cell Biol. 13:470-477.

Indrigo J., R.L. Hunter Jr, J.K. Actor (2003) Cord factor trehalose 6,6'-dimycolate (TDM) mediates trafficking events during mycobacterial infection of murine macrophages. Microbiology 149:2049-2059.

Ipsen J., G. Karlstrom, O. Mouritsen, H. Wennerstrom, M. Zuckermann (1987) Phase equilibria in the phosphatidylcholine-cholesterol system. Biochem. Biophys. Acta 905:162- 172.

Israelachvili J.N. (1985) Intermolecular and surface forces - with application to colloidal and biological systems. Academic Press, Inc., London.

Israelachvili J.N., D.J. Mitchell, B.W. Ninham (1976) Theory of self-assembly of hydrocarbon amphiphiles into micelles and bilayers. J. Chem. Soc., Faraday Trans. II 72:1525-1568.

Jackson M. and H.H. Mantsch (1996) Infrared Spectroscopy of Biomolecules. Mantsch HH, Chapman D, editors. Wiley-Liss; Toronto. p. 311.

Jacobson K., O.G. Mouritsen, R.G. Anderson (2007) Lipid rafts: at a crossroad between cell biology and physics Nat Cell Biol. 9:7-14.

Janeway C., P. Travers, M. Walport, M. Shlomchik (2001). Immunobiology; Fifth Edition. New York and London: Garland Science.

Jarlier V. and H. Nikaido (1994) Mycobacterial cell wall: structure and role in natural resistance to antibiotics. FEMS Microbiol. Lett. 123:11-18.

Jass J., T. Tjarnhage, G. Puu. (2000) From liposomes to supported, planar bilayer structures on hydrophilic and hydrophobic surfaces: an atomic force microscopy study. Biophys. J. 79:3153-3163.

Johnson R., E.M. Streicher, G.E. Louw, R.M. Warren, P.D. van Helden, T.C. Victor (2006) Drug Resistance in Mycobacterium tuberculosis. Curr. Issues Mol. Biol. 8:97-112.

Karima R., S. Matsumoto, H. Higashi, K. Matsushima (1999) The molecular pathogenesis of endotoxic shock and organ failure. Mol. Med. Today 5:123-132.

Kawabuchi M., Y. Satomi, T. Takao, Y. Shimonishi, S. Nada, K. Nagai, A. Tarakhovsky, M. Okada (2000) Transmembrane phosphoprotein Chp regulates the activity of Src-family of tyrosine kinase. Nature 404:999-1003.

Kitano H. (2002) Systems Biology: a brief overview. Science 295:1662-1664.

Kleinig H. (1999) Die äußere Membran gramnegativer Bakterien. In Zellbiologie. H. Kleinig and U. Maier, editors. G. Fischer, Stuttgart.

Kubiak J., J. Brewer, S. Hansen, L.A. Bagatolli (2011) Lipid lateral organization on giant unilamellar vesicles containing lipopolysaccharides. Biophys. J. 100:978-86.

Kucerka N., Y. Liu, N. Chu, H.I. Petrache, S. Tristram-Nagle, J.F. Nagle (2005) Structure of fully hydrated fluid phase DMPC and DLPC lipid bilayers using X-ray scattering from oriented multilamellar arrays and from unilamellar vesicles. Biophys. J. 88:2626-2637.

Kusumi A., I. Koyama-Honda, K. Suzuki (2004) Molecular dynamics and interactions for creation of stimulation-induced stabilized rafts from small unstable steady-state rafts. Traffic 5:213-230.

Lafont F., P. Verkade, T. Galli, C. Wimmer, D. Louvard, K. Simons (1999) Raft association of SNAP receptors acting in apical trafficking in Madin-Darby canine kidney cells. Proc. Natl. Acad. Sci. USA 96:3734-3738.

Lakowicz J.R. (1999) Principles of Fluorescence Spectroscopy, Kluwer Academic/Plenum, New York.

Lang T., D. Bruns, D. Wenzel, D. Riedel, P. Holroyd, C. Thiele, R. Jahn (2001) SNAREs are concentrated in cholesterol-dependent clusters that define docking and fusion sites for exocytosis. EMBO J. 20:2202-2213.

Langmuir I. and V.J. Schaefer (1938) Activities of urease and pepsin monolayers. J.Am Chem.-Soc. 60:1351-1360.

Lewis B.A. and D.M. Engelman (1983) Lipid bilayer thickness varies linearly with acyl chain length in fluid phosphatidylcholine vesicles. J. Mol. Biol. 166:211-217.

Li L. and J.X. Cheng (2006) Coexisting stripe- and patch-shaped domains in giant unilamellar vesicles. Biochemistry 45:11819-11826.

Lichtenberg D., F.M. Goni, H. Heerklotz (2005) Detergent-resistant membranes should not be identified with membrane rafts. Trends Biochem Sci. 30:430-436.

Lichtman J.W. and J.-A. Conchello (2005) Fluorescence microscopy. Nat. Methods 2:910-919.

Lima V.M., V.L. Bonato, K.M. Lima, S.A. Dos Santos, R.R. Dos Santos, E.D. Goncalves, L.H. Faccioli, I.T. Brandao, J.M. Rodrigues Jr, C.L. Silva (2001) Role of trehalose dimycolate in recruitment of cells and modulation of production of cytokines and NO in tuberculosis. Infect Immun. 69:5305-5312.

Luisi P.L. and P. Walde (2000) Giant Vesicles. John Wiley & Sons: Chichester, U.K.

Luisi P.L., F. Ferri, P. Stano (2006) Approaches to semi-synthetic minimal cells: a review. Naturwissenschaften 93:1-13.

Marsh D. (1991) General features of phospholipid phase transitions. Chemistry and Physics of Lipids 57:109-120.

Martin Y., C. Williams, H. Wickramasinghe (1987) Atomic force microscope-force mapping and profiling on a sub 100-a scale. J Appl Phys. 61:4723-4729.

Matsuzaki K., K. Sugishita, N. Fujii, K. Miyajima (1995) Molecular Basis for Membrane Selectivity of an Antimicrobial Peptide, Magainin 2. Biochemistry 34:3423-3429.

McMullen T., R. Lewis, R. McElhaney (2000) Differential Scanning Calorimetric and Fourier Transform Infrared Spectroscopic Studies of the Effects of Cholesterol on the Thermotropic Phase Behavior and Organization of a Homologous Series of Linear Saturated Phosphatidylserine Bilayer Membranes. Biophys. J. 79:2056-2065.

Meena LS, Rajni (2010) Survival mechanisms of pathogenic Mycobacterium tuberculosis H37Rv. FEBS J. 277:2416-27.

Minnikin, D.E. (1982) Lipids: complex lipids, their chemistry, biosynthesis and roles. In The Biology of the Mycobacteria: Physiology, Identification and Classification (Ratledge, C. and Stanford, J., eds, pp. 95-184, Academic Press, Inc., New York, NY.

Miyawaki, A. (2011) Development of Probes for Cellular Functions Using Fluorescent Proteins and Fluorescence Resonance Energy Transfer. Annu Rev Biochem. 80:357-73.

Moffett S., D.A. Brown, M.E. Linder (2000) Lipid-dependent targeting of G proteins into rafts. J. Biol. Chem. 275:2191-2192.

Montal M. and P. Mueller (1972). Formation of bimolecular membranes from lipid monolayers and a study of their electrical properties. Proc. Natl. Acad. Sci. USA 69:3561-3566.

Montes L.R., A. Alonso, F.M. Goni, L.A. Bagatolli (2007) Giant Unilamellar Vesicles Electroformed from Native Membranes and Organic Lipid Mixtures under Physiological Conditions; Biophys. J. 93:3548-3554.

Morales-Penningston N.F., J. Wu, E.R. Farkas, S.L. Goh, T.M. Konyakhina, J.Y. Zheng, W.W. Webb, G.W. Feigenson (2010) GUV Preparation and Imaging: Minimizing Artifacts. Biochim. Biophys. Acta 1798:1324-32.

Moscho A., O. Orwar, D. Chiu, B. Modi, R. Zare (1996) Rapid preparation of giant unilamellar vesicles. Proc. Natl. Acad. Sci. 93:11443-11447.

Munro S. (2003) Lipid rafts: elusive or illusive? Cell 115:377-388.

Nagel E. (1961) The structure of science; problems in the logic of scientific explanation. New York, Harcourt, Brace and World.

Nakhla A.N., J.H. Banoub, J. Hernandez-Borrell, K.M.W Keough (1996) Incorporation of the lipopolysaccharide and polysaccharide from Aeromonas salmonicida into liposomes. Journal of liposome Research 6:141-154.

Neville F., M. Cahuzac, O. Konovalov, Y. Ishitsuka, K.Y. Lee, I. Kuzmenko, G.M. Kale, D. Gidalevitz (2006) Lipid headgroup discrimination by antimicrobial peptide LL-37: insight into mechanism of action. Biophys. J. 90:1275-87.

Nielsen M., L. Miao, J. Ipsen, M.Zuckermann, O. Mouritsen (1999) Off-lattice model for the phase behavior of lipid-cholesterol bilayers. Phys. Rev. E. 59:5790-5803.

Nikaido H. (1994) Prevention of drug access to bacterial targets: role of permeability barriers and active efflux. Science 264:382-388.

Nikaido H. and M. Vaara (1985) Molecular basis of bacterial outer membrane permeability. Microbial. Rev. 49:1-32.

Noble, D. (2006). The music of life: Biology beyond the genome. Oxford: Oxford University Press. pp. 176.

Noireaux V. and A. Libchaber (2004) A vesicle bioreactor as a step toward an artificial cell assembly Proc. Natl Acad.Sci. 101:17669-74.

Noll H., H. Bloch, J. Asselineau, E. Lederer (1956) The chemical structure of the cord factor of Mycobacterium tuberculosis. Biochim Biophys Acta 20:299-309.

O'hara P. B., K.M. Gorski, M. A. Rosen (1988) Thermal profiles of förster energy transfer preliminary studies of luminescent probes of protein dynamics in transferrin and calmodulin. Analytrca Chimica Acta 205:161-173.

Osborn M.J., J.E. Gander, E. Parisi, J. Carson (1972) Mechanism and assembly of the outer membrane of Salmonella typhimurium. J. Biol. Chem. 247:3962-3972.

Parasassi T., G. De Stasio, A. d'Ubaldo, and E. Gratton (1990) Phase fluctuation in phospholipid membranes revealed by Laurdan fluorescence. Biophys. J. 57:1179-1186.

Pautot, S., B.J. Frisken, D.A. Weitz (2003) Engineering asymmetric vesicles. Proc. Natl. Acad. Sci. USA 100:10718-10721.

Peschel, A., M. Otto, R.W. Jack, H. Kalbacher, G. Jung, F. Götz (1999) Inactivation of the dlt operon in Staphylococcus aureus confers sensitivity to defensins, protegrins, and other antimicrobial peptides. Journal of Biological Chemistry 274:8405-8410.

Pike L.J. (2006) Rafts defined. J. Lipid Res. 47:1597-1598.

Pott T., H. Bouvrais, P. Méléard (2008) Giant unilamellar vesicle formation under physiologically relevant conditions, Chemistry and Physics of Lipids 154:115-119.

Raetz C. and C. Whitfield (2002) Lipopolysaccharide Endotoxins. Annu. Rev. Biochem. 71:635-700.

Raetz C.R.H. (1993) Bacterial endotoxins: extraordinary lipids that activate eucaryotic signal transduction. J. Bacteriol. 175:5745-5753.

Rajendran L and K. Simons (2005) Lipid rafts and membrane dynamics. J Cell Sci. 118:1099-1102.

Ramstedt B. and J.P. Slotte (2002) Membrane properties of sphingomyelins. FEBS Lett. 531:33-37.

Rao V., N. Fujiwara, S.A. Porcelli, M.S. Glickman (2005) Mycobacterium tuberculosis controls host innate immune activation through cyclopropane modification of a glycolipid effector molecule. J Exp Med. 201:535-543.

Retzinger G.S., S.C. Meredith, K. Takayama, R.L. Hunter, F.J. Kezdy (1981) The role of surface in the biological activities of trehalose 6,6'-dimycolate. Surface properties and development of a model system. J Biol Chem. 256:8208-8216.

Retzinger G.S., S.C. Meredith, R.L. Hunter, K. Takayama, F.J. Kezdy. (1982) Identification of the physiologically active state of the mycobacterial glycolipid trehalose 6,6'- dimycolate and the role of fibrinogen in the biologic activities of trehalose 6,6'-dimycolate monolayers. J Immunol. 129:735-744.

Rietschel E.T., H. Brade, L. Brade, K. Brandenburg, U. Schade, U. Seydel, U. Zahringer, C. Galanos, O. Luderitz, O. Westphal (1987) Lipid a, the endotoxic center of bacterial lipopolysaccharides: relation of chemical structure to biological activity. Progress in Clinical and Biological Research 231:25-53.

Rietveld A. and K. Simons (1998) The differential miscibility of lipids as the basis for the formation of functional membrane rafts. Biochim. Biophys. Acta 1376:467-79.

Rittig M.G., A. Kaufmann, A. Robins, B. Shaw, H. Sprenger, D. Gemsa, V. Foulongne, B. Rouot, J. Dornand (2003) Smooth and rough lipopolysaccharide phenotypes of Brucella induce different intracellular trafficking and cytokine/chemokine release in human monocytes. Journal of Leukocyte Biology 74:1045-1055.

Rivest S., S. Lacroix, L. Vallieres, S. Nadeau, J. Zhang, N. Laflamme (2000) How the blood talks to the brain parenchyma and the paraventricular nucleus of the hypothalamus during systemic inflammatory and infectious stimuli. Proc. Soc. Exp. Biol. Med. 223:22-38.

Rodgers W., B. Crise, J.K. Rose (1994) Signals determining protein tyrosine kinase and glycosyl-phosphatidylinositol-anchored proteins targeting to a glycolipid-enriched membrane fraction. Mol. Cell Biol. 14:5384 -5391.

Rodriguez N., F. Pincet, S. Cribier (2005) Giant vesicles formed by gentle hydration and electroformation: a comparison by fluorescence microscopy. Colloids Surf. B Biointerfaces 42:125-130.

Roes S., U. Seydel, T. Gutsmann (2005) Probing the Properties of Lipopolysaccharide Monolayers and Their Interaction with the Antimicrobial Peptide Polymyxin B by Atomic Force Microscopy. Langmuir 21:6970-6978.

Rohl C.A., W. Fiori, R.L. Baldwin (1999) Alanine is helix-stabilizing in both template nucleated and standard peptide helices. Proc.Natl.Acad.Sci. USA 96:3682-3687.

Roux A., D. Cuvelier, P. Nassoy, J. Prost, P. Bassereau, B. Goud (2005) Role of curvature and phase transition in lipid sorting and fission of membrane tubules. EMBO J. 24:1537-45.

Roy H., K. Dare, M. Ibba (2009) Adaptation of the bacterial membrane to changing environments using aminoacylated phospholipids. Mol. Microbiol. 71:547-550.

Salton M.J.R. and K.S. Kim (1996) Structure; in: Baron's Medical Microbiology (Baron S et al., eds.) (4th ed.). Univ of Texas Medical Branch.

Sankaram M. and T. Thompson (1990). Interaction of cholesterol with various glycerophospholipids and sphingomyelin. Biochemistry 29:10670-10675.

Schibli D.J., H.N. Hunter, V. Aseyev, T.D. Starner, J.M. Wiencek, P.B.J. McCray, B.F. Tack, H.J. Vogel (2002) The solution structures of the human beta-defensins lead to a better understanding of the potent bactericidal activity of hbd3 against staphylococcus aureus. J Biol Chem. 277:8279-8289.

Schmitz G. and E. Orsó (2002) CD14 signalling in lipid rafts: new ligands and co-receptors. Curr Opin Lipidol. 13:513-21.

Schroeder R., E. London, D. Brown (1994) Interactions between saturated acyl chains confer detergent resistance on lipids and glycosylphosphatidylinositol (GPI)-anchored proteins: GPI-anchored proteins in liposomes and cells show similar behavior. Proc. Natl. Acad. Sci. USA 91:12130-12134.

Shaw A.S. (2006) Lipid rafts: now you see them, now you don't. Nat Immunol. 7:1139-42.

Shimshick E.J. and H.M. McConnell (1973) (I) Lateral phase separation in phospholipid membranes. Biochemistry 12:2351-2360.

Shimshick E.J. and H.M. McConnell (1973) (II) Lateral phase separation in binary mixtures of cholesterol and phospholipids. Biochem. Biophys. Res. Commun. 53:446-451.

Silva C.L., S.M. Ekizlerian, R.A. Fazioli (1985) Role of cord factor in the modulation of infection caused by mycobacteria. Am J Pathol. 118:238-247.

Simons K. and E. Ikonen (1997) Functional rafts in cell membranes. Nature 387:569-572.

Simons K. and E. Ikonen (2000) How cells handle cholesterol. Science 290:1721-1726.

Simons K. and G. van Meer (1988) Lipid sorting in epithelial cells. Biochemistry 27:6197-6202.

Singer S.J. and G.L. Nicolson (1972) The fluid mosaic model of cell membranes. Science 175:720-731.

Solomon K.R., E.A. Kurt-Jones, R.A. Saladino, A.M. Stack, I.F. Dunn, M. Ferretti, D. Golenbock, G.R. Fleisher, R.W. Finberg (1998) Heterotrimeric G proteins physically associated with the

lipopolysaccharide receptor CD14 modulate both in vivo and in vitro responses to lipopolysaccharide. J. Clin. Invest. 102:2019-2027.

Steck P.A., B.A. Schwartz, M.S. Rosendahl, G.R. Gray (1978) Mycolic acids. A reinvestigation. J. Biol. Chem. 253:5625-5629.

Steiner H., D. Hultmark, A. Engstrom, H. Bennich, H.G. Boman (1981) Sequence and specificity of two antibacterial proteins involved in insect immunity. Nature 292:246-248.

Stott B.M., M.P. Vu, C.O. McLemore, M.S. Lund, E. Gibbons, T.J. Brueseke, H.A. Wilson-Ashworth, J. Bell (2008) Use of Fluorescence to Determine the Effects of Cholesterol on Lipid Behavior in Sphingomyelin Liposomes and Erythrocyte Membranes. Journal of Lipid Research 49:1202-1215.

Syed S.S. and R.L. Hunter (1997) Studies on the toxic effects of quartz and a mycobacterial glycolipid, trehalose 6,6'-dimycolate. Ann Clin Lab Sci. 27:375-383.

Thompson H.J. (2005) Fever: a concept analysis. Journal of Advanced Nursing 51:484-492.]

Tonge P.J. (2000) Another brick in the wall. Nat Struct Biol. 7:94-96.

Triantafilou M., K. Miyake, D.T. Golenbock, K. Triantafilou (2002) Mediators of innate immune recognition of bacteria concentrate in lipid rafts and facilitate lipopolysaccharide-induced cell activation. Journal of Cell Science 115:2603-2611.

Tristram-Nagle S., Y. Liu, J. Legleiter, J.F. Nagle (2002) Structure of gel phase DMPC determined by X-ray diffraction. Biophys. J. 83:3324-3335.

Urban E., A. Bota, B. Kocsis (2006) Non-bilayer formation in the DPPE-DPPG vesicle system induced by deep rough mutant of Salmonella minnesota R595 lipopolysaccharide. Colloids Surf., B. 48:106-11.

Vaara M. (1992) Agents that increase the permeability of the outer membrane. Microbiol Rev. 56:395-411.

Valeva A., N. Hellmann, I. Walev, D. Strand, M. Plate, F. Boukhallouk, A. Brack, K. Hanada, H. Decker, S. Bhakdi (2006). Evidence that clustered phosphocholine head groups serve as sites for binding and assembly of an oligomeric protein pore. J. Biol. Chem. 28:26014-21.

van der Meer B.W., Coker G. III, Chen S.Y.S. (1994) Resonance Energy Transfer: Theory and Data New York: VCH Press.

van Dijck P.W.M., A.J. Laper, M.A.J. Oonk, J. de Gier (1977) Miscibility properties of binary phosphatidylcholine mixtures. Biochim. Biophys. Acta 470:58-69.

van Meer G. and W.L.C. Vaz (2005) Membrane curvature sorts lipids. EMBO reports 6:418-419.

van Meer G., D.R Voelker, G.W. Feigenson (2008) Membrane lipids: where they are and how they behave. Nature Rev. Mol. Cell. Biology. 9:112-124.

Veatch S.L (2007) Lipid Rafts (Methods in Molecular Biology), Bookchapter on Liposome preparation, Editor: T. McIntosh, Humana Press, New York.

Veatch S.L. and S.L. Keller (2003) Separation of liquid phases in giant vesicles of ternary mixtures of phospholipids and cholesterol. Biophys. J. 85:3074-3083.

Veatch S.L. and S.L. Keller (2005) Seeing spots: Complex phase behavior in simple membranes. Biochimica et Biophysica Acta 1746:172-185.

Vinckier A. and G. Semenza (1998) Measuring elasticity of biological materials by atomic force microscopy. FEBS Lett. 430:12-16.

Walde P., K. Cosentino, H. Engel, P. Stano (2010) Giant vesicles: preparations and applications. Chembiochem. 11:848-65.

Waugh A. and A. Grant (2007) Anatomy and Physiology in Health and Illness, 10th edition (Churchill Livingstone Elsevier, Glassgow, UK, pp. 22.

Wesołowska O., K. Michalak, J. Maniewska, A.B. Hendrich (2009) Giant unilamellar vesicles - a perfect tool to visualize phase separation and lipid rafts in model systems. Acta Biochi. Pol. 56:33-39.

Wiese A. and U. Seydel. (1999) Electrophysiological measurements on reconstituted outer membranes. Methods in Molecular Biology 145:355-370.

World Health Organization (2009) "Epidemiology". Global tuberculosis control: epidemiology, strategy, financing. pp. 6-33

World Health Organization (2010)Tuberculosis Fact sheet N° 104.

Yamashita Y., M. Oka, T. Tanaka, M. Yamazaki (2002) A new method for the preparation of giant liposomes in high salt concentrations and growth of protein microcrystals in them. Biochim. Biophys. Acta 1561:129-34.

Yang D., O. Chertov, J.J. Oppenheim (2001) The role of mammalian antimicrobial peptides and proteins in awakening of innate host defenses and adaptive immunity. Cell. Mol. Life Sci. 58:978-989.

Youmans G.P. (1979) (I) Chapter 2, Morphology and metabolism of mycobacteria. In: Tuberculosis (Youmans GP, Ed), Saunders, Philadelphia, pp 8-45.

Youmans GP. (1979) (II) Mycobacterial lipids: chemistry and biologic activities. In: Tuberculosis (Youmans GP, Ed), Saunders, Philadelphia, pp 63-193.

Yuan Y., R.E. Lee, G.S. Besra, J.T. Belisle, C.E. Barry (1995) Identification of a gene involved in the biosynthesis of cyclopropanated mycolic acids in Mycobacterium tuberculosis. Proc Natl Acad Sci USA 92:6630-6634.

Zachowski, A. (1993) Phospholipids in animal eukaryotic membranes: transverse asymmetry and movement. Biochem. J. 294:1-14.

Zähringer U., B. Lindner, E.T. Rietschel (1994) Molecular structure of lipid A, the endotoxic center of bacterial lipopolysaccharides. Adv. Carbohydr. Chem. Biochem. 50:211-276.

Zasloff M. (2002) Antimicrobial peptides of multicellular organisms. Nature 415:389-95.

Zuber, B., M. Chami, C. Houssin, J. Dubochet, G. Griffiths, M. Daffé (2008) Direct visualization of the outer membrane of native mycobacteria and corynebacteria. J. Bacteriol. 190:5672-5680.

7 ACKNOWLEDGMENT

I would like to thank:

- my supervisor, Prof. Dr. Thomas Gutsmann, for giving me the opportunity to carry out this thesis in his lab group, for his intellectual and practical support during all phases of the work, for fruitful discussions, teaching of laboratory techniques and granting of additional data.
- Prof. Dr. Christian Hübner, for agreeing to examine this thesis as a second referee.
- Prof. Dr. Ulrich Schaible, for his supply with purified trehalose dimycolate and the ongoing collaboration.
- Sam Willcocks PhD, for providing data about the effects of antimicrobial peptides on mycobacteria.
- Rainer Bartels, for his supply with antimicrobial peptides.
- Annemarie Brauser, for the initial establishment of the preparation protocol for asymmetric vesicles and her collaboration during the first experiments.
- Dr. Buko Lindner, for quality control by mass spectrometry and for his help with some chemical issues.
- Sebastian Stengl, for his great effort in building a temperature cell.
- Dr. Thomas Scholzen, for teaching me how to use a confocal fluorescence microscope.
- Nina Halbrock, for IR spectroscopic measurements.
- Christine Hamann, for fluorescence spectroscopic measurements and for supporting me with virtually unlimited amounts of small unilamellar vesicles.
- Dr. Martin Ernst, for his occasional advice and nice conversations.
- Dr. Nadja Hellmann, for teaching me some concepts of membrane biophysics back then at the University of Mainz. Without this knowledge parts of this thesis would not have been possible.
- Dr. Andre Beerlink, for his theoretical and practical support concerning small-angle X-ray scattering experiments at the Deutsche Elektronen Synchrotron in Hamburg.
- Dr. Gordon Freeman, for nice evening discussions.
- Dr. Malte Hammer, for collaboration regarding the effects of polymyxin B on membranes.
- the technicians and all the other members of the biophysics laboratory group at the Research Center Borstel, for various help with small and bigger problems.
- the Research Center Borstel, for providing a place for scientific research.
- my girlfriend, family and friends for encouragement and support.
- all those, who allowed me to learn something and contribute to the spread of free knowledge.

8 Deutsche Zusammenfassung

Charakterisierung rekonstituierter bakterieller Membranen

und deren Interaktion mit antimikrobiellen Peptiden

Diese Arbeit behandelt den Aufbau eukaryotischer, Gram-negativer und mykobakterieller Membranen, deren Rolle im Infektionsgeschehen der Sepsis und Tuberkulose sowie deren Interaktion mit anti-mikrobiellen Substanzen, vornehmlich anti-mikrobiellen Peptiden (AMPs). Die experimentelle Durchführung der Arbeit basierte auf Membranmodellen als Abbild natürlicher Membranen. Zusammenfassend konnten drei verschiedene Aktivitäten für einzelne der untersuchten Substanzen beschrieben werden: (i) eine Schwächung von Sphingomyelin(SM)-Cholesterol reichen Domänen, die ein Model für *lipid rafts* in Makrophagen darstellen; (ii) eine Fusion von Lipidmembranen, die ein Modell für bakterielle Membranen bilden; und (iii) eine Permeabilisierung von asymmetrischen LPS/Lipid-Membranen als Modell für die äußere Membran Gram-negativer Bakterien. Zu Beginn der Doktorarbeit wurden zwei Standartprotokolle zur Präparation von unilamellaren Vesikeln in der Größe eukaryotischer Zellen (*giant unilamellar vesicles*, GUVs) etabliert. Nachfolgend wurden GUVs zur Untersuchung des medizinisch relevanten Komplexes der Sepsis und des septischen Schocks genutzt. Bei diesem Krankheitsbild verursachen Lipopolysaccharide (LPS) aus einer lokalen Infektion mit Gram-negativen Bakterien eine ernste, systemische Entzündungsreaktion und bewirken somit unter Umständen einen lebensbedrohlichen Abfall des Blutdrucks. Die im Menschen beobachteten Immunreaktionen sind letztlich auf eine Erkennung von LPS durch Makrophagen und andere Zellen des Immunsystems zurückzuführen. Die Funktion des hierbei aktiven Rezeptorkomplexes ist mit dessen Lokalisation innerhalb besonderer Membranareale, den *lipid rafts*, verbunden. Dies legt eine mögliche Verhinderung der LPS-induzierten Entzündungsreaktion durch Auflösen der *lipid raft* Strukturen in der Makrophagenmembran und eine dadurch erfolgende Inhibierung des Rezeptorkomplexes nahe. In diesem Zusammenhang wurden SM-Cholesterol reiche Domänen in GUVs als ein künstliches Modell der natürlichen *lipid raft* Struktur erzeugt und auf ihre Interaktion mit verschiedenen AMPs hin untersucht. Die Ergebnisse zeigen, dass alle getesteten AMPs zunächst außerhalb der SM-Cholesterol reichen Domänen an die Membran banden und die Auflösung der Domänen vermutlich von deren Rand her begann. Die induzierten Veränderungen in der Domänengröße waren jedoch im Nanometerbereich und daher nur mittels Rasterkraftmikroskopie (AFM) aber nicht durch Fluoreszenzmikroskopie abbildbar. Weitere Experimente nutzten GUVs aus den bakteriellen Phospholipiden Phosphatidylethanolamin und Phosphatidylglycerol und eventuell LPS als Membranmodell für bakterielle Membranen. Ein Teilaspekt dieser Arbeit zeigte hierbei die Fähigkeit des Antibiotikums Polymyxin B (PMB) und dessen Nonapeptids (PMBN), GUV

Membranen zu fusionieren. Die Ergebnisse legen die Induktion von Membranfusionen auch als natürlichen Wirkmechanismus des PMBs nahe. Weiterhin dienten LPS-haltige GUVs als Membranmodell für die äußere Membran Gram-negativer Bakterien und konnten auch als asymmetrische Vesikel mit LPS in der äußeren Membranmonoschicht und Phospholipiden in der inneren Membranmonoschicht präpariert werden. Asymmetrische Vesikel spiegelten die natürliche Asymmetrie der äußeren Membran Gram-negativer Bakterien wieder und wurden zunächst für Versuche mit AMPs genutzt. Hierbei konnte die Membranen permeabilisierende Wirkung verschiedener AMPs prinzipiell bestätigt werden. Das so etablierte Testsystem ermöglicht eine systematische Überprüfung der Aktivität verschiedener AMPs in der Zukunft. Neben Versuchen mit AMPs wurden asymmetrische Vesikel auch zur Untersuchung der thermodynamischen Kopplung zwischen innerer und äußerer Membranmonoschicht genutzt. In diesem Zusammenhang konnte gezeigt werden, dass eine innere Lipidmonoschicht in der flüssigkristallinen Phase die Fluidität einer äußeren, rigiden LPS Schicht erhöhen kann. Die beobachtete Kopplung zwischen den Schichten einer Membran könnte einen neuen Mechanismus zur Regulation der Fluidität in der äußeren Membran Gram-negativer Bakterien darstellen und dort das Auftreten von Gel Phasen in der äußeren Monoschicht verhindern. Weitere Teile der Arbeit behandeln die äußere Membran von *Mycobacterium tuberculosis*, dem Erreger der Tuberkulose im Menschen. Da die äußere Membran dieser Bakterien eine entscheidende Rolle bei der mykobakteriellen Virulenz und Resistenz gegen AMPs spielt, wurde sie als Membranmodel nachgebildet. Dieses Model enthielt das für Mykobakterien charakteristische Glykolipid Trehalose-Dimykolat (TDM), dessen strukturellen Eigenschaften und Interaktionen mit AMPs eingehend untersucht wurden. Die Ergebnisse zeigen, dass TDM in Lipiddoppelschichten Domänen bildete und in der Lage war Lipidmembranen zu stabilisieren. In den in eine Lipidmatrix eingebetteten TDM Domänen waren die Alkylketten des TDM gefaltet, was vermutlich eine vermehrte Ausbildung von Wasserstoffbrückenbindungen und van-der-Waals Interaktionen mit benachbarten Molekülen begünstigt. In Übereinstimmung mit anderen Autoren legen unsere Erkenntnisse nahe, dass TDM zur mechanischen Stabilität der äußeren Membran von Mykobakterien beiträgt. Zusätzliche Versuche mit AMPs verdeutlichten die besondere Bedeutung des TDM im Zusammenhang mit mykobakterieller Resistenz gegen AMPs. Hier konnte gezeigt werden, dass das aktive humane AMP hBD-3-l in der Lage war, TDM haltige Membranen zu permeabilisieren. Das Peptid band dabei an Lipidbereiche der Membran außerhalb TDM haltiger Domänen und aggregierte zu kleinen Peptiddomänen mit einer sehr hohen lokalen Peptidkonzentration. Interessanterweise wurde die hBD-3-l Aktivität aufgehoben, wenn TDM haltige Membranen zuvor mit einem anderen humanen AMP namens LL32 behandelt wurden. LL32 war selbst nicht in der Lage, TDM haltige Membranen zu permeabilisieren, erzeugte jedoch eine partielle Auflösung der enthaltenen TDM Domänen. Bei einer nachfolgenden hBD-3-l Zugabe konnte dieses AMP nun nicht mehr an TDM-freie Bereiche binden, da sich Lipide und TDM vermischt hatten. Die hBD-3-l Aktivität wurde so entweder durch eine direkte Interaktion zwischen hBD-3-l und TDM oder durch eine vom TDM hervorgerufene Stabilisierung der Lipide verhindert. Eine durch vorherige LL32 Zugabe

ausgelöste Inhibierung der hBD-3-l Aktivität konnte nicht nur in Modellmembranen gezeigt werden, sondern trat auch in Versuchen unserer Kooperationspartner mit *Mycobacterium tuberculosis* Keimen auf. Auch wenn zur endgültigen Klärung dieses Phänomens weitere Untersuchungen notwendig sein werden, legen die bisher erzielten Ergebnisse einen neuen Mechanismus der bakteriellen Resistenz nahe. Mykobakterien könnten humane AMPs, welche vom Körper zur Beseitigung der Bakterien produziert werden, nutzen um sich selbst durch Membranveränderungen vor anderen AMPs zu schützen.